

**QUANTIFICATION OF SAHARAN DUST INFLUENCES ON EASTERN  
MEDITERRANEAN AIR QUALITY VIA ATMOSPHERIC MODELING**



**Ph.D. THESIS**

**Burcu KABATAŞ**

**Climate and Marine Sciences**

**Earth System Sciences**

**OCTOBER 2016**



**QUANTIFICATION OF SAHARAN DUST INFLUENCES ON EASTERN  
MEDITERRANEAN AIR QUALITY VIA ATMOSPHERIC MODELING**



**Ph.D. THESIS**

**Burcu KABATAŞ  
(601102002)**

**Climate and Marine Sciences**

**Earth System Sciences**

**Thesis Advisor: Prof. Dr. Alper ÜNAL**

**OCTOBER 2016**



**SAHRA TOZUNUN DOĞU AKDENİZ HAVA KALİTESİ ÜZERİNDEKİ  
ETKİLERİNİN ATMOSFER MODELİYLE BELİRLENMESİ**

**DOKTORA TEZİ**

**Burcu KABATAŞ  
(601102002)**

**İklim ve Deniz Bilimleri**

**Yer Sistem Bilimleri**

**Tez Danışmanı: Prof. Dr. Alper ÜNAL**

**EKİM 2016**



Burcu Kabataş a Ph.D. student of ITU Eurasia Institute of Earth Sciences student ID 601102002, successfully defended the dissertation entitled “QUANTIFICATION OF SAHARAN DUST INFLUENCES ON EASTERN MEDITERRANEAN AIR QUALITY VIA ATMOSPHERIC MODELING”, which she prepared after fulfilling the requirements specified in the associated legislations, before the jury whose signatures are below.

**Thesis Advisor :** **Prof. Dr. Alper ÜNAL** .....  
Istanbul Technical University

**Jury Members :** **Dr. Bradley R. PIERCE** .....  
NOAA/NESDIS/STAR

**Prof. Dr. Tayfun KINDAP** .....  
Istanbul Technical University

**Prof. Dr. Mete TAYANÇ** .....  
Marmara University

**Asst. Prof. Dr. Burçak KAYNAK TEZEL**.....  
Istanbul Technical University

**Date of Submission : 05 September 2016**

**Date of Defense : 04 October 2016**





## FOREWORD

First, I would like to gratefully and sincerely thank my Ph.D. advisor Prof. Alper Ünal for his continuous support, understanding, guidance and most importantly, his friendship during my graduate studies at Istanbul Technical University. I also would like to express my sincere gratitude to Dr. Brad Pierce for his patience, motivation, and immense knowledge during my research. Without their precious support and help, it would not be possible to conduct this research. I appreciate and treasure everything that I have learned from them.

I am also very grateful to Liam Gumley for giving me the opportunity to visit Space Science and Engineering Center at University of Wisconsin-Madison. His contribution to my future success has been invaluable.

My sincere thanks also goes to Dr. Marek Rogal not only for helping me throughout my research and answering my every question, but also for his friendship, and Todd Schaack and Dr. Allen Lenzen for providing the data and technical support that was essential to this study.

I will forever be thankful to my former M.Sc. advisor Prof. Dr. Paul Menzel and his beloved wife Nancy Jesse for sharing the most amazing moments with me. Dr. Menzel is not only my former M.Sc. adviser but has also been a tremendous mentor. He's always been motivating, encouraging, and enlightening.

I would like to thank my steering committee members, Prof. Dr. Tayfun Kındap and Prof. Dr. Mete Tayanç for generously offering their time and guidance throughout the progress of this research.

I have been extremely lucky to have great friends such as Pamela and Sinan Taş, Kaba Bah, who cheered me up and were always there whenever I needed them, as well as my other Madisonian friends Nathaniel Shay, Adel Ardalan, Lidka and Arun Rao, Fırat Yaşar, and Mat Gunshor who provided me a fun environment during this “long and winding road”.

Besides the Madisonian gang, my lifetime friends from home Hande Aladağ, Semra Kepenek, M. Nezhil Muşlu, Cenk Avcı, Duygu Sancak Salarvan, Cihan Bulut and Utkan Kolat always encouraged me despite the long distance between us. Thank you to all of my friends for supporting me through this entire process.

I thank my fellow office mates, Seden Baltacıbaşı, who ended up not only being one of my closest friends, but also a tremendous help since the day I started at the Eurasia Institute of Earth Sciences at ITU, Merve Gökğöz Ergül, Elvin Öksüz, Müge Kafadar, Burak Öztaner, Metin Baykara, Tuğba Ağaçayak, Hakkı Baltacı, post-docs Luca Pazzoli, Yasemin Ezber, Yasemin Ergüner and Ozan Mert Gökürk and my geologist fellows Sibel Üsküplü Bulkan, Nalan Lom, Semih Can Ülgen, Emir Altıntaş, Gönenç Göçmengil, Esta Çetin, Remziye Akdoğan, Özge Tekeşin and Ömer Özden Akbaş for sharing the most weary moments we have been through together, for the things we learned together, and for all the fun we have had in the last couple of years.

Words cannot express how grateful I am to my parents, Hülya and Ertuğrul Kabataş, and my brother Burak, for their never-ending support, unconditional trust, love and encouragement. My parents instilled many great qualities in me and I may never have gotten to where I am today without their support. They are the heroes behind my success. My dear cousins Ebru Eren and Ceren Çelebi, it was great to know that I was always in your thoughts and that helped me get through this agonizing period in the most positive way.

Last, but not least, I would like to thank all the scientists around the world for conducting research that inspires the world around them and for enlightening us to understand the dynamics driven by nature in order to do science.

September 2016

Burcu KABATAŞ

## TABLE OF CONTENTS

	<u>Page</u>
<b>FOREWORD</b> .....	<b>ix</b>
<b>TABLE OF CONTENTS</b> .....	<b>xi</b>
<b>ABBREVIATION</b> .....	<b>xiii</b>
<b>SYMBOLS</b> .....	<b>xv</b>
<b>LIST OF FIGURES</b> .....	<b>xvii</b>
<b>SUMMARY</b> .....	<b>xxi</b>
<b>ÖZET</b> .....	<b>xxv</b>
<b>1. INTRODUCTION</b> .....	<b>1</b>
1.1 Background Information .....	1
1.2 Hypothesis .....	2
1.3 Research Questions .....	2
1.4 Literature Study .....	3
1.4.1 Mediterranean region facts .....	5
1.4.2 Air quality management systems .....	7
<b>2. REAL-TIME AIR QUALITY MODELING SYSTEM EXPERIMENT</b> .....	<b>13</b>
2.1 Data .....	13
2.1.1 Ground-based data .....	13
2.1.2 RAQMS model description .....	15
2.1.3 Satellite data overview .....	16
2.2 Results of RAQMS Experiment .....	17
2.3 Discussion of RAQMS Experiment .....	22
<b>3. WRF-CHEM CONTROL EXPERIMENT</b> .....	<b>25</b>
3.1 Ground Observation and Model Description .....	25
3.2 Results of the WRF-Chem Experiment .....	28
3.3 Discussion of the WRF-Chem Experiment .....	36
<b>4. WRF-CHEM MODIS ASSIMILATION EXPERIMENT</b> .....	<b>41</b>
4.1 Data Description .....	41
4.1.1 Data assimilation GSI/3D-VAR and calculating background error covariances .....	41
4.1.2 MODIS aerosol optical depth (AOD) retrieval product.....	43
4.2 Results of the WRF-Chem Assimilation Experiments.....	44
4.3 Discussion of the WRF-Chem Assimilation Experiment.....	49
<b>5. CONCLUSIONS</b> .....	<b>55</b>
<b>REFERENCES</b> .....	<b>61</b>
<b>CURRICULUM VITAE</b> .....	<b>73</b>



## ABBREVIATIONS

<b>AOD</b>	: Aerosol Optical Depth
<b>BC</b>	: Black Carbon
<b>BEC</b>	: Background Error Covariances
<b>BUFR</b>	: Binary Universal Form for the Representation of meteorological data
<b>CALIPSO</b>	: Cloud-Aerosol Lidar and Infrared Pathfinder Satellite Observations
<b>CCN</b>	: Cloud Condensation Nuclei
<b>CMAQ</b>	: Community Multi-scale Air Quality Model
<b>COPD</b>	: Chronic Obstructive Pulmonary Disease
<b>CRTM</b>	: The Community Radiative Transfer Model
<b>DA</b>	: Data Assimilation
<b>EDGAR</b>	: Emission Database for Global Atmospheric Research
<b>GDAS</b>	: Global Data Assimilation System
<b>GFS</b>	: Global Forecast System
<b>GISS</b>	: Goddard Institute for Space Studies
<b>GOCART</b>	: Goddard Chemistry Aerosol Radiation and Transport
<b>GSI</b>	: Gridpoint Statistical Interpolation
<b>HTAP</b>	: Task Force on Hemispheric Transport of Air Pollution
<b>LBC</b>	: Lateral Boundary Conditions
<b>MODIS</b>	: The Moderate Resolution Imaging Spectroradiometer
<b>NCEP</b>	: National Centers for Environmental Prediction
<b>NMC</b>	: National Meteorological Center
<b>NOAA</b>	: National Ocean and Atmospheric Administration
<b>OC</b>	: Organic Carbon
<b>PBL</b>	: Planetary Boundary Layer
<b>PM</b>	: Particulate Matter
<b>PM<sub>10</sub></b>	: Particulate Matter less than or equal to 10 micrometers in diameter
<b>PM<sub>2.5</sub></b>	: Particles less than 2.5 micrometers in diameter
<b>RAQMS</b>	: Real-time Air Quality Modeling System
<b>RETRO</b>	: REanalysis of the TROpospheric
<b>RRTM</b>	: Rapid Radiative Transfer Model
<b>SST</b>	: Sea Surface Temperatures
<b>sd</b>	: Standard Deviation
<b>SO<sub>4</sub><sup>2-</sup></b>	: Sulfate Aerosol
<b>SOA</b>	: Secondary Organic Aerosol
<b>WF-ABBA</b>	: Wild Fire Automated Biomass Burning Algorithm
<b>WRF</b>	: Weather Research and Forecasting
<b>WRF-Chem</b>	: Weather Research and Forecasting model with Chemistry
<b>YSU</b>	: Yonsei University Scheme



## **SYMBOLS**

<b>km</b>	: Kilometers
<b>%</b>	: Percent
<b>μm</b>	: Micrometers
<b>μg</b>	: Microgram
<b>m<sup>3</sup></b>	: Cubic meter
<b>nm</b>	: Nanometers







## LIST OF FIGURES

	<u>Page</u>
<b>Figure 2.1</b> : Monthly PM <sub>10</sub> concentration of 2008 for Anatolian Peninsula (Kabatás et al, 2014).....	14
<b>Figure 2.2</b> : Boxplot of daily PM <sub>10</sub> concentration for April 2008. Red dots show daily mean PM <sub>10</sub> concentrations and the European Commission daily PM <sub>10</sub> standard (50 µg/m <sup>3</sup> ) is shown with red line (Kabatás et al, 2014).....	15
<b>Figure 2.3</b> : AOD obtained from (a) MOD04 (Terra) and (b) MYD04 (Aqua) aerosol product for Eastern Mediterranean basin analyzed for April 14, 2008, when the maximum PM <sub>10</sub> level was recorded (Kabatás et al, 2014).....	17
<b>Figure 2.4</b> : Boxplot of daily PM <sub>10</sub> concentration for April 2008 obtained from RAQMS (Kabatás et al, 2014).....	18
<b>Figure 2.5</b> : RAQMS output of dust concentrations at the surface for Eastern Mediterranean for the selected episode (a–h refers to April 11–18, 2008, respectively) (Kabatás et al, 2014) .....	19
<b>Figure 2.5 (Continued)</b> : RAQMS outputs of dust concentrations at surface for Eastern Mediterranean for the selected episode (a–h refers to April 11–18, 2008, respectively) (Kabatás et al, 2014).....	20
<b>Figure 2.6</b> : Synoptic conditions obtained from (a) RAQMS and (b) WRF for April 15, 2008, at 00:00 UTC. Both of the model results show mean sea-level pressure along with the wind vectors at the peak of the episode (Kabatás et al, 2014) .....	21
<b>Figure 2.7</b> : Path of CALIPSO and its total extinction output over Turkey on April 14, 2008. CALIPSO shows deeper mixing of the aerosol over Turkey starting from south to north part of the peninsula (Kabatás et al, 2014).....	22
<b>Figure 2.8</b> : RAQMS total extinction output over Turkey on April 14, 2008. It shows a shallow (and stronger) layer near the surface, where there is a very strong inversion over Turkey (Kabatás et al, 2014).....	23
<b>Figure 2.9</b> : Cross section of WRF potential temperature (K) along CALIPSO track at 00:00 UTC on April 15, 2008. The bold lines indicate the surface elevation (solid) and planetary boundary layer height (dashed) for the 30km WRF (black) and 2° × 2° RAQMS (red) models (Kabatás et al, 2014).....	24
<b>Figure 3.1</b> : WRF-Chem domains configured to cover Eastern Mediterranean (30km outer domain) and Anatolian Peninsula (10km inner domain) with topography map .....	26
<b>Figure 3.2</b> : Daily mean (red line) and boxplots of daily PM <sub>10</sub> concentration obtained from WRF-Chem EDGAR 30 km outer domain (a), WRF-Chem HTAP 30km outer domain (b), WRF-Chem HTAP 10km nested domain (c) and time series comparisons for daily PM <sub>10</sub> concentration (d). Red dashed lines show European Commission daily PM <sub>10</sub> standard (50 µg/m <sup>3</sup> ) .....	29
<b>Figure 3.2 (Continued)</b> : Daily mean (red line) and boxplots of daily PM <sub>10</sub> concentration obtained from WRF-Chem EDGAR 30 km outer domain (a),	

	WRF-Chem HTAP 30km outer domain (b), WRF-Chem HTAP 10km nested domain (c) and time series comparisons for daily PM <sub>10</sub> concentration (d). Red dashed lines show European Commission daily PM <sub>10</sub> standard (50 µg/m <sup>3</sup> ) .....	30
<b>Figure 3.3</b>	: Scatter plots for WRF-Chem HTAP outer (30 km horizontal resolution) (a), nested (10 km horizontal resolution) (b), and WRF-Chem EDGAR outer (30 km horizontal resolution) (c) runs, respectively.....	31
<b>Figure 3.4</b>	: Surface monthly PM <sub>10</sub> Concentration for April 2008 from HTAP (upper left panel), EDGAR (upper right panel) and difference between HTAP and EDGAR (lower left panel).....	33
<b>Figure 3.5</b>	: WRF-Chem HTAP daily output for outer and nested domain with ground observations (colored circles) for April 11-18, 2008 (a-h, respectively) episode. Surface wind vectors are shown in black arrows .....	34
<b>Figure 3.5 (continued)</b>	: WRF-Chem HTAP daily output for outer and nested domain with ground observations (colored circles) for April 11-18, 2008 (a-h, respectively) episode. Surface wind vectors are shown in black arrows.....	35
<b>Figure 3.6</b>	: Lateral boundary conditions obtained from RAQMS for south, north, west and east directions for WRF-Chem HTAP 10km nested domain .....	36
<b>Figure 3.7</b>	: Time series for ground observations, WRF-Chem HTAP outer (30KM) (red) and nested (10KM) (green) domains, and WRF-Chem EDGAR outer domain (30KM) (blue) (upper panel); and AOD speciation for the WRF-Chem HTAP nested (10KM) domain only (lower panel) for two different ground observation stations ((a) Denizli and (b) Kocaeli sites). Locations of both stations are shown on the map with a blue circle. HTAP_O refers to WRF-Chem HTAP outer domain, HTAP_N refers to WRF-Chem HTAP nested domain, and EDGAR_O refers to WRF-Chem EDGAR outer domain in the upper panel. Key for speciation is given for the lower panel with each color representing different species .....	37
<b>Figure 4.1</b>	: Time series comparisons for daily PM <sub>10</sub> concentration of WRF-Chem 30km_Assim and WRF-Chem 30km_Control runs to ground observations.....	44
<b>Figure 4.2</b>	: WRF-Chem 30km_Assim with RAQMS LBC (a), WRF-Chem 10km_NoAssim with 30km_Assim LBC (b), WRF-Chem 10km_Assim with 30km_Assim LBC (c) and time series comparisons for daily PM <sub>10</sub> concentration of three WRF-Chem runs and ground observations (d). Red dashed lines indicate the threshold of European Commission daily PM <sub>10</sub> standard (50 µg/m <sup>3</sup> ).....	45
<b>Figure 4.2 (continued)</b>	: WRF-Chem 30km_Assim with RAQMS LBC (a), WRF-Chem 10km_NoAssim with 30km_Assim LBC (b), WRF-Chem 10km_Assim with 30km_Assim LBC (c) and time series comparisons for daily PM <sub>10</sub> concentration of three WRF-Chem runs and ground observations (d). Red dashed lines indicate the threshold of European Commission daily PM <sub>10</sub> standard (50 µg/m <sup>3</sup> ).....	46
<b>Figure 4.2 (continued)</b>	: WRF-Chem 30km_Assim with RAQMS LBC (a), WRF-Chem 10km_NoAssim with 30km_Assim LBC (b), WRF-Chem 10km_Assim with 30km_Assim LBC (c) and time series comparisons for daily PM <sub>10</sub> concentration of three WRF-Chem runs and ground observations (d). Red dashed lines indicate the threshold of European Commission daily PM <sub>10</sub> standard (50 µg/m <sup>3</sup> ).....	47
<b>Figure 4.3</b>	: Scatter plots for WRF-Chem 30KM_Assim with RAQMS LBC (a), for	

	WRF-Chem 10km_NoAssim with 30km_Assim LBC (b), and WRF-Chem 10km_Assim with 30km_Assim LBC (c) runs, respectively.....	48
<b>Figure 4.4 :</b>	Timeseries of PM10 differences averaged over the sites for 30km runs (30km_Assim and 30km_Control) and 10km runs (10km_Assim and 10km_NoAssim).....	49
<b>Figure 4.5 :</b>	Difference of surface daily PM <sub>10</sub> concentration between 30km_Assim with RAQMS-LBC and 30km_Control with RAQMS-LBC (upper left panel), 10km_Assim with 30km_Assim-LBC and 10km_NoAssim with 30km_Assim-LBC (upper right panel), 30km_Assim interpolation over 10 km grid and 10km_NoAssim with 30km_Assim-LBC (lower left panel) for April 1, 2008.....	51
<b>Figure 4.6 :</b>	Difference of surface daily PM <sub>10</sub> concentration between 30km_Assim with RAQMS-LBC and 30km_Control with RAQMS-LBC (upper left panel), 10km_Assim with 30km_Assim-LBC and 10km_NoAssim with 30km_Assim-LBC (upper right panel), 30km_Assim interpolation over 10 km grid and 10km_NoAssim with 30km_Assim-LBC (lower left panel) for April 13, 2008.....	52





# QUANTIFICATION OF SAHARAN DUST INFLUENCES ON EASTERN MEDITERRANEAN AIR QUALITY VIA ATMOSPHERIC MODELING

## SUMMARY

According to the World Health Organization (WHO), air pollution is a major environmental risk to health for urban population in both developed and developing countries and particulate matter (PM) affects more people than any other pollutant. Particles less than 10 micrometers are called PM<sub>10</sub>, and fine inhalable particles, with diameters that are generally 2.5 micrometers and smaller are called PM<sub>2.5</sub>. Among sources of particulate matter, mineral dust is one of main contributors of natural aerosol emissions on a global basis contributing around 22% and Sahara is the main contributor to the global dust budget.

Epidemiologic studies show that there is a clear link between the dust and adverse health problems such as respiratory diseases, cardiovascular diseases, pulmonary and systemic inflammation. Aside from its effects on human health, transported dust also affects ecosystem by transporting a variety of chemicals and microbial agents (such as bacteria, fungi, and viruses) from source area to other regions. Dust can have both physical and chemical impacts on plants. For instance, it may serve essential nutrients for plant growth such as iron, and phosphorus, yet microbial agents that can be carried thousands of miles in the atmosphere, might be pathogenic to the plants causing rust and other plant disorders. Mineral dust also has a direct role on the radiation budget and regional climate and has a semi-direct effect on cloud cover.

Air pollution is one of the major environmental problems in the Mediterranean basin since the limit values of the pollutants are often exceeded. Saharan dust intrusions into the Mediterranean Basin affects 427 million people living in the 21 countries surrounding it. Considering its location, Turkey is downwind of Europe and on the crossroad of long-range dust transport and local emissions, meaning high amount of population living in Turkey are exposed to high PM concentration. The contribution of Saharan dust on PM concentration is still unclear in the Eastern Mediterranean, especially in Western Turkey, where significant industrial sources and metropolitan areas (i.e., Istanbul, Ankara and Izmir) are located. This study aims to quantify the contribution of Saharan dust on high levels of PM<sub>10</sub> that was measured in April 2008 via ground observations, satellite data and atmospheric models.

Ground observations that is used in this study were obtained from the Turkish Ministry of Environment and Urbanization for the year 2008. Data analysis of the ground observations showed April 2008 had significantly higher values compared to other warm season months with a monthly mean of  $\sim 87 \mu\text{g}/\text{m}^3$ , where the annual mean PM<sub>10</sub> concentration of 2008 was found to be  $\sim 82 \mu\text{g}/\text{m}^3$ . It is known from the literature that the transition seasons are usually associated with dust transport from Sahara Desert in the Mediterranean Basin. One method to understand the complex nature of aerosol formation is via atmospheric models. In the real atmosphere, both meteorological factors (such as wind speed and direction, turbulence, radiation, clouds, and

precipitation) and chemical processes (such as deposition, and transformations) play important roles on air quality and they are coupled. The interaction of meteorological factors on air quality and atmospheric transport of pollutants is well accepted and they can no longer be conducted separate from each other.

Within this scope, we utilized the Real-time Air Quality Modeling System (RAQMS), which is an online global aerosol and chemistry assimilation and forecasting system that was run at 2x2 degrees horizontal resolution, to explore the possible effects of Saharan dust on high levels of PM<sub>10</sub> measured in Turkey in April 2008. The RAQMS chemical scheme was developed at NASA Langley Research Center, and the aerosol module incorporates the Goddard Ozone Chemistry Aerosol Radiation and Transport (GOCART) mechanism. RAQMS simulates sulfate (SO<sub>4</sub><sup>-2</sup>), dust, black carbon (BC), organic carbon (OC) and sea-salt aerosols that are known as the major tropospheric aerosol components. The model results showed that the high levels of PM<sub>10</sub> observed for April 2008 are related to a Saharan dust outbreak. Due to its coarse resolution (2x2 degree) and inability to resolve local topographic variations, RAQMS was found to over predict the surface PM<sub>10</sub> concentration over Turkey by up to a factor of 5.

Continuation of the RAQMS research, the higher resolution (30km outer and 10 km nested domains) online-coupled regional Weather Research and Forecasting/Chemistry model (WRF-Chem), a version of the non-hydrostatic model WRF, was utilized. In order to include dust transport from North Africa through lateral boundary conditions (LBC), 6 hourly RAQMS 2x2 degree global analyses was used for 30km run. For background aerosol, GOCART simple aerosol module within the WRF-chem is used. For anthropogenic emissions, two different emission inventories are used, 1x1 degree spatial resolution RETRO (REanalysis of the TROpospheric)/EDGAR (Emission Database for Global Atmospheric Research) and 0.1x0.1 degree spatial resolution EDGAR HTAP (EDGAR: Emission Database for Global Atmospheric Research of the Joint Research Centre, JRC, in cooperation with the Task Force on Hemispheric Transport of Air Pollution (TF HTAP)), to investigate the spatial and temporal distribution of Saharan mineral dust transport over the Eastern Mediterranean (-10.0° W–60.0° E, 30.0° S–70.0° N) for the same time period. The WRF-Chem results were found to be significantly improved compared to the previous RAQMS study. WRF-Chem HTAP outer and nest domain were able to more accurately resolve local emissions that influence the ground observations than the WRF-Chem EDGAR run. The comparison between ground observations to the WRF-Chem HTAP model predictions indicated that the model was able to simulate dust transport patterns and the concentrations in a successful way.

Followed by WRF-Chem study, we investigated the impacts of satellite data assimilation through assimilation of the Moderate Resolution Imaging Spectroradiometer (MODIS (collection 6)) total aerosol optical depth (AOD) retrieval products (at 550 nm wavelength) from Terra satellite within the National Centers for Environmental Prediction (NCEP) Gridpoint Statistical Interpolation (GSI) three-dimensional variational (3DVAR) data assimilation system by using the same configuration that was used for WRF-Chem experiment. The simple GOCART aerosol module that is implemented in WRF-Chem modeling system was used to assimilate 3-D mass concentration of 14 aerosol variables within the model including hydrophilic and hydrophobic components of atmospheric aerosols such as sea salt, dust, organic carbon (OC), black carbon (BC), and sulfate. Two nested domain (10km) experiments were designed to evaluate the impact of AOD DA on predicted PM<sub>10</sub> concentrations over Turkey by using the same LBC obtained from 30km domain. Both 10km

experiments used the same physical and chemistry options, but one experiment did not employ DA (10km\_NoAssim) and the other employed 3DVAR DA (10km\_Assim) that updated the 14 aerosol profiles of GOCART aerosol module.

When we compared average model outputs with the observation means, we found that both 10km (10km\_NoAssim and 10km\_Assim) analyses show higher level of variability in the PM<sub>10</sub> values compared to 30km\_Assim run. Among the 10km runs though, 10km\_NoAssim run showed higher level of variability than the 10km\_Assim run. So, assimilation lowers the variability especially for the days when high dust event occurred. Daily comparison of surface PM<sub>10</sub> measurements to model outputs showed that higher resolution domains (10km\_Assim and 10km\_NoAssim) overestimate daily surface mean PM<sub>10</sub> values more than lower resolution domain (30km\_Assim) does for the high dust event days.

In order to explore differences in aerosol AOD assimilation between the high resolution domain (10km) and the 30km runs, we have interpolated 30km\_Assim run to the 10km grid. Based on the PM<sub>10</sub> differences averaged over the surface sites for 30km runs and 10km runs, April 1 and April 13, 2008 are chosen in order to further explore the consistency of the aerosol assimilation at 30 and 10km resolution.

On April 1<sup>st</sup> low dust event day, over the central Anatolia, within the higher resolution domain, the predictions tend to increase due to the 30km\_Assim domain influence through the LBC. This increase in higher resolution domain is corrected by employing assimilation by moving the predictions towards the observations. For the eastern part of the domain on April 1, the impacts of assimilation are similar for the 30 and 10km experiments indicating LBC impact is small.

On April 13<sup>th</sup>, when dust is the dominant aerosol, 30km\_Assim run shows higher PM<sub>10</sub> concentrations than the 30km\_Control run. The local emissions, as well as LBC from the 30km domain, add additional enhancements to 10km domain resulting an overestimation in 10km\_NoAssim domain (due the large negative differences between 30km\_Assim and 10km\_NoAssim). Relatively small differences between the two 10km domains again shows that assimilation tends to move the 10km predictions closer to the surface observations during this high dust event.

This demonstrates that, in our study, although the nested domains tend to over predict the PM<sub>10</sub> concentrations comparing to the 30km domain, assimilation of satellite AOD retrievals moves the model forecasts towards the surface observations within the 10km resolution domains especially on high dust event days.





## SAHRA TOZUNUN DOĞU AKDENİZ HAVA KALİTESİ ÜZERİNDEKİ ETKİLERİNİN ATMOSFER MODELİYLE BELİRLENMESİ

### ÖZET

Dünya Sağlık Örgütü (WHO)'ne göre hava kirliliği, Dünya'daki tüm canlı türlerini etkileyen ve insan sağlığı üzerinde ciddi etkileri olan çevresel bir risktir. Amerika Birleşik Devletleri Çevre Koruma Ajansı (USA EPA)'nın altı yaygın kirleticisinden bir tanesi olan Partikül Madde (PM), hava içinde uzun süre askıda kalabilen, katı ve sıvı halde bulunan maddelerdir. PM boyut olarak aerodinamik çapı 0.1  $\mu\text{m}$ 'den küçük olan çok (ultra) ince partiküller, 0.1  $\mu\text{m}$  ile 2.5  $\mu\text{m}$  (2.5  $\mu\text{m}$  dahil) arasında olan ince partiküller, 2.5  $\mu\text{m}$  ile 10  $\mu\text{m}$  arasında olan kaba (course) partiküller ve 10  $\mu\text{m}$ 'den büyük kaba partiküller olarak sınıflandırılmaktadır. Partikül madde insan kaynaklı olabildiği gibi doğal kaynaklı da olabilir. Doğal partikül madde kaynaklarının %22'lik bölümünü mineral çöl tozu oluşturmaktadır ve Sahra Çölü bilinen en büyük çöl tozu kaynağıdır. Partikül madde (PM) diğer tüm hava kirleticilerine oranla insan sağlığı üzerinde en fazla negatif etkisi olan kirleticidir.

Son yıllarda yapılan epidemiolojik çalışmalar hava kirliliğinin insan sağlığı üzerindeki ciddi etkilerini açıkça ortaya koymaktadır. Dolaşım yolları hastalıkları, akciğer iltihabı, sistemik inflamasyon gibi hastalıklar bu etkilerden birkaçına örnektir. Bunu yanı sıra özellikle çöl tozlarının astım hastalarının kriz sıklığını artırdığı, dünyada çöl tozlarından etkilenen bölgelerde astım hastalığı oranının fazla olduğu literatürde birçok çalışmayla ortaya konmuştur. İnsan sağlığı üzerindeki olumsuz etkilerinin yanı sıra toz taşınımının ekosistemler üzerinde de etkisi vardır. Örneğin; rüzgârlar vasıtasıyla çöllerden kalkarak atmosfere karışan toz partikülleri atmosferik taşınım ile çok uzak bölgelere kadar ulaşırken aynı zamanda kaynak bölgeye ait kimyasal ve mikrobiyal ajanları (bakteri, fungus, virüs) da beraberlerinde getirirler. Çöl tozları içerisinde barındırdığı demir, alüminyum gibi mineraller bitkilerin gelişimini hızlandırırken aynı zamanda mikrobiyal ajanlar sebebiyle bitkilerde çeşitli hastalık ve bozulmalara neden olmaktadır. Mineral tozun iklim sistemi üzerindeki etkileri de literatürde büyük yer kaplamaktadır. Tozun iklim sistemi üzerinde güneş ve yer kaynaklı radyasyonunu yansıtma ve absorplama özellikleri ile bulut albedosu ve yağış özelliklerini değiştirmek gibi etkileri vardır.

Akdeniz Havzası'nda hava kirliliği sınır değerleri çoğunlukla aşıldığı için bu bölgede yaşayan toplam 427 milyon kişi hava kirliliğinden negatif bir şekilde etkilenmektedir. Bu bölge için yapılan çalışmalarda yüksek partikül madde konsantrasyonu ile özellikle bahar aylarında olan Sahra Çölü kaynaklı toz taşınımı arasında bir ilişki olduğu bulunmuştur. Sahra Çölü'nden taşınan tozun yanı sıra, Türkiye bulunduğu coğrafya nedeniyle gerek Avrupa'dan gelen antropojenik kaynaklı kirleticilere, gerekse lokal kaynaklı kirleticilere maruz kalmaktadır. Her ne kadar yüksek partikül madde konsantrasyonu ile Sahra Çölü tozu arasında bir bağlantı olduğu bilinse de, Sahra tozunun özellikle endüstriyel aktivitenin yoğun olduğu metropolitan alanlardaki kirliliğe olan katkısının ne kadar olduğu belirsizliği de hala sürmektedir. Bu çalışma

Sahra tozunun yüksek partikül madde konsantrasyonuna olan katkısının yer gözlemleri, uydu verileri ve fiziksel modeller kullanılarak belirlenmesini amaçlanmaktadır.

Çalışmada kullanılan ve 2008 senesine ait olan PM<sub>10</sub> yer gözlemleri T.C. Çevre ve Şehircilik Bakanlığı'ndan alınmıştır. Yapılan veri analizine göre 2008 yılı Nisan ayına ait veriler diğer ılıman aylara kıyasla daha yüksek PM<sub>10</sub> konsantrasyon değerlerine sahiptir. 2008 yılına ait ortalama PM<sub>10</sub> konsantrasyonu ~82 µg/m<sup>3</sup> olarak hesaplanmışken, Nisan ayı ortalaması ~87 µg/m<sup>3</sup> olarak bulunmuştur. Nisan ayı içindeki en yüksek günlük PM<sub>10</sub> konsantrasyon ortalaması 14 Nisan 2008 tarihinde ~170 µg/m<sup>3</sup> olarak hesaplanmıştır. Bu değer sadece Nisan ayı içinde değil, 2008 yılı içinde ölçülen en yüksek konsantrasyon değeridir. Nisan ayı günlük PM<sub>10</sub> konsantrasyon değerleri Avrupa Komisyonu'nun belirlediği günlük PM<sub>10</sub> konsantrasyon sınır değeri olan 50 µg/m<sup>3</sup>'den daha yüksek seviyelerde hesaplanmıştır.

Aerosollerin kompleks yapısını anlamak için atmosferik modeller kullanılmaktadır. Gerçek atmosferde rüzgar hızı ve yönü, radyasyon, bulut oluşumu, yağış oluşumu ve türbülans gibi meteorolojik faktörler hava kalitesi üzerinde önemli etkiye sahiptir ve bu etkiler birbirlerinden ayrı düşünülemez. Örneğin; atmosfer kimyası meteorolojiyi Dünya'nın enerji bütçesini değiştirerek doğrudan veya bulut yoğunlaşma çekirdeği gibi davranarak dolaylı olarak etkileyebilir. Bulutlar, rüzgarlar ve yağış gibi meteorolojik parametreler ise atmosferdeki kimyasal madde dönüşümü, taşınımı ve depozisyonu gibi prosesler üzerinde etkilidir.

Bu çalışmada, Sahra tozunun Türkiye üzerindeki etkilerini görebilmek ve yer gözlemlerinden hesaplanan yüksek PM<sub>10</sub> konsantrasyonuna katkısını anlamak amacıyla ilk aşamada RAQMS (Real-time Air Quality Modeling System) modeli çalıştırılmıştır. RAQMS 2x2 derece yatay çözünürlüğe sahip, online, yani atmosferik prosesler ve kimyasal proseslerin birlikte çalıştırıldığı, global bir aerosol asimilasyon ve tahmin modelidir. RAQMS kimyasal şeması NASA Langley Araştırma Merkezi'nde geliştirilmiştir, aerosol modülü olarak Goddard Ozone Chemistry Aerosol Radiation and Transport (GOCART) kullanılmıştır. RAMQS modeli sülfat (SO<sub>4</sub><sup>-2</sup>), toz, karbon (BC), organik carbon (OC) ve deniz tuzu aerosollerini simule eder (hidrofilik ve hidrofobik bileşenler de dahildir.). RAQMS model sonuçları Nisan 2008'de gözlemlenen yüksek PM<sub>10</sub> konsantrasyonunun Sahra tozuyla ilişkili olduğunu göstermiştir. Model tahmini yer gözlemleriyle benzer sonuçlar göstermiştir. Ancak RAQMS modelinin düşük çözünürlüklü olması ve lokal topografik etkileri tam olarak çözememiş olmasından dolayı tahmin değerleri gözlem değerlerinden yaklaşık 5 kat daha fazla çıkmıştır.

Bu çalışmanın ikinci aşamasında daha yüksek çözünürlüklü (30km ana domain ve 10 km nest domain), online, bölgesel WRF-Chem (Weather Research and Forecasting/Chemistry) modeli kullanılmıştır. WRF-Chem, hidrostatik olmayan WRF modelinin kimya içeren versiyonudur. WRF-Chem atmosferdeki küçük miktardaki gaz karışımları ve partikül maddeleri meteorolojik alanlarla birlikte eş zamanlı olarak simule eder. Modelin meteorolojik bileşenleri ile hava kalitesi bileşenleri aynı grid içinde çalışır ve aynı taşınım şemasına sahiptir. WRF-Chem 30km çözünürlüklü ana domain batıda Avrupa, doğuda Hazar Denizi, kuzeyde İskandinavya ve güneyde Sahra Çölü ile sınırlıdır (-10.0° Batı boylamı–60.0° Doğu boylamı, 30.0° Güney paraleli–70.0° Kuzey paraleli). Doğu-batı yönünde 190 grid, kuzey güney yönünde 158 grid noktasına, düşeyde 35 seviyeye sahiptir. 10km çözünürlüklü nest domain ise Türkiye'yi içine alacak şekilde doğu-batı yönünde 262 grid, kuzey güney yönünde 181 grid noktasına, düşeyde de 35 seviyeye sahiptir. Kuzey Afrika'dan taşınan tozu model

alanı içine katabilmek amacıyla 2x2 derecelik RAQMS global model kullanılarak yanal sınır koşulları (LBC) oluşturulmuştur. Bu çalışmada iki farklı emisyon envanteri kullanılarak yüksek toz taşınımının olduğu günlerde lokal emisyonların etkisi belirlenmeye çalışılmıştır. Bu envanterlerden ilki 1x1 derece yersel çözünürlüğe sahip RETRO (REanalysis of the TROpospheric)/EDGAR (Emission Database for Global Atmospheric Research) emisyon envanteri, diğeri de 0.1×0.1 derece yersel çözünürlüğe sahip EDGAR HTAP (EDGAR: Emission Database for Global Atmospheric Research of the Joint Research Centre, JRC, Task Force on Hemispheric Transport of Air Pollution (TF HTAP)) emisyon envanteridir. EDGAR emisyon envanteri kullanılarak çalıştırılan model sonuçları, özellikle antropojenik kirleticiler lokal bağlamda çözümlenemediği için, HTAP emisyon envanteri kullanılarak oluşturulan model sonuçlarına kıyasla daha düşük değerler vermiştir. Öte yandan daha yüksek çözünürlüğe sahip emisyon envanteri olan HTAP lokal emisyonları hesaplamalara katabilmiş ve tozun etkisinin az olduğu günlerde model sonuçlarını gözlemlere yaklaştırmıştır. WRF-Chem model sonuçları RAQMS model sonuçlarına kıyasla yer gözlemleri ve model sonuçları arasındaki hata/yanlılık (bias) değerlerini azaltarak sonuçların geliştirilmesini sağlamıştır.

Çalışmanın bir sonraki bölümünde Terra uydusu üzerinde bulunan MODIS (collection 6) (Moderate Resolution Imaging Spectroradiometer) sensörüne ait Aerosol Optik Kalınlık (AOD) (550 nm dalgaboyuna ait) değerleri algoritması kullanılarak WRF-Chem modeli içinde bulunan GOCART aerosol modülüne ait AOD verileri asimile edilmiştir. Data asimilasyonu için Amerika Birleşik Devletleri Milli Çevresel Tahmin Merkezi (U.S. National Centers for Environmental Prediction (NCEP)) tarafından geliştirilmiş Gridpoint Statistical Interpolation (GSI) üç boyutlu değişken (3DVAR) data asimilasyon sistemi kullanılmıştır. WRF-Chem modelini koşturmak için kullanılan konfigürasyonun aynısı GSI veri asimilasyon sistemi kullanılarak koşturulan WRF-Chem deneyi için de kullanılmıştır. WRF-Chem model sistemi kapsamında bulunan GOCART aerosol modülüne ait 14 aerosol tipinin kütle konsantrasyonu 3 boyutlu olarak asimile edilmiştir. 30km çözünürlüklü ana domainin Sınır Tabaka koşulları (LBC); daha önceki deneyde olduğu gibi yine 2 derece yatay çözünürlüğe sahip global model olan RAQMS model kullanılarak oluşturulmuştur. Daha sonra 30km çözünürlüğe sahip model kullanılarak 10km nest domain için gerekli olan LBC belirlenmiştir. 30km\_Assim sınır koşulları kullanılarak koşturulan 10km çözünürlüğe sahip domain için iki farklı analiz yapılmıştır. Bunlardan ilki 10km domain içine veri asimilasyon yöntemi uygulanarak (10km\_Assim), diğeri de asimilasyon yöntemi uygulanmayarak (10km\_NoAssim) yapılmıştır. Model sonuçları yer gözlemleriyle karşılaştırıldığında 10km\_Assim ve 10km\_NoAssim model sonuçları 30km\_Assim model sonuçlarına göre daha yüksek çıkmıştır. 10km model sonuçları arasında ise 10km\_NoAssim sonuçları 10km\_Assim'e oranla daha yüksek değerler gösterme eğilimindedir.

Aerosol data asimilasyon tekniğinin farklı çözünürlüğe sahip domainler (30km ve 10km) üzerindeki etkisini anlamak amacıyla interpolasyon yöntemi uygulanarak 30km\_Assim model gridleri 10km grid için hesaplanmıştır. Türkiye geneli için model alanı içinde bulunan yer gözlem istasyon lokasyonlarındaki model tahminlerinin günlük ortalamaları hesaplanmış ve 30km (30km\_Assim ve 30km\_Control) ve 10km (10km\_Assim ve 10km\_NoAssim) domainler arasındaki farklar kullanılarak asimilasyonun etkileri daha detaylı incelenmiştir. Bu analiz için düşük toz konsantrasyonunun olduğu 1 Nisan günü ile yüksek toz konsantrasyonunun olduğu 13 Nisan tarihleri seçilmiştir.

1 Nisan'da 30km model (30km\_Assim ve 30km\_Control) sonuç farkları kullanılarak hazırlanan yer haritalarına göre 30km\_Assim daha düşük tahmin değerleri göstermektedir (İç Anadolu ve çevresi için). 10km domainde ise asimilasyon tekniği uygulanmadan çalıştırılan model sonucu (10km\_NoAssim) asimilasyon uygulanarak oluşturulan modele kıyasla daha yüksek değerler göstermiştir. Yani 10km domain içerisinde asimilasyon model sonuçlarını yer gözlemlerine yaklaştırma eğilimindedir. Model alanının doğu sınırı için gerek 30km gerekse 10km model sonuçları benzer değerler vermiştir. 10km domain içinde asimilasyon hesaplamaları düzelterek 30km domainden gelen yüksek konsantrasyon değerlerini yer gözlemlerine yaklaştırmıştır. Bunun sonucu olarak da model alanının doğusu için model farkları birbirlerine yakın çıkmıştır.

Yüksek toz taşınımının olduğu 13 Nisan günü, 30km çözünürlüğe sahip model sonuçları arasından asimilasyon uygulanan deney kontrol deneyine kıyasla daha yüksek değerler vermiştir. Bu yüksek lokal emisyon değerleri 30km\_Assim LBC vasıtasıyla 10km domain içindeki tahmin değerlerinin daha da artmasına sebep olmuştur. Fakat 10km domainlerin arasındaki farklar asimilasyon uygulanarak çalıştırılan modelin PM<sub>10</sub> tahminlerini düşürerek tahminlerin yer gözlemlerine yaklaşmasını sağladığını göstermiştir.

Her iki gün için de 10km çözünürlüğe sahip domain tahmin sonuçları 30km çözünürlüğe sahip domain tahmin sonuçlarından yüksek çıkmıştır. Bunun sebeplerinden biri 30km\_Assim domaininin 10km domaine yanal sınırlar vasıtasıyla olan etkisidir. Düşük çözünürlüklü domainden daha yüksek çözünürlüklü domaine geçiş sırasında da emisyon alanlarının daha detaylı çözümlenmesinden dolayı emisyon değerleri artmaktadır. Fakat her iki gün için de asimilasyon yüksek çözünürlükteki domain içinde bu etkiyi düzeltme ve tahminleri yer gözlemlerine yaklaştırma eğilimindedir. Bu eğilim yüksek toz taşınımının olduğu günlerde düşük toz taşınımının olduğu günlere kıyasla daha fazladır.

## **1. INTRODUCTION**

### **1.1 Background Information**

Fine solid particles or liquid droplets suspended in the atmosphere are defined as aerosols (Prospero et al, 1983; Hinds, 1999). Particulate matter (PM) is an end product of complex chemical and physical processes, and they can be classified based on their source characteristics indicated by aerosol composition. Aerosol types can be defined as natural (e.g. sea-salt, windblown mineral dust, biogenic materials, natural gas-to-particle conversion products) and anthropogenic (e.g. soot, smoke, road dust, products from the conversion of anthropogenic gases) on the basis of sources. They can also be classified as tropospheric and stratospheric, which impacts their atmospheric residence time, which can vary from days to weeks. Particle production occurs by either being directly emitted into the atmosphere (primary) or indirectly (secondary) derived from the subsequent reactions of emitted gases. Chemical processes and physical modifications changes size distribution and chemical composition of the particle (Prospero et al, 1983).

Among sources of particulate matter, sea-salt and mineral dust are main contributors of natural aerosol emission contributing around 90% (68% for sea salt aerosol and 22% for natural dust) (Bellouin and Haywood, 2015). Sahara considered to be the largest dust source on Earth with estimation of annual dust emission ranges between 130 to 760 Tg yr<sup>-1</sup> while global dust emission estimates range between 1000 to 3000 Tg yr<sup>-1</sup> (Engelstaedter et al, 2006). In a study conducted by Tanaka and Chiba, a comparison is made between nine potential dust source regions including North and South Africa, the Arabian Peninsula, Central Asia, eastern and western China, North and South America, and Australia to investigate the contribution of those dust sources to the global dust budget (2006).

A six-year simulation (1990 to 1995) done by MASINGAR (Model of Aerosol Species IN the Global AtmospHeRe) model showed that North Africa (the Sahara Desert) is the greatest contributor to the global dust budget accounting for 58% of the total global dust emission (Tanaka and Chiba, 2006). Sahara produces around  $2 \times 10^8$  tons of

aerosols annually, and they get transported towards the Atlantic Ocean, to the Mediterranean Sea and as well Southern Europe (Mitsakou et al, 2008; Kallos et al, 2007; Querol et al, 2004). In the Mediterranean it has been shown that high levels of PM<sub>10</sub> is correlated with the African dust intrusion (Querol et al, 2009). One of the recent studies indicated that African dust contribution to PM<sub>10</sub> concentration decreases exponentially with latitude (from south to north) and increases longitudinally from 25°E eastwards (Pey et al, 2013).

## **1.2 Hypothesis**

Saharan desert is known to be the largest natural dust source in the world. Literature reviews suggest that dust transport from North Africa to Mediterranean Basin occurs in the transition seasons. Under certain conditions, such as cyclones, dust plumes reach as far as Anatolian Peninsula (Kubilay et al, 2000). Contributions of natural sources to high PM values in the eastern Mediterranean is studied by Koçak et al. (2007) and it is found that 40% of the PM<sub>10</sub> exceedances originated as consequence of mineral dust particles from the Saharan Desert.

One of the areas with largest aerosol optical depth (AOD)s (up to about 1.0 or 0.6 according to TOMS and MODIS, respectively) is the Anatolian plateau, which is mainly affected by desert dust (Hatzianastassiou et al, 2009). Therefore, it is suspected that Saharan dust has a major effect on Eastern Mediterranean air quality.

## **1.3 Research Questions**

The overall research question is to understand and quantify the effect of Saharan dust in the Eastern Mediterranean. Specifically, the research questions to be addressed in this study are:

- 1) Is there any quantitative impact of Saharan dust on Eastern Mediterranean air quality, especially in Anatolian Peninsula?
- 2) What is the effect of other aerosols on Eastern Mediterranean's, especially Anatolian peninsula's, air quality during a dust outbreak?
- 3) What is the impact of emission inventories in terms of identifying local emissions during the dust outbreak in order to improve the results?
- 4) What is the impact of model resolution on dust predictions?

5) How does assimilation of satellite data impact dust predictions?

#### 1.4 Literature Study

When dust is transported from the source area to other regions, a variety of chemicals and microbial agents (such as bacteria, fungi, and viruses) are also transported affecting ecosystem and human health (Griffin, 2007; Grishkan et al, 2012). Epidemiologic studies show that there is a clear link between the particulate matter (PM) and adverse health problems such as respiratory (i.e., asthma) disease, cardiovascular diseases (i.e., accelerated atherosclerosis, altered cardiac), pulmonary and systemic inflammation, lung cancer and even death (Pope III. et al, 2004; Atkinson et al, 2001; Peters et al, 2000). Moreover, it is stated that there is a less well-understood, sporadic linkage between PM and cerebrovascular disease (such as stroke). A  $10\text{-}\mu\text{g}/\text{m}^3$  increase in  $\text{PM}_{10}$  results in a 1.03% increase for hospital admission for ischemic stroke, while a  $10\text{ }\mu\text{g}/\text{m}^3$  increase in ambient  $\text{PM}_{2.5}$  increases the risk of hospitalization for cerebrovascular events by 0.8% (Anderson et al, 2012).

Association between short-term exposure to major air pollutants (ozone, carbon monoxide, nitrogen dioxide, sulfur dioxide, and  $\text{PM}_{10}$  and  $\text{PM}_{2.5}$ ) is assessed and all of them except ozone is found to be significantly associated with a near-term increase in myocardial infarction risk (Mustafic et al, 2012). Air pollution is also listed as one of the trigger factors of myocardial infarction. A change of  $30\text{ }\mu\text{g}/\text{m}^3$  in the daily mean  $\text{PM}_{10}$  would result a change in myocardial infarction incidence by 4.8% while a change of  $10\text{ }\mu\text{g}/\text{m}^3$  would be associated with a 1.6% change. Even  $1\text{ }\mu\text{g}/\text{m}^3$  change in  $\text{PM}_{10}$  would change incidence by 0.16% (Nawrot et al, 2011).

In their study, Tobias et al. (2011) showed a  $10\text{ }\mu\text{g}/\text{m}^3$  increase in coarse particulate matter ( $\text{PM}_{2.5-10}$ ) during Saharan dust outbreaks also increases total mortality by 2.8% compared to 0.6% increase during non-dust days in Madrid. Sajani et al. (2011) stated that for people over 75 years old, the respiratory death rates increase by 22% on the days with Sahara dust. Even though literature shows an association of PM to adverse health problems, further explorations such as chemical characterization and toxicity of the particle are needed to understand impact of Sahara dust outbreak on human health, especially in Mediterranean Basin (Karanasiou et. al, 2012). In their study, Vodonos et al. (2014) stated that in the Eastern Mediterranean, high  $\text{PM}_{10}$  concentration due to dust transport exacerbates the rate of hospitalization for chronic obstructive pulmonary

disease (COPD) mainly for elderly people and women. Mallone (2011) showed that during Saharan dust episodes, cardiac and circulatory mortality rate increases due to the toxicological and inflammatory effects of particles originating from desert sources.

Mineral dust also affects other important processes in the Earth's system such as marine ecosystems. Increases in transatlantic dust transport decreases the vitality of Caribbean coral reefs (Shinn et al, 2000). Long-range dust transport from North Africa causes an increase in the numbers of viable fungal spores and other microorganisms by factor 2 to 3 where they settle in the Caribbean marine environment (Griffin et al, 2001). Saharan dust has an important impact on nutrient cycles, soil formation and sediment cycles in both oceanic and terrestrial ecosystems not only in the source area but also around the world due to its long range transport across the Atlantic Ocean, the Mediterranean Sea and the Red Sea, to the Americas, Europe and the Middle East (Goudie and Middleton, 2001). The dust observed during the wet seasons of Amazon Basin is believed to be of Saharan origin, which is delivered by storm systems with horizontal scales of thousands of kilometers that associated with major pulses of rainfall (Swap et al, 1992). Saharan dust decreases the solubility of trace metals such as Cu, Zn and Pb, thus increases the pH of rainwater (Guerzoni et al, 1997).

Particulate matter influences climate system due to either direct effect through scattering and absorbing the shortwave solar radiation or indirect effects by acting as cloud condensation nuclei (CCN). Studies show that Saharan dust particles commonly act as CCN, modifying the cloud development and precipitation formation. (Twohy et al, 2009; Levin et al, 2005). In their study Smoydzin et al. (2012), showed that high concentration of mineral dust can enhance ice crystal formation, however it does not make a significant change in total precipitation amount, except when there is an orographic ascent. This causes glaciation of the clouds and increasing local rainfall amount. It is predicted that annual average contribution of mineral dust to cloud condensation nuclei is around 40% and to cloud droplet number concentration is around 23.8% (Karydis et al, 2011).

In their study Perlwitz and Miller (2010) reexamined the link between aerosols and clouds that depends on changes in specific humidity induced by aerosol heating using Goddard Institute for Space Studies (GISS) climate model. Although in some areas, their model agreed with the conventional description of the semi-direct effect of reducing the low cloud cover due to aerosol heating, overall net effect is an



enhancement of low cloud cover with increasing soil dust particle absorption for all seasons except for winter in Northern Hemisphere (Huang et al, 2014).

Change in the amount of dust load is shown to affect surface radiative heat flux and sea surface temperatures (SST), as well (Foltz and McPhaden 2008). Mineral dust has a direct role on radiation budget and regional climate while having a semi-direct effect on cloud cover by reducing it. After a severe dust storm originated in the Gobi desert, it is found that dust radiative forcing accounts for 42% total aerosol forcing at the surface (Han et al, 2012). For the same dust event, it is stated that direct radiative forcing by dust aerosols decreases ground temperature and wind speed in dust deflation region and the dust radiative forcing causes a surface cooling of  $-0.6\text{ }^{\circ}\text{C}$  to  $-1.0\text{ }^{\circ}\text{C}$  (Han et al, 2013).

In their study, Zhao et al. (2011) investigated radiative forcing of dust and its impact on precipitation over the West Africa monsoon (WAM) region and results show that dust modified the surface energy budget and increased atmospheric stability in the daytime leading to a reduction of late afternoon precipitation. Chemical and physical analyses also show that mineral dust aerosols act like ice nuclei seed particles on which cirrus ice crystals form by sublimating (Cziczo et al, 2013).

#### **1.4.1 Mediterranean region facts**

Communication from the Commission to the Council and the European Parliament Establishing an Environment Strategy for the Mediterranean (2006) defines the Mediterranean as the largest European sea. It is shared by 427 million people living in the 21 countries and territories surrounding it.

Pollution is a major problem in the area having a direct effect on neighboring countries and natural systems such as air, soil, water and biodiversity since pollutant air quality limits are often exceeded. The Environmental Performance Index (EPI) (Hsu et al, 2014) scores a country's performance on high-priority environmental issues including air, water and soil pollution with 100 being considered the best performance.

The mean overall score for 178 countries around the world is 50.68. European countries score 68.83 and countries within the Mediterranean Basin score 60.84 out of 100. Although the Mediterranean Basin score is higher than world average, it is still lower than the European countries. The Mediterranean has a fragile environment and for several countries, ongoing deterioration costs billions of Euros annually. This is mainly

due to its location being a crossroad of air masses, where anthropogenic emissions, mainly from Europe, Balkans and the Black Sea, meet with natural emissions from Northern Africa.

In addition to regional transport of natural and anthropogenic pollution sources, local sources also have significant effects on air pollution levels in the area (Kanakidou et al, 2011). Studies conducted to identify the major factors controlling the variability of the background aerosols in Mediterranean region indicate that PM in the Eastern Mediterranean region specified by higher levels of crustal material and sulphate than Western Mediterranean region (Querol et al, 2009). Atmospheric dynamics and emission sources of the Mediterranean Basin have an absolute impact on complex nature of aerosol chemical composition and levels in the Mediterranean Basin making it distinguishable from the other parts of Europe (Querol et al, 2009). It is found that Mediterranean lower troposphere has lower air quality, especially in summer due to Mediterranean being a crossroad of the intercontinental transport of aerosols (Lelieveld et al, 2002). In southeastern part of the Mediterranean, during the February–April period, contribution of African dust is shown to be as high as 80% to the PM<sub>10</sub> concentration (Pey et al, 2013). Even in the urban regions of Eastern Mediterranean, there is a significant contribution of long-range pollution transport (i.e. African dust) (Kanakidou et al, 2011).

There are studies conducted for the Mediterranean to quantify the relationship between Saharan dust outbreaks and PM<sub>10</sub> concentration using satellite data, ground measurements and modeling systems. The Mediterranean Sea is one of the areas in the world having a particularly optically thick aerosol layer. It is shown that Saharan dust outbreaks over the Eastern Mediterranean follow a pathway starting from the Northern Africa to the Eastern Mediterranean Sea (Papayannis et al, 2005).

In their work, Gerasopoulos et al. (2006) identified the factors that control PM levels in Eastern Mediterranean region and they stated that the significant PM<sub>10</sub> levels should be attributed to dust outbreaks that are transported via southerly air mass from the Sahara Desert. Bouchlaghem et al. (2009) presented Saharan dust outbreaks affecting Tunisian coast and its impact on PM<sub>10</sub>. The relationship between high levels of PM<sub>10</sub> and intrusions of Saharan dust over the Iberian Peninsula is studied by Rodriguez et al. (2001). In both studies it is found that the average daily PM<sub>10</sub> concentration values are higher on the days with Saharan dust contribution than the days with no dust event.

Kallos et al. (2006) and Mitsakou et al. (2008) both used SKIRON atmospheric modeling system to compare dust event forecasts with PM<sub>10</sub> concentrations obtained from monitoring stations. It is found that contribution of annual dust concentration to daily mean PM<sub>10</sub> concentration is greater than 10%. In another study, particulate matter samples collected in the North Atlantic free troposphere at Izaña Global Atmospheric Watch (GAW) observatory were analyzed. The results show that there is a repeated mixing of desert dust with pollution aerosols (Rodríguez et al, 2011). CALIOPE (CALIdad del aire Operacional Para España) modeling system is used to characterize aerosols over Europe and it is found that local anthropogenic emissions, Saharan dust and atmospheric dynamics at synoptic scale are dominantly effecting aerosol levels over Europe. High levels of PM<sub>10</sub> and aerosol optical depth (AOD) are linked to the desert dust transport from North Africa that has a 40% contribution to the total aerosol budget in Southern Europe (Basart et al, 2012).

In a previous study an integrated air quality system is used to see the interaction of anthropogenic emissions sources on Sahara dust concentrations. CMAQ (Community Multi-scale Air Quality Model) anthropogenic outputs DREAM (Dust REgional Atmospheric Model) desert dust forecasts are coupled in an online operational way (Jiménez-Guerrero et al, 2008). However, with this approach physical and chemical interaction of natural aerosols with man-made aerosol is neglected.

#### **1.4.2 Air quality management systems**

In order to give a complete deterministic description, such as emission sources, meteorological processes, physical and chemical transformations, of the ambient pollutant concentrations that threaten public health, atmospheric chemistry modeling systems are often used. The use of atmospheric models plays an important role due to their capability to simulate aerosol distributions, emission and transport (Daly and Zannetti, 2007). In the real atmosphere meteorological factors and chemical processes are coupled, meaning atmospheric composition can influence both Earth's radiation budget and climate directly by scattering and absorbing radiation or indirectly by acting as a cloud condensation nuclei affecting cloud formation and precipitation. The interaction of meteorological factors on air quality and atmospheric transport of pollutants is well accepted and they can no longer be conducted separate from each other (Grell et al, 2005; Baklanov et al, 2014). An “online” Weather Research and Forecasting/Chemistry model (WRF-Chem), a version of the non-hydrostatic model

WRF (Skamarock et al, 2001), simulates trace gases and particulates simultaneously with the meteorological fields by using the same transport scheme (mass and scalar preserving) and the same grid (horizontal and vertical components) (Grell et al, 2005; Fast et al, 2006).

While there are many studies that use WRF-Chem to understand atmospheric phenomenon, such as ozone chemical formation (Tie et al, 2007; Tie et al, 2013), NO<sub>x</sub> emissions, ozone chemistry and NO<sub>x</sub> oxidation productions analysis (Chen et al, 2013), annual simulations of tropospheric ozone and related species (Kumar et al, 2012), simulation of wildfire plume transport (Sessions et al, 2011), quantification of spatial and temporal variability of column integrated trace gases (Follette-Cook et al, 2015), only a few examples exist that focus on natural dust related problems. Khan et al. (2015) utilized WRF-Chem to reproduce the meteorological environment and spatial and size distributions of dust over northwest Africa. It was found that orographic lifting, land and sea breeze interactions are the key mechanisms that form the aerosol plume.

In another study, the WRF-Chem model was used to investigate seasonal and inter-annual variations of Asian dust balance, its direct radiative forcing, and estimates of the dust lifecycle contributions from transport, and dry and wet deposition (Chen et al, 2014). In this study it was found that the WRF-Chem model was successful in simulating overall characteristics of mineral dust over the dust source region and dust direct radiative forcing, which resulted in atmospheric warming and surface and TOA (top of atmospheric) cooling over East Asia. Kumar et al. (2014) used WRF-Chem over northern India to simulate the spatial and temporal distributions of dust plumes. The results showed an underestimation of aerosol optical depth compared to the Aerosol Optical Depth (AOD) values obtained from AERONET sites.

Remote sensing is another useful tool for air quality for surface concentration estimations, and improvement of emission inventories of trace gases and aerosol. Capabilities of satellite remote sensing of tropospheric aerosols and physical processes affecting their accuracy and precision are well explained in Martin V. R.'s review (2008). Although it is difficult to detect dust aerosols due to having short lifetime, strong interactions with local and regional aerosols and synoptic conditions, both visible (VS) and infrared (IR) spectral bands can be used to detect dust plumes in the atmosphere. In order to distinguish dust particles, magnitude of the difference of

reflectance in VS bands or brightness temperature (BT) in IR bands can be used (Zhao, 2012). Four satellite dust retrieval products (MODIS, SEVIRI, MIRS and IASI) are compared to each other to identify strengths and weaknesses of each algorithm in order to detect dust loading over the Sahara Desert. MODIS is found to retrieve dust loading better at low dust events. It is shown that other than dust loading, meteorological conditions and land surface properties also plays a critical role for dust detection (Banks et al, 2013). The inference of ground PM concentration is primarily retrieved from GOES over the eastern United States. MODIS (The Moderate Resolution Imaging Spectroradiometer) sensor on board of Aqua and Terra satellite and MIRS (Multi-angle Imaging SpectroRadiometer) on board of Terra satellite is being used to retrieve aerosol optical depth (AOD), which is columnar aerosol loading of the atmosphere (Martin 2008; Streets et al, 2013). MODIS can also be used to distinguish dust from smoke and maritime aerosols for evaluation of the African dust column concentration. Using satellite data, Kaufman et al. (2005) found that  $240 \pm 80$  Tg of dust are transported annually from Africa to the Atlantic Ocean. They also established that  $140 \pm 40$  Tg of the dust deposits in the Atlantic Ocean, 50 Tg fertilizes the Amazon Basin, 50 Tg reaches the Caribbean and 20 Tg returns to Africa and Europe (Kaufman et al, 2005).

A coupled meteorology–chemistry model is often utilized to forecast aerosol concentrations in air quality modeling. However, it is limited to spatial and temporal resolutions as well as physical and chemical processes, which are often simplified the real atmosphere. Pollutant transport and transformations in coupled atmospheric models are also strongly driven by uncertain external parameters, such as input data (emissions), initial and boundary conditions of pollutants from a larger-scale simulation, and meteorological fields, they introduce uncertainties and contribute to inaccurate Air Quality (AQ) forecasts (Wang et al, 2014; Bocquet et al, 2015). In order to improve the accuracy of the input data of model forecasts (e.g. initial conditions and/or boundary conditions), and correct the errors caused by the uncertainties of the model inputs in order to improve model forecasts of aerosols, aerosol data assimilation (DA) methods are used in atmospheric models (Talagrand, 1997, Niu et al, 2008; Liu et al, 2011; Schwartz et al., 2012; Wang et al, 2014; Pagowski et al, 2014). These previous studies have shown that the use of satellite observations and aerosol optical depth (AOD) products can improve the accuracy of the analyzed aerosol distributions and forecasts during the times when the satellite data are available (Zhang et al, 2008; Shi et al, 2011).

There are many DA studies that use satellite-derived aerosol products in chemical transport models. Collins et al. (2001) used optimal interpolation (OI) approach in order to constrain AOD forecasts for planning the deployment of ships and aircraft by using AVHRR (Advanced Very High Resolution Radiometer) data. Zhang et al. (2008) used a two-dimensional variational (2DVAR) approach to integrate satellite observations from the Moderate Resolution Imaging Spectroradiometer (MODIS) product in order to improve aerosol forecasts and global AOD analyses. In their study Saide et al. (2013) developed an ability to use the NOAA Grid-point Statistical Interpolation (GSI) (Wu et al., 2002), a three dimensional variational (3DVAR) approach to assimilate AOD products within WRF-Chem forecasts. Sekiyama et. al., (2010) successfully assimilated aerosol backscatter measurements from the Cloud-Aerosol Lidar and Infrared Pathfinder Satellite Observations (CALIPSO) by using a four-dimensional ensemble Kalman filter approach. Benedetti et al. (2009) focused on the theoretical architecture and practical implementation of the operational four-dimensional variational (4D-Var) aerosol assimilation system that uses retrievals of optical depth from the MODIS sensor on the Aqua and Terra satellites. Their analysis showed that the DA brought the model AOD closer to the observations and assimilation tended to improve the aerosol distribution over the polluted areas. Liu et al. (2011) used 3DVAR approach in their study to assimilate MODIS total AOD retrieval products from both Terra and Aqua satellites to constrain dust storm predictions over East Asia. In order to assimilate AOD, they developed a single-step aerosol DA system within the National Centers for Environmental Prediction (NCEP) operational GSI (Kleist et al., 2009) 3DVAR meteorological DA tool, which is coupled to the WRF-Chem model. They showed that assimilating MODIS AOD improves aerosol analyses compared to independent AOD observations from the Aerosol Robotic Network (AERONET) and Cloud-Aerosol Lidar with Orthogonal Polarization (CALIOP) instrument, and surface  $PM_{10}$  observations and that the system can be used as a tool to generate better dust storm forecasts. In 2014 Pagowski et al. developed a package that consists of software for calculating background error covariance statistics and for converting satellite data to BUFR (Binary Universal Form for the Representation of meteorological data) format, which GSI requires. This implementation of the GSI can be used to assimilate MODIS aerosol optical depth at 550 nm with WRF-Chem and is used in the present study. The studies mentioned above contributed significantly for our understanding of the extent of global and regional dust influences, however the dust contribution in

Eastern Mediterranean is still unclear, where significant industrial sources and metropolitan areas with population higher than 3 million people (i.e. Istanbul, Ankara, Izmir) are located. In this study we aim to fill this gap via analysis of satellite data and atmospheric models.

The following chapters present the data (i.e. ground observations), the models utilized to quantify the effect of Saharan dust on high levels of  $PM_{10}$  measured in the Anatolian Peninsula, results and discussions of RAQMS experiment (Chapter 2), WRF-Chem Control experiment (Chapter 3), WRF-Chem MODIS Assimilation experiment (Chapter 4) and overall conclusions (Chapter 5).







## **2. REAL-TIME AIR QUALITY MODELING SYSTEM EXPERIMENT**

This chapter gives information about the Real-time Air Quality Modeling System (RAQMS) that is utilized to explore the possible effects of Saharan dust on high levels of PM<sub>10</sub> measured in Turkey and its results. RAQMS model is compared with 118-air quality stations distributed throughout Turkey (81 cities) for April 2008.

This chapter is published in Science of the Total Environment in 2014 that is entitled as “The contribution of Saharan dust in PM<sub>10</sub> concentration levels in Anatolian Peninsula of Turkey” (Kabatas, B., Unal, A., Pierce, R.B., Kindap, T., and Pozzoli, L.: The contribution of Saharan dust in PM<sub>10</sub> concentration levels in Anatolian Peninsula of Turkey, *Sci. Total Environ.*, 488–489, 413–421, 2014).

### **2.1 Data**

#### **2.1.1 Ground-based data**

This study used the ground observations conducted in Turkey by Turkish Ministry of Environment and Urbanization. Daily averages of PM<sub>10</sub> data are computed from the hourly data obtained from 118-air quality stations distributed throughout Turkey (81 cities) for 2008. The monitoring system’s instrument is using beta Gauge, which allows an accurate determination of particulate concentration under all conditions, to measure mass of particulates. US EPA also certifies beta Gauge monitoring system due to advantages of its being automated and reduced sample handling. The data provided by the Turkish Ministry of Environment and Urbanization undergoes QA/QC (Quality Assurance, Quality Control). However, we further conducted a QA/QC of our own. The original data is hourly. When estimating daily average values we have ignored the days where more than 25 % of the data are missing. Furthermore, data were checked individually to identify possible outliers. However, we have not observed such data. Figure 2.1 presents the monthly box plots of PM<sub>10</sub> obtained from the 118 air quality stations throughout the year 2008. In box plot, the box boundaries represent the upper (75%) and lower quartiles (25%) while the horizontal line shows the median of the data.

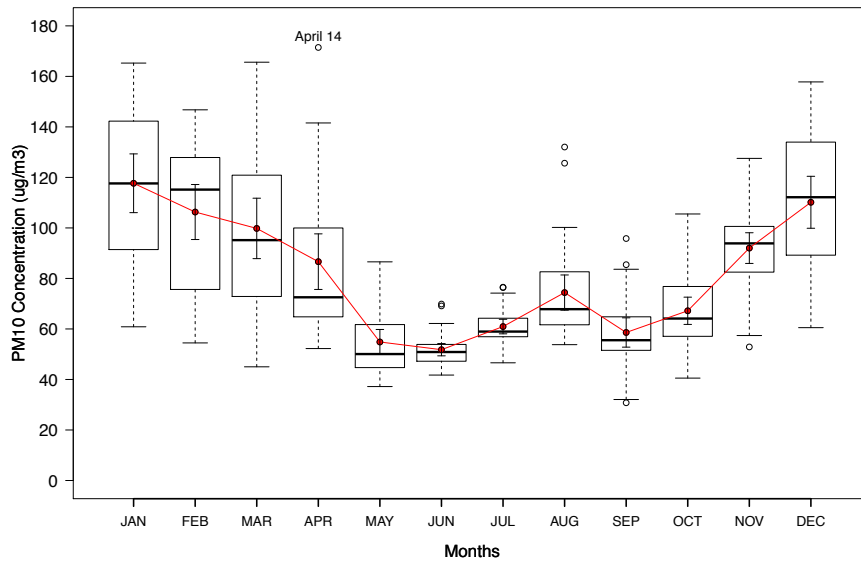


**Figure 2.1 :** Monthly PM<sub>10</sub> concentration of 2008 for Anatolian Peninsula (Kabatás et al, 2014).

Whiskers above and below the box show the locations of the smallest and largest values of dataset. Mean values of the data are shown with red dots in the box plot with the confidence intervals around them (within 1.96 standard deviations). The length of the box indicates data variability. In this case, months of January, February, March, April, August and December have more variation in the data while the rest of the months have small variation. In some months, the mean value seems to be larger than median, as in March, April, May, June, July, August, September and October, where most of the values are small, but there are some exceptionally large values. As seen in the figure, monthly PM<sub>10</sub> averages are smaller in the warm seasons, except August. Annual average of PM<sub>10</sub> concentration in 2008 was 81.7 µg/m<sup>3</sup> with a standard deviation (sd) of 23.4 µg/m<sup>3</sup>. Seasonal averages reach 111.5 µg/m<sup>3</sup> in winter (sd=29.6 µg/m<sup>3</sup>), 80.3 µg/m<sup>3</sup> in spring (sd=32.5 µg/ m<sup>3</sup>), 62.5 µg/ m<sup>3</sup> in summer (sd=15.5 µg/ m<sup>3</sup>) and 72.5 µg/ m<sup>3</sup> in fall months (sd= 20.9 µg/ m<sup>3</sup>). High levels of PM<sub>10</sub> during the winter is expected since during this period pollution sources (both local and regional) are significant and atmospheric conditions do not favor dispersion. High PM concentration measured in summer months (in this case August) are expected due to biomass burning. In July 31, 2008, a forest fire broke out in the Mediterranean province of Antalya. It lasted 5 days and was extinguished on August 4, 2008, resulting in the destruction of more than 15000 hectares of woodlands (Ayberk et al, 2010; Kavgacı et al, 2010). Thus, high values of PM<sub>10</sub> observed in August can be explained by biomass burning. Also, it is important to note that month of April had significantly high PM<sub>10</sub> values with an average of 86.7 µg/ m<sup>3</sup> with standard deviation of 29.5 µg/ m<sup>3</sup>. Maximum PM<sub>10</sub>

values were recorded on April 14, 2008 with a daily average of  $170 \mu\text{g}/\text{m}^3$  (which is also the maximum  $\text{PM}_{10}$  observation measured in the year 2008). As known from the studies, peak  $\text{PM}_{10}$  values caused by Saharan dust outbreaks occur in the transition seasons (Rodriguez et al, 2001; Gerasopoulos et al, 2006; Kallos et al, 2007; Mitsakou et al, 2008; Querol et al, 2009, Gkikas et al, 2012). A recent study states that dust transport occurs over the Mediterranean to Europe during all seasons, however, the highest AOD due to Saharan dust aerosol is observed in spring in Western Europe ( $15^\circ\text{W}$ – $5^\circ\text{E}$ ), it is in spring and summer season over Central Europe ( $5^\circ\text{E}$ – $25^\circ\text{E}$ ) and in spring and autumn over Eastern Europe ( $25^\circ$ – $40^\circ\text{E}$ ) (Israelevich et al, 2012).  $\text{PM}_{10}$  data for April 2008, as seen in Figure 2.2, suggests a possible contribution of Saharan dust to high  $\text{PM}_{10}$  levels over Turkey at this time.

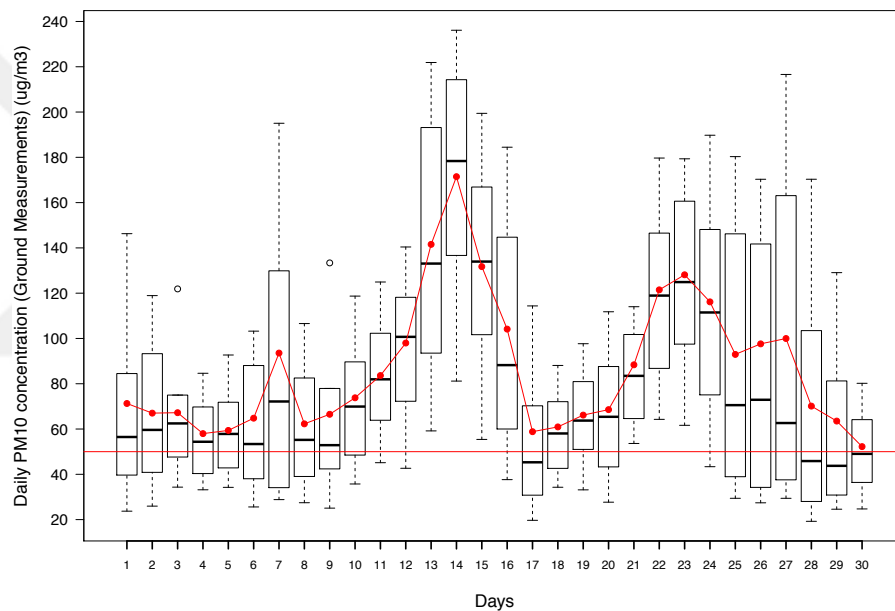


**Figure 2.2 :** Boxplot of daily  $\text{PM}_{10}$  concentration for April 2008. Red dots show daily mean  $\text{PM}_{10}$  concentrations and the European Commission daily  $\text{PM}_{10}$  standard ( $50 \mu\text{g}/\text{m}^3$ ) is shown with red line (Kabatas et al, 2014).

Since all the values are above European Commission’s air quality standard for  $\text{PM}_{10}$ , daily  $50 \mu\text{g}/\text{m}^3$ , another threshold is used to determine episode. First, days lying within 2 standard deviations ( $59 \mu\text{g}/\text{m}^3$ ) of the mean ( $86.6 \mu\text{g}/\text{m}^3$ ) are identified. Including  $\pm 2$  days to this identified range; period between April 11 and April 18, 2008 is selected as our episode in this analysis.

### 2.1.2 RAQMS model description

The Real-time Air Quality Modeling System (RAQMS) is a unified, meteorological and chemical modeling system for assimilating satellite observations of atmospheric

chemical composition throughout the troposphere and stratosphere. The model also provides real time forecasts of trace gas and aerosol distributions (Pierce et al, 2003, 2007; Verma et al, 2009). It extends from surface to around 60 km with 35 vertical levels. The University of Wisconsin-Madison hybrid isentropic coordinate model is the RAQMS dynamical core (Schaack et al, 2004; Pierce et al, 2007). The RAQMS chemical scheme was developed at NASA Langley Research Center (Pierce et al, 2003, 2007) and the aerosol module incorporates the Goddard Ozone Chemistry Aerosol Radiation and Transport (GOCART) mechanism (Chin et al, 2002, 2003). RAQMS simulates sulfate ( $\text{SO}_4^{2-}$ ), dust, black carbon (BC), organic carbon (OC), and sea-salt aerosols that are known as the major tropospheric aerosol components (Chin et al, 2002). RAQMS predicts dust loadings for four size bins (effective radius of 0.8, 1.5, 2.5, and 4.0 microns). Dust emissions are determined based on a static dust source function associated with regions of topographic depressions, soil composition, 10-meter wind speed, and a threshold velocity which is dependent on dust size and surface wetness (Ginoux, 2001).

The RAQMS aerosol analysis used in the current study is from a retrospective 4-month (February–May 2008)  $2 \times 2^\circ$  that includes hourly assimilation of MODIS Aerosol Optical Depth (AOD) from instruments onboard the Terra and Aqua satellites (Remer et al, 2005). RAQMS aerosol concentrations were initially set to zero on February 15th and assimilation of the MODIS AOD retrievals began on March 1st, 2008. RAQMS meteorological forecasts were re-initialized at 6-hour intervals using the National Ocean and Atmospheric Administration (NOAA) Global Data Assimilation System (GDAS) meteorological analyses. The RAQMS aerosol analysis is in good agreement with April 2008 global Aeronet aerosol optical depth measurements with a correlation coefficient of 0.7 and a mean bias of 0.05 (Natarajan et al, 2012).

### **2.1.3 Satellite data overview**

Satellite data are used for validation of the RAQMS predictions of the impact of long range transport on high  $\text{PM}_{10}$  values measured in ground air quality stations located in Turkey. High-resolution vertical profiles of clouds and aerosols are provided from CALIOP, which is the primary instrument carried by the Cloud-Aerosol Lidar and Infrared Pathfinder Satellite Observations (CALIPSO) satellite. CALIPSO includes a two-channel (532 and 1064 nm) polarization lidar that provides qualitative information on particle size. It helps not only in discrimination of cloud and aerosol, but also the

identification of aerosol types (Winker et al, 2007). MODIS (The Moderate Resolution Imaging Spectroradiometer) Aerosol Product (MOD04 for Terra, MYD04 for Aqua), Collection 5 is used to get information about AOD (at 550 nm), which represents columnar aerosol loading of the atmosphere. Figure 2.3 (a) and (b) shows the aerosol optical depth (AOD) obtained from Terra and Aqua MODIS for April 14, 2008, respectively.

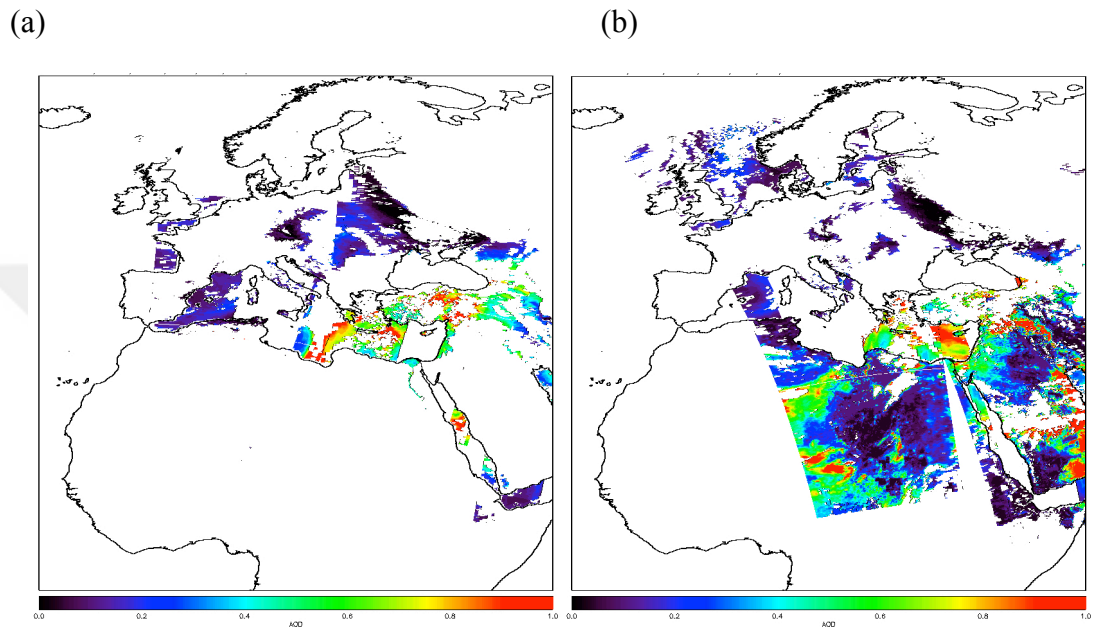


**Figure 2.3 :** AOD obtained from (a) MOD04 (Terra) and (b) MYD04 (Aqua) aerosol product for Eastern Mediterranean basin analyzed for April 14, 2008, when the maximum  $PM_{10}$  level was recorded (Kabatas et al., 2014).

In figure 2.3 AOD values vary between a minimum of 0 and a maximum of 1. AOD ranges between 0.5 and 0.7 for the western part of the peninsula whereas it is between 0.7 and 1.0 for the eastern part (which could be related to dust contribution in cloud free condition) for Terra MODIS. For Aqua MODIS, similar conclusions can be made with a slight change in the AOD values. Since Aqua and Terra MODIS have different viewing angles and over pass time, visualization of the data differs in the same way. Dust load transport and its path from North Africa to Turkey can better be seen on Aqua MODIS imaginary with higher AOD values than its vicinity over the desert.

## 2.2 Results of RAQMS Experiment

The lowest model level output ( $\sim 60\text{m}$  above the surface) from the RAQMS model is extrapolated to the surface and used for the comparison of in-situ  $PM_{10}$  observations. For this purpose, we have utilized total  $PM_{10}$  ( $\mu\text{g}/\text{m}^3$ ) concentration, which includes

dust, sea salt, BC, OC and  $\text{SO}_4^{2-}$ . RAQMS analyses show that in April 2008, dust aerosols account for 96.6% of total  $\text{PM}_{10}$  mass at the surface  $\text{PM}_{10}$  sites while other species (i.e. sea salt, BC, OC,  $\text{SO}_4^{2-}$ ) account for only 3.4%. Figure 2.4 shows box plot of daily  $\text{PM}_{10}$  surface concentration for April 2008 obtained from RAQMS aerosol analysis. Red dots on the figure show daily mean values and whiskers show 10% and 90% range of data.

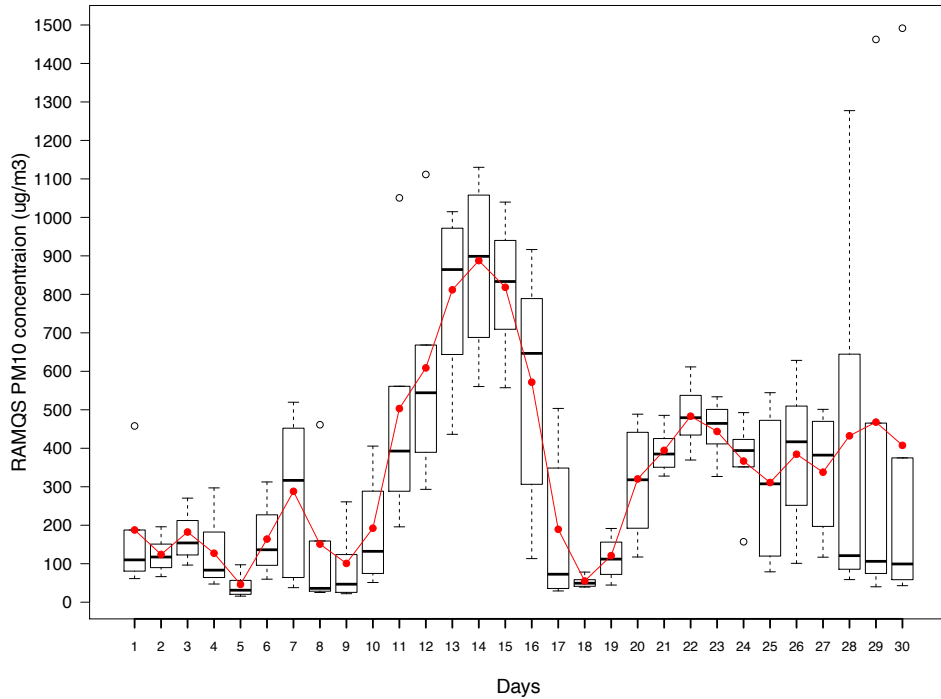


**Figure 2.4 :** Box plot of daily  $\text{PM}_{10}$  concentration for April 2008 obtained from RAQMS (Kabatas et al, 2014).

Maximum mean value is observed via RAQMS on April 14 with value of  $898 \mu\text{g}/\text{m}^3$  while the maximum mean value observed on April 14 via ground observations was  $170 \mu\text{g}/\text{m}^3$ . Unlike ground observations, model output show higher values on the last three days of April (28-29-30 April) with daily mean values higher than their medians, with values of  $121 \mu\text{g}/\text{m}^3$ ,  $106 \mu\text{g}/\text{m}^3$ ,  $99 \mu\text{g}/\text{m}^3$  and  $432 \mu\text{g}/\text{m}^3$ ,  $468 \mu\text{g}/\text{m}^3$ ,  $407 \mu\text{g}/\text{m}^3$  respectively. Overall, the model prediction is consistent with the 118 ground station observations as the model captures the temporal variability and spatial distribution. The only exception is for the period between 28 and 30 April, where the model shows an increasing trend while the observations have a decreasing trend. A significant correlation is found between the model and in situ observations (The correlation coefficient is 0.87). Since dust is the primary component of  $\text{PM}_{10}$  load according to the model, we used the surface dust prediction to understand the effect of dust transport on surface  $\text{PM}_{10}$  in Turkey. Figure 2.5 shows RAQMS surface level dust mass for Eastern

Mediterranean for 11-18 April 2008. In Figure 2.5a (11 April) high levels of PM<sub>10</sub> can be seen over Italy and Greece and southeastern part of Turkey. It is likely that high levels of PM<sub>10</sub> over the Southeastern Turkey are due to previous dust intrusions from Sahara or other source regions. The dust cloud moves towards northwestern part of Turkey on April 12 (figure 2.5b) and on April 13 (figure 2.5c), the cloud dominates the whole region. Saharan dust clouds cover the entire Turkey on April 14, coinciding with the maximum PM<sub>10</sub> concentration measured at the ground stations.

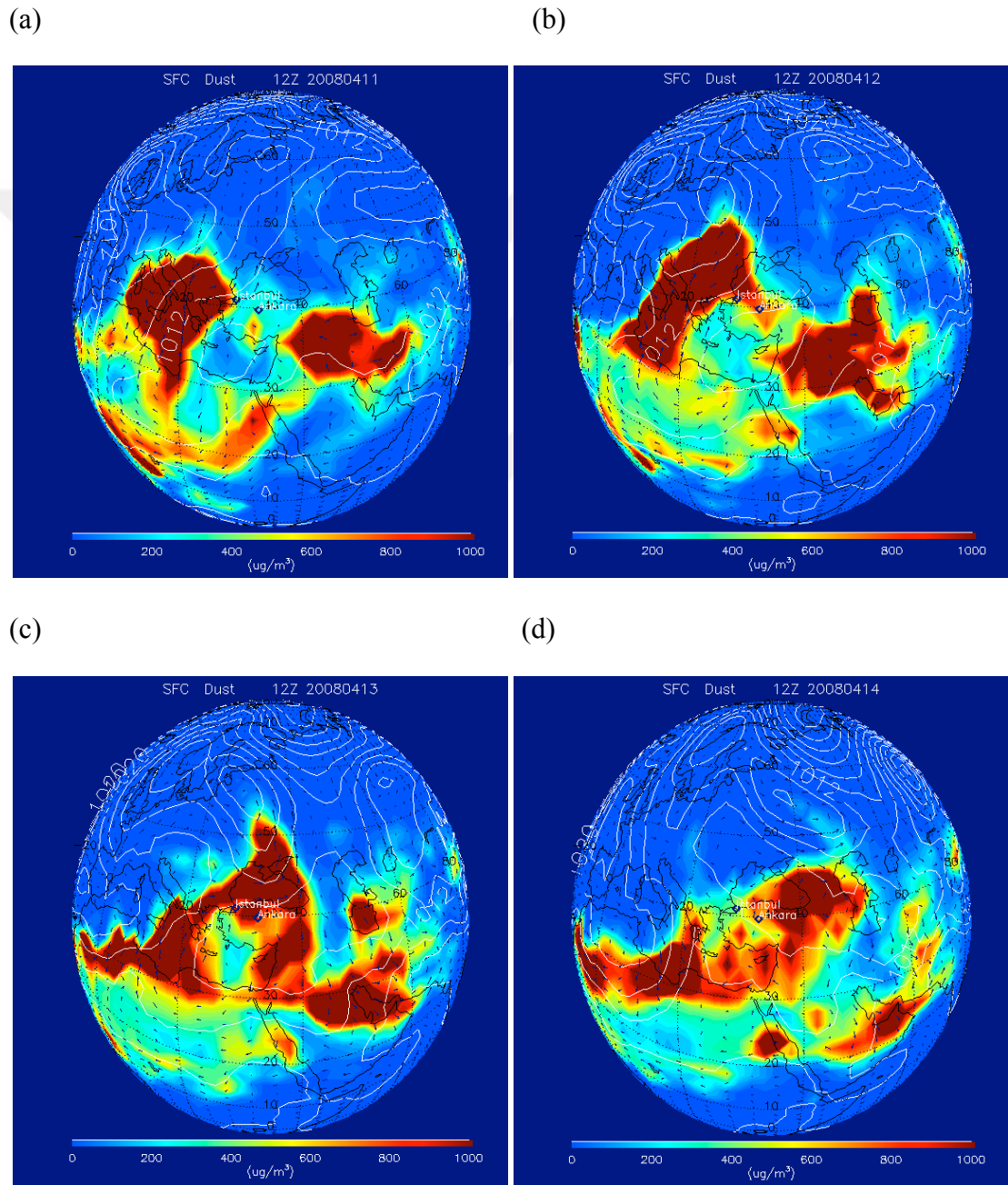


**Figure 2.5 :** RAQMS outputs of dust concentrations at the surface for Eastern Mediterranean for the selected episode (a–h refers to April 11–18, 2008, respectively) (Kabatas et al, 2014).

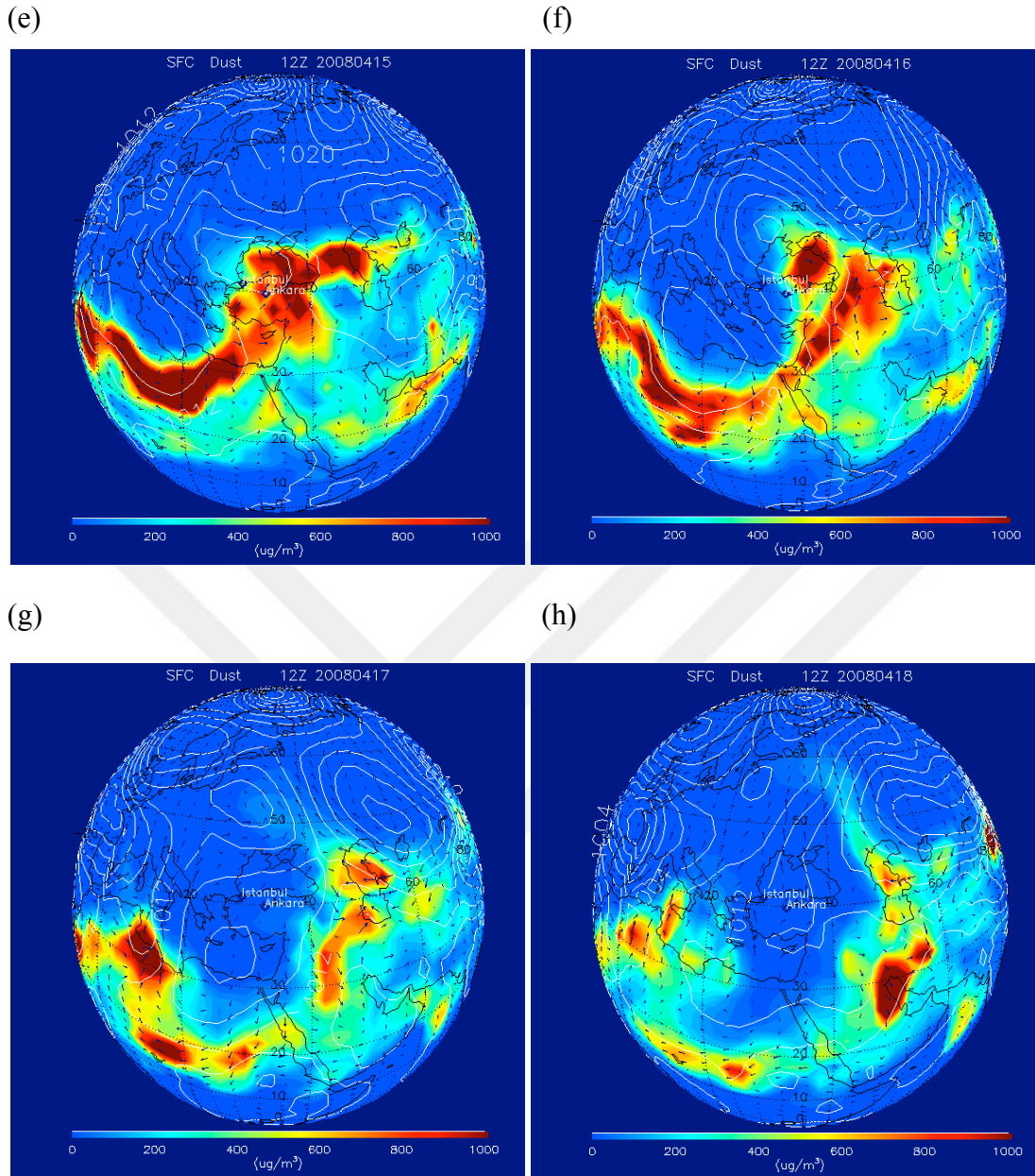


**Figure 2.5 (continued) :** RAQMS outputs of dust concentrations at the surface for Eastern Mediterranean for the selected episode (a–h refers to April 11–18, 2008, respectively) (Kabatas et al, 2014).

The Saharan dust transport continues on April 15 and then gets weaker by the end of the episode. Atmospheric conditions are also favorable for dust transport from North Africa to Turkey. Since RAQMS has spatial resolution by  $2^\circ$ , a mesoscale, non-hydrostatic meteorological model WRF (Weather Research and Forecasting) is also used to simulate higher resolution meteorological conditions (Skamarock et al, 2001; Michalakes et al, 2001; Skamarock and Klemp, 2008). Figure 2.6a shows the synoptic conditions simulated with RAQMS meteorological parameters (Mean sea level pressure along with wind vectors at 00Z on April 15th, 2008).





Kain–Fritsch (new Eta) cumulus scheme, YSU (Yonsei University scheme) boundary layer parameterization scheme.

Figure 2.6 (b) shows atmospheric conditions obtained via WRF for April 15, 2008 at 00:00 UTC. The similar pressure and wind pattern that is obtained via RAQMS can be seen in WRF simulation. Although the synoptic patterns from both models show similar pattern, WRF shows mesoscale features that are not present in the RAQMS analysis. High-pressure system located on eastern Mediterranean Sea and low-pressure system located on central Europe creates a channel that helps Saharan dust transport over Mediterranean Sea to Turkey.

### 2.3 Discussion of RAQMS Experiment

The comparison with Turkey surface  $PM_{10}$  measurements shows that RAQMS overestimates maximum daily mean  $PM_{10}$  values by a factor of 5.25 on April 14, 2008. We use CALIPSO measurements to verify the RAQMS aerosol analysis and understand why this overestimate occurs. Figure 2.7 shows CALIPSO total aerosol extinction at 23:55Z on April 14, 2008 during the period of maximum  $PM_{10}$  concentrations.

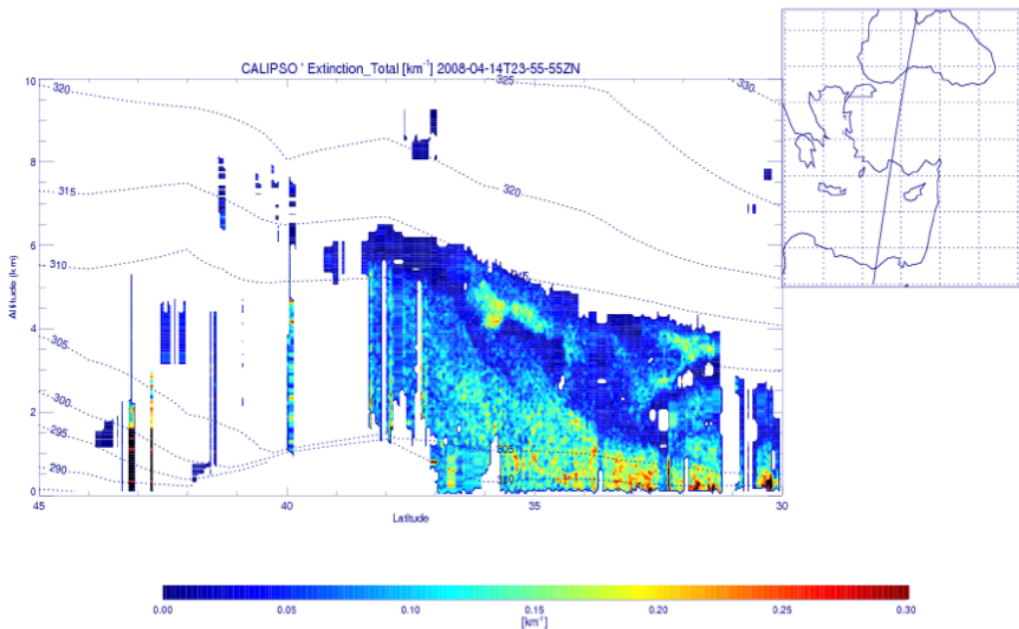


**Figure 2.7 :** Path of CALIPSO and its total extinction output over Turkey on April 14, 2008. CALIPSO shows deeper mixing of the aerosol over Turkey starting from south to north part of the peninsula (Kabatas et al, 2014).

Extinction is a measure of attenuation of the light passing through the atmosphere due to the scattering and absorption by aerosol particles. The satellite’s path extends from

Turkey south to the North African coast. Dashed lines show the altitude of potential temperature surfaces from the RAQMS analysis. Figure 2.8 shows RAQMS analyzed aerosol extinction profiles along the CALIPSO path. RAQMS shows a shallow layer of enhanced aerosol extinction below 2 km with uniform aerosol extinctions in excess of  $0.2 \text{ km}^{-1}$  over the Mediterranean and generally larger than  $0.1 \text{ km}^{-1}$  over Turkey, where the enhanced aerosol extinction is restricted to a shallow inversion layer near the surface. CALIPSO shows similar, although less uniform, extinction enhancements below 2 km over the Mediterranean but shows aerosol extinctions up to nearly 6 km over Turkey.

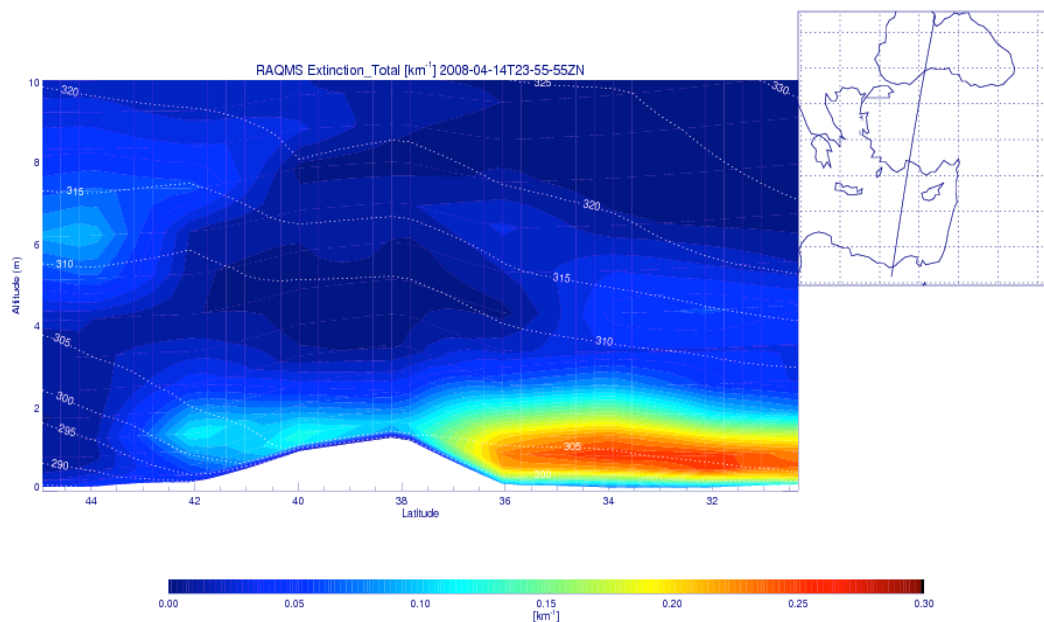


**Figure 2.8 :** RAQMS total extinction output over Turkey on April 14, 2008. It shows a shallow (and stronger) layer near the surface, where there is a very strong inversion over Turkey (Kabatas et al, 2014).

In order to understand why RAQMS may underestimate aerosol lofting over Turkey, we compared the RAQMS and a higher resolution atmospheric model (Weather Research and Forecasting (WRF) model) surface elevation, planetary boundary layer depths, and potential temperature distributions along the CALIPSO track at 00:00UTC on April 15, 2008 (Figure 2.9). Red color represents RAQMS model outputs and black color represents WRF model outputs while dashed lines show the planetary boundary layer height and solid lines show surface elevation. The 30km WRF simulation is able to better represent the topographic features along the CALIPSO track and shows a deeper planetary boundary layer over the Southern Coast of Turkey. The WRF potential temperature distribution does not show the shallow inversion layer near the

surface that was found in the RAQMS model. These comparisons suggest that RAQMS underestimates the lofting of the dust aerosols over Turkey due to the surface inversion and consequently overestimates the surface concentrations.

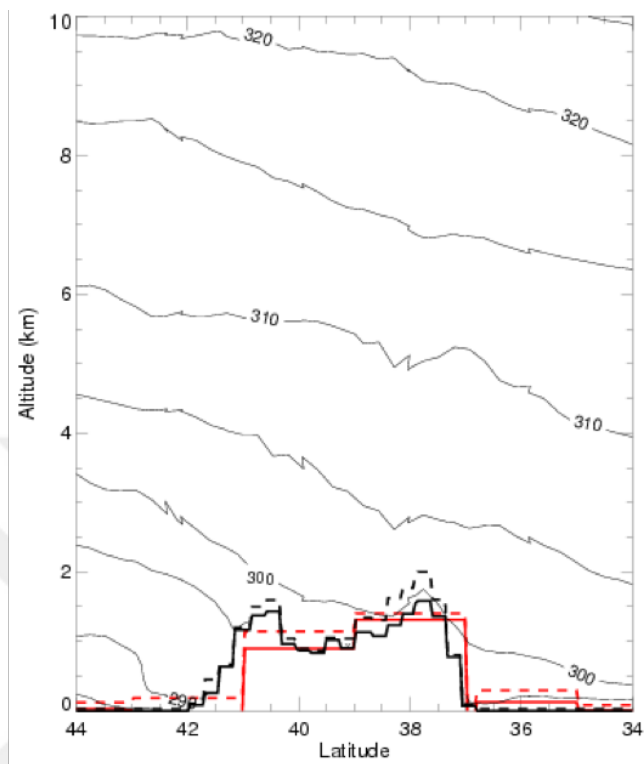


**Figure 2.9** : Cross section of WRF potential temperature (K) along CALIPSO track at 00:00 UTC on April 15, 2008. The bold lines indicate the surface elevation (solid) and planetary boundary layer height (dashed) for the 30km WRF (black) and  $2^\circ \times 2^\circ$  RAQMS (red) models (Kabatas et al, 2014).

### **3. WRF-CHEM CONTROL EXPERIMENT**

In this chapter, the higher resolution online-coupled regional Weather Research and Forecasting model with chemistry (WRF-Chem) model, driven by RAQMS lateral boundary conditions, is utilized using two different emission inventories (RETRO/EDGAR and EDGAR HTAP) to investigate the spatial and temporal distribution of Saharan mineral dust transport over the Eastern Mediterranean for the same time period. This is the first WRF-Chem study investigating natural dust influences on air quality in the Eastern Mediterranean, especially in Anatolian Peninsula.

#### **3.1 Ground Observations and Model Description**

Same dataset that is analyzed in the first chapter is used as ground observations for WRF-Chem experiment. Ground observations used in this study are conducted by the Turkish Ministry of Environment and Urbanization. Analysis of ground observations are well explained in Figure 2.1 and Figure 2.2. Mean value of PM<sub>10</sub> concentration for April 2008 was found to be  $\sim 87 \mu\text{g}/\text{m}^3$  (annual mean PM<sub>10</sub> concentration in 2008 was  $81.7 \mu\text{g}/\text{m}^3$ ). Maximum mean PM<sub>10</sub> values were found on April 14, 2008 with a daily average around  $170 \mu\text{g}/\text{m}^3$ , which was also the highest PM<sub>10</sub> value of the year 2008 (Kabatas et al, 2014).

In this chapter, we have utilized a regional online atmospheric model, Weather Research and Forecasting model with chemistry (WRF-Chem) (Grell et al, 2005), with higher resolution (30km outer and 10 km nested domains) to investigate the spatial and temporal distribution of Saharan mineral dust transport over Eastern Mediterranean in April 2008. We use RAQMS lateral boundary conditions coupled to an online WRF-Chem version 3.5.1 configured to cover Eastern Mediterranean (30km outer domain) and Anatolian Peninsula (10km nested domain) to determine how model resolution effects the PM<sub>10</sub> predictions. Figure 3.1 shows both domains on top of a topography map showing terrain height. WRF-Chem, a version of WRF (Skamarock et al, 2001), is an online coupled model that allows aerosol, air quality, weather and climate

interactions simultaneously. For this study, we used the simple GOCART aerosol option in WRF-Chem. GOCART (Chin et al, 2000) simulates five major tropospheric aerosol types within the model including hydrophilic and hydrophobic components of atmospheric aerosols such as sea salt, dust, organic carbon (OC), black carbon (BC), and sulfate.

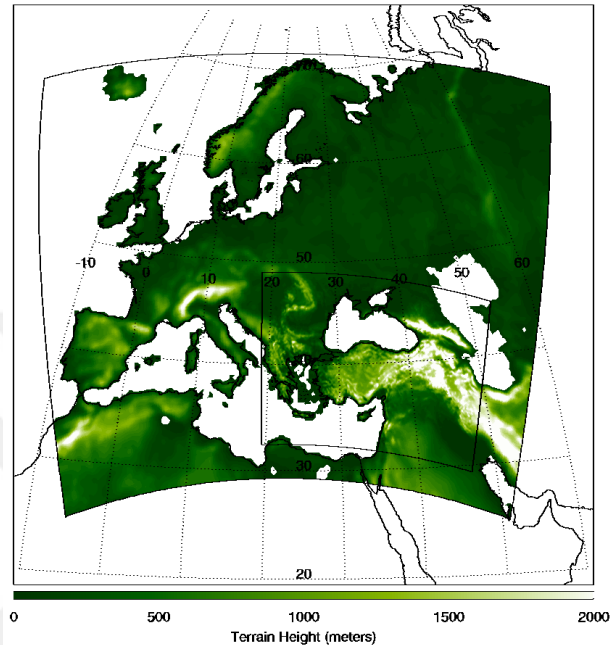


**Figure 3.1 :** WRF-Chem domains configured to cover Eastern Mediterranean (30km outer domain) and Anatolian Peninsula (10km inner domain) with topography map.

GOCART module represents emission, advection, convection, diffusion, dry deposition and wet deposition that are related to aerosol species' evolution. GOCART dust emission scheme simulates the dust emission as a function of surface wind speed, and surface wetness. Sea salt emission from the ocean is mainly a function of wind speed at 10 m, similar to dust uplifting (Chin et al, 2000, 2002; Ginoux et al., 2001). In this study, the size distribution is modeled into five size bins for dust and four size bins for sea salt. For the first part of the study, the global anthropogenic emission inventories are obtained from the RETRO (REanalysis of the TROpospheric) chemical composition data collected over the past 40 years (available for the 1960–2000) (Schultz et al, 2007) and the EDGAR (Emission Database for Global Atmospheric Research) (Olivier et al, 1996). The RETRO emission data has a  $0.5^\circ \times 0.5^\circ$  spatial resolution and global coverage, with monthly temporal resolution, and is based on the year 2000. It provides global annual emission data of several greenhouse gases (e.g.,  $\text{CO}_2$ ,  $\text{CH}_4$  and  $\text{N}_2\text{O}$ ) as well as some precursor gases. EDGAR provides past and present global anthropogenic emissions of greenhouse gases and air pollutants (such as  $\text{N}_2\text{O}$ ,

CO<sub>2</sub>, CO, CH<sub>4</sub>, SO<sub>2</sub>, SF<sub>6</sub>, NO<sub>x</sub> and NMVOC) with a 1° x 1° spatial resolution. EDGAR emissions do not vary in time. In order to prepare emission fields from a large set of source databases, WRF-Chem uses a preprocessor (PREP-CHEM-SRC). This comprehensive tool aims at preparing emission fields of trace gases and aerosols for use in the model (Freitas et al, 2011). For the second part of this experiment, we used EDGAR HTAP anthropogenic emission inventory (EDGAR: Emission Database for Global Atmospheric Research of the Joint Research Centre, JRC, in cooperation with the Task Force on Hemispheric Transport of Air Pollution (TF HTAP)) (Janssens-Maenhout et al, 2012) that consists monthly 0.1° x 0.1° global grids for year 2008. We substituted HTAP SO<sub>2</sub>, OC, BC, PM<sub>10</sub>, PM<sub>2.5</sub> emissions from Energy, Industry, Transport, and Residential sectors in original EDGAR emission inventory that is implemented in WRF-Chem modeling system to create higher resolution anthropogenic emissions. Hereafter RETRO/EDGAR emission inventory referred to as EDGAR and EDGAR/HTAP emission inventory referred to as HTAP. Biomass burning emissions are produced from Wild Fire Automated Biomass Burning Algorithm (WF-ABBA) wildfire products (Prins and Menzel, 1994). For the region of this study, WF-ABBA uses SEVIRI data to detect and characterize biomass burning. Biomass emissions are updated every 24 hours.

The simulation presented here is the dust storm that impacted Eastern Mediterranean, especially Anatolian Peninsula, for April 2008. The outer WRF-Chem domain, with a horizontal resolution of 30 km, covers Europe in the west, Caspian Sea in the east, Scandinavia in the north and Sahara in the south (Figure 3.1). WRF-Chem version 3.5.1 is configured to cover Eastern Mediterranean (-10.0°W–60.0°E, 30.0° S–70.0°N) with 190 west-east and 158 north-south grid points and 35 vertical layers up to 10 hPa. The high-resolution nested domain has 10 km horizontal resolution, 262 west-east, 181 north-south grid points and the same 35 vertical layers as the 30 km outer domain.

The following physical parameterizations were included for both outer and nested runs: the Noah land surface model, Mellor-Yamada-Janjic Planetary Boundary Layer (PBL) (Zaviša and Janjić, 1994) and the New Grell Cumulus Parameterization scheme. Meteorological fields are initialized and lateral boundary conditions are obtained from 6 hourly NOAA NCEP GFS (Global Forecast System) analyses. Aerosol lateral boundary conditions are obtained from 6 hourly RAQMS 2x2 degree global analyses. Since the simulation domain of this study does not cover North Africa, a significant

portion of main dust source area is not included in the outer domain. However, by using 2x2 degree global RAQMS analysis, dust transport from North Africa is included through lateral boundary conditions. WRF-Chem was run in the above configuration for entire month of April 2008.

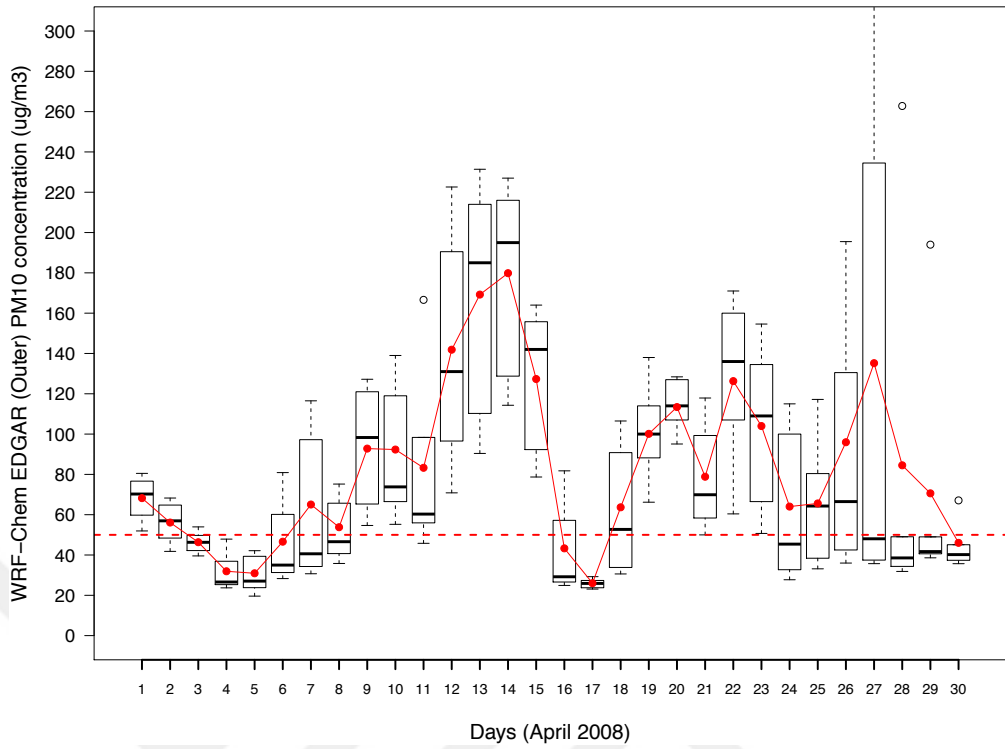
### **3.2 Results of the WRF-Chem Experiment**

From the ground observations, the maximum mean daily PM<sub>10</sub> concentration was observed on April 14, 2008 with a daily mean value of ~170 µg/m<sup>3</sup>, which is also the maximum PM<sub>10</sub> concentration measured throughout 2008, and the minimum mean daily PM<sub>10</sub> concentration was observed on April 17, 2008 with a daily mean value of (~53 µg/m<sup>3</sup>) (see Figure 2.2). WRF-Chem EDGAR 30km outer domain, WRF-Chem HTAP 30km outer and 10 km nested domain box plot results are presented in Figures 3.2a, 3.2b and 3.2c, respectively. Lower and upper hinges of the boxplot represent 10<sup>th</sup> and 90<sup>th</sup> percentile of the data. Presence of outliers in some of the data points (both models and observations) results in mean values being greater, on average, than median values. Comparison of daily PM<sub>10</sub> concentration of ground observations, WRF-Chem HTAP outer domain (30km) and nested domain (10 km), and WRF-Chem EDGAR outer domain (30km) can be seen from Figure 3.2d.

The model daily mean prediction averaged over all ground observation sites (118 stations) is consistent with observations suggesting that the model captures the overall temporal evolution very well, yet all runs tend to overestimate the high values of PM<sub>10</sub> (high dust event on April 14) while they underestimate low PM<sub>10</sub> events (low dust event on April 17). It should be noted that there is high variability in the PM<sub>10</sub> observation data especially on April 7<sup>th</sup>, 13<sup>th</sup>, 14<sup>th</sup>, 19<sup>th</sup>, 20<sup>th</sup>, 25<sup>th</sup>, and 27<sup>th</sup>. When we compare the model output specifically on high PM<sub>10</sub> event days (April 13<sup>th</sup>, 14<sup>th</sup>, 15<sup>th</sup>) that we calculated from 118 ground observations distributed throughout Turkey (figure 2.2), we observe that WRF-Chem EDGAR (Outer) and WRF-Chem HTAP (Inner) has similar level of variability while WRF-Chem HTAP (Outer) has significantly lower variability. It should be noted that the over prediction of WRF-Chem is much less than the RAQMS over prediction (see Figure 2.4). Utilizing a higher resolution regional model has improved the representation of planetary boundary layer (PBL) dynamics which resulted in an overestimation of the predictions by factor of 5 from the previous 2x2 degree resolution RAQMS model analysis.



(a)



(b)

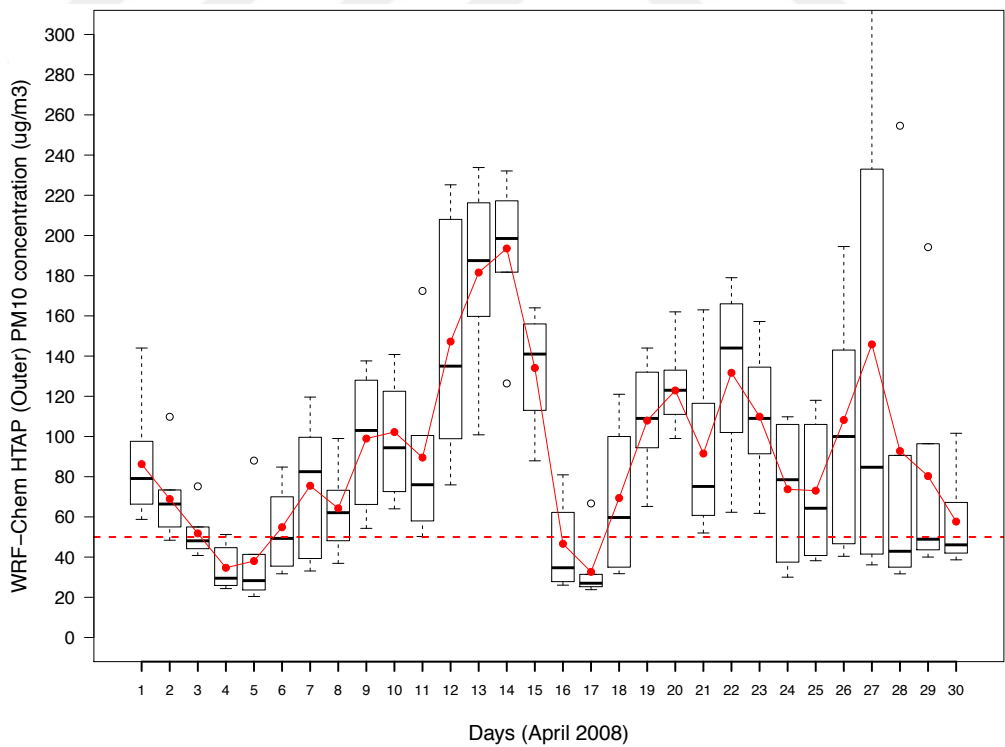
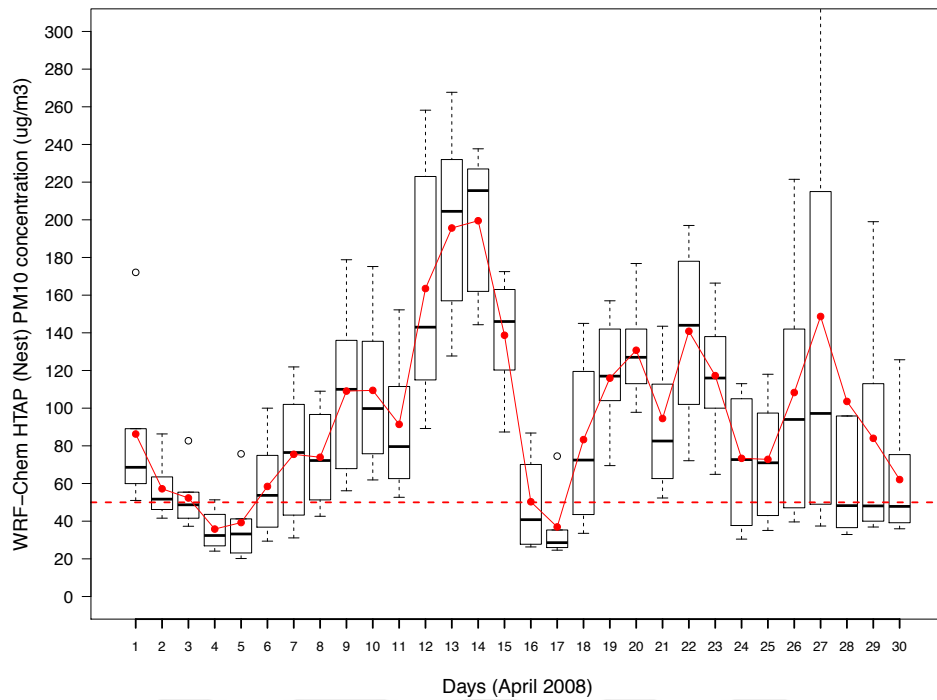


**Figure 3.2 :** Daily mean (red line) and boxplots of daily PM<sub>10</sub> concentration obtained from WRF-Chem EDGAR 30 km outer domain (a), WRF-Chem HTAP 30km outer domain (b), WRF-Chem HTAP 10 km nested domain (c) and time series comparisons for daily PM<sub>10</sub> concentration (d). Red dashed lines show European Commission daily PM<sub>10</sub> standard (50  $\mu\text{g}/\text{m}^3$ ).

(c)



(d)

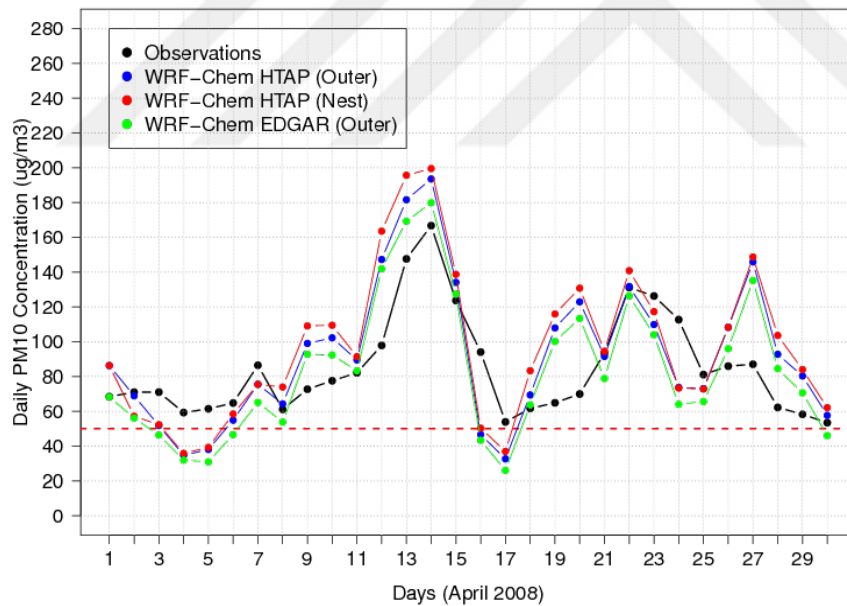


**Figure 3.2 (continued)** : Daily mean (red line) and boxplots of daily PM<sub>10</sub> concentration obtained from WRF-Chem EDGAR 30 km outer domain (a), WRF-Chem HTAP 30km outer domain (b), WRF-Chem HTAP 10 km nested domain (c) and time series comparisons for daily PM<sub>10</sub> concentration (d). Red dashed lines show European Commission daily PM<sub>10</sub> standard ( $50 \mu\text{g}/\text{m}^3$ ).

Figures 3.3a, b and c show the scatterplots for comparison of individual daily ground observations to the WRF-Chem HTAP outer domain (30km), WRF-Chem HTAP nested domain (10km), and WRF-Chem EDGAR outer domain (30km), respectively. Each color in the scatterplot represents the number of data points falling into each

scatterplot bin. Both the 30 km and 10 km WRF-Chem HTAP runs overestimate the ground observations with observations minus model biases of  $-6.75 \mu\text{g}/\text{m}^3$  and  $-11.14 \mu\text{g}/\text{m}^3$ , respectively.

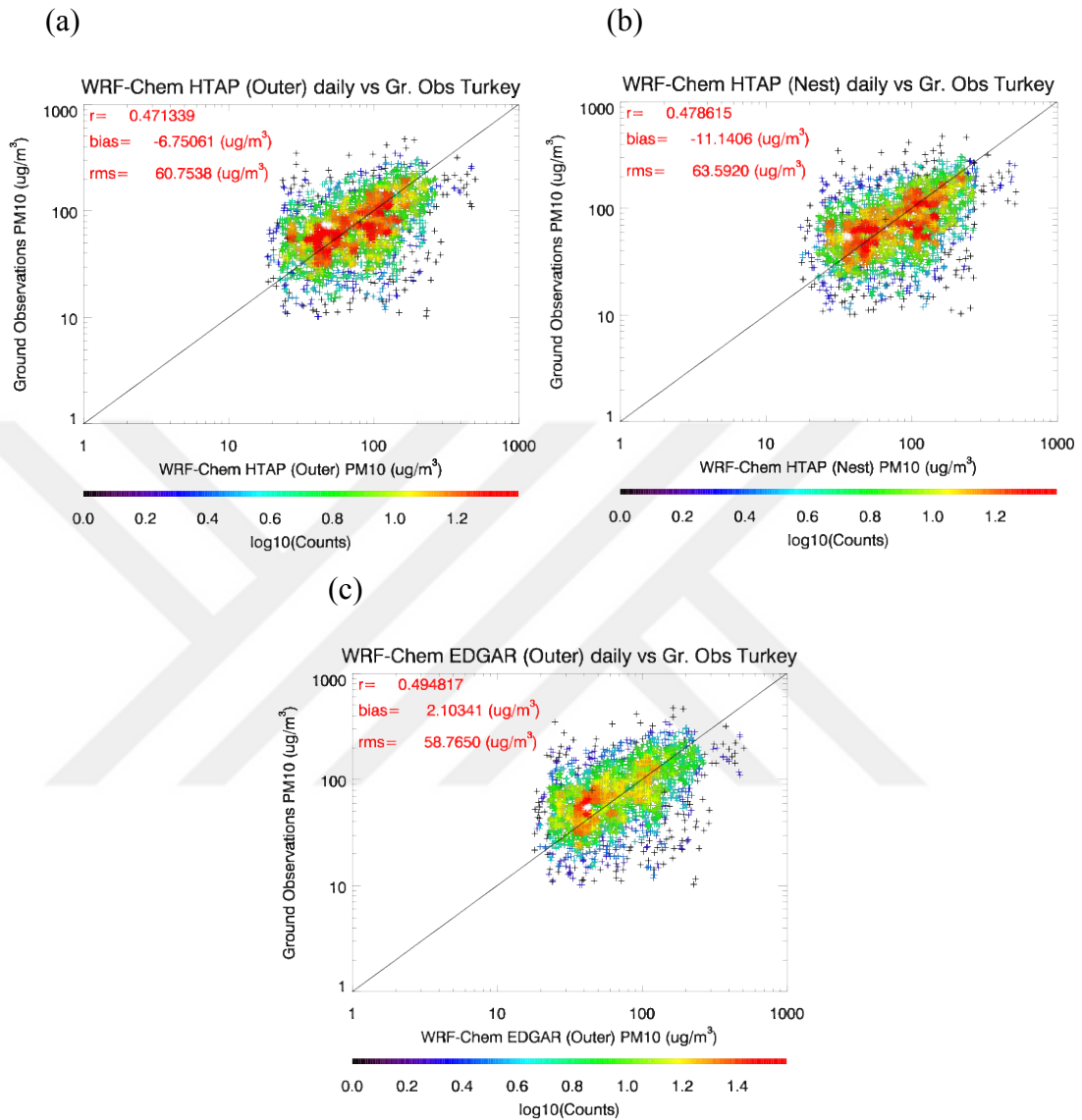


**Figure 3.3 :** Scatter plots for WRF-Chem HTAP outer (30 km horizontal resolution) (a), nested (10 km horizontal resolution) (b), and WRF-Chem EDGAR outer (30 km horizontal resolution) (c) runs, respectively.

The 30km WRF-Chem EDGAR run underestimates the ground observations with observations minus model biases of  $(2.10 \mu\text{g}/\text{m}^3)$ . Although the number of data points falling within each scatterplot bin is higher and along the linear line in HTAP runs, the correlation of both HTAP runs is slightly lower (0.471 for 30 km outer domain and 0.478 for the 10 km nested domain) than the 30km EDGAR run (0.494). WRF-Chem EDGAR run underestimates the frequency of relatively high observed  $\text{PM}_{10}$  values ( $>50 \mu\text{g}/\text{m}^3$ ). Root mean squared error (RMSE) of WRF-Chem EDGAR is smaller than

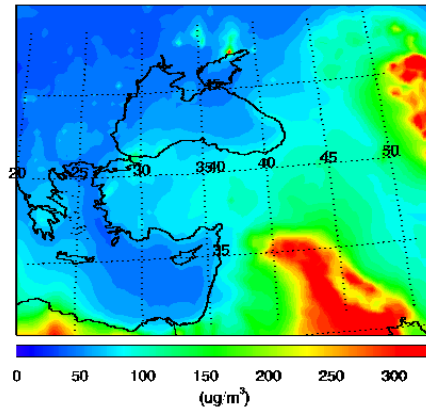
WRF-Chem HTAP 30km and 10km runs ( $58.7 \mu\text{g}/\text{m}^3$ ,  $60.75 \mu\text{g}/\text{m}^3$ ,  $63.59 \mu\text{g}/\text{m}^3$ , respectively). Using a higher resolution emission inventory leads to changes in biases from low values to higher values in different signs. That causes HTAP to overestimate the observations more than the EDGAR does. Higher resolution emission inventory adds more variance leading to the increase in RMSE values.

Correlations between ground observations from all 118-ground stations and the WRF-Chem HTAP 10km nested run is found to be 0.48 when dust fraction is over 50% and 0.247 when the dust fraction is less than 50%. Correlations between ground observations and WRF-Chem HTAP 30km run is found to be 45% when the dust fraction is more than 50% and 31% when the dust fraction is less than 50%. For WRF-Chem EDGAR run, however, when dust is not the dominant aerosol (dust fraction is less than 50%), the correlation between WRF-Chem EDGAR output to ground observations is found to be lower than 0.1 and when dust is the dominant aerosol the correlation between the model outputs and the ground observations are found to be 0.49. This points out that, the higher resolution emission inventory HTAP improves the overall predictions compared to EDGAR results when the dust fraction is less than 50%, and among two HTAP runs (30km and 10km), the WRF-Chem 10km HTAP run cannot adequately predict the  $\text{PM}_{10}$  that is associated with the local emissions especially when dust is not the dominated aerosol as well as explains the high RMSE results for 10km HTAP run (See Figure 3.3b).

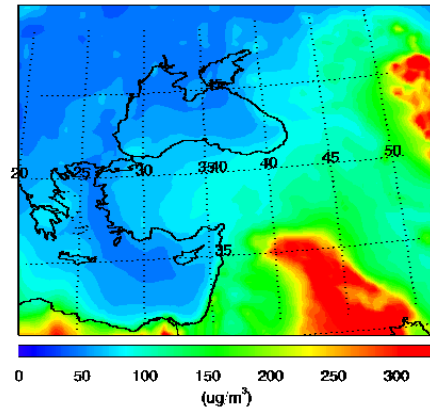
In order to understand the impact of utilizing two different anthropogenic emission inventories, monthly mean surface  $\text{PM}_{10}$  concentrations of HTAP run, EDGAR run, and the difference between HTAP and EDGAR runs are plotted for April 2008 and shown in Figure 3.4. In the figure, the upper left panel shows the monthly mean  $\text{PM}_{10}$  concentration of the WRF-Chem HTAP (Outer) run, upper right panel shows the monthly mean  $\text{PM}_{10}$  concentration of the WRF-Chem EDGAR (Outer) run, lower left panel shows the difference between the two runs (HTAP–EDGAR).

Although the monthly mean predictions from both runs show similar concentrations to each other over Turkey with higher values in the eastern part of the country ( $\sim 150 \mu\text{g}/\text{m}^3$ ), and lower values in the western part of the country ( $\sim 70 \mu\text{g}/\text{m}^3$ ), the difference map indicates that HTAP run suggest  $\sim 50 \mu\text{g}/\text{m}^3$  higher  $\text{PM}_{10}$  predictions than EDGAR run, especially in the western and northwestern part of Turkey, where the most industrialized zones are located (i.e. Istanbul, Izmir, Kocaeli).

WRF-Chem 30KM HTAP Surface Monthly PM10 (APRIL 2008)



WRF-Chem 30KM EDGAR Surface Monthly PM10 (APRIL 2008)



WRF-Chem 30KM HTAP and 30KM EDGAR Differences of Surface Monthly PM10 (APRIL 2008)

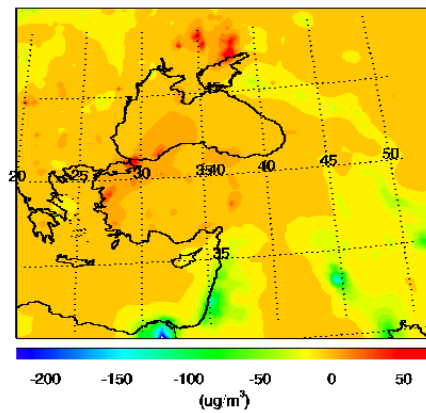
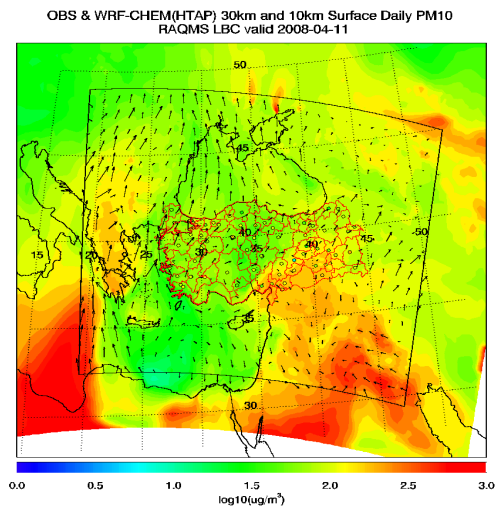


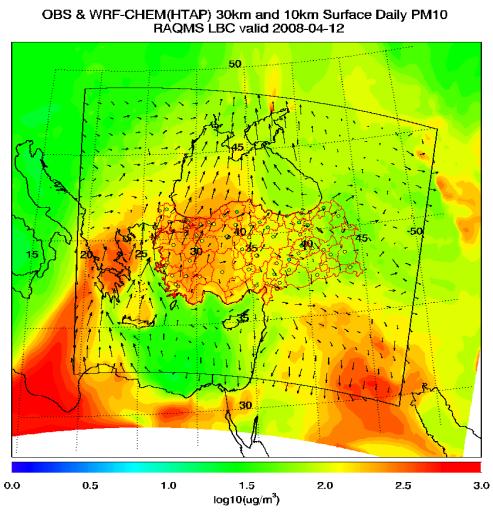
**Figure 3.4 :** Surface monthly PM<sub>10</sub> Concentration for April 2008 from HTAP (upper left panel), EDGAR (upper right panel) and difference between HTAP and EDGAR (lower left panel).

Model results can be used to understand the aerosol transport during the dust event as can be seen from Figures 3.5a-h for both WRF-Chem HTAP outer (30km horizontal resolution) and nested (10km horizontal resolution) domains for April 11-18, 2008 in order to include high PM<sub>10</sub> event days. During the high dust event that occurred on April 14, 2008 (Figure 3.5d), WRF-Chem HTAP nested run shows higher daily surface aerosol concentrations ( $\sim 2.3 \log_{10}$  or  $200 \mu\text{g}/\text{m}^3$ ) than the daily mean ground observations (colored circles,  $\sim 170 \mu\text{g}/\text{m}^3$ ) for the same day, while during the low dust event that occurred on April 17, 2008 (Figure 3.5g), WRF-Chem HTAP nested shows lower ( $\sim 1.56 \log_{10}$  or  $37 \mu\text{g}/\text{m}^3$ ) values than the measured surface aerosol concentrations ( $\sim 53 \mu\text{g}/\text{m}^3$ ). Saharan dust dominates the whole region when it is transported from North Africa over the Mediterranean Sea to Turkey with surface values around  $250 \mu\text{g}/\text{m}^3$  ( $\sim 2.4 \log_{10}$ ) throughout the high dust event episode (11-18 April 2008). During the dust event starting on April 11, 2008, dust is transported from North Africa over the Mediterranean Sea to Turkey from the southwest (Figure 3.5a).

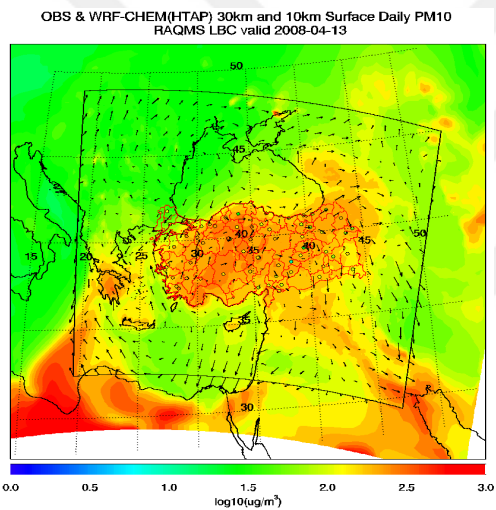
(a)



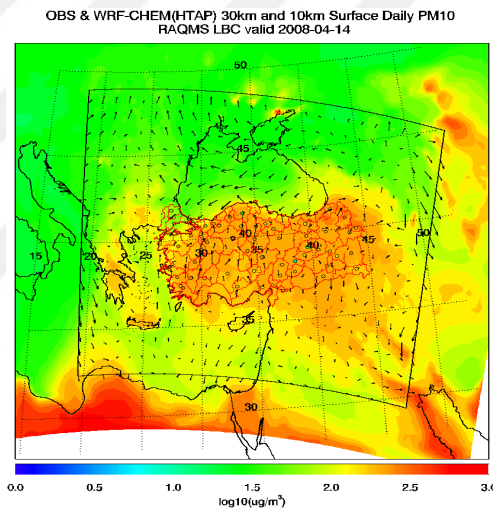
(b)



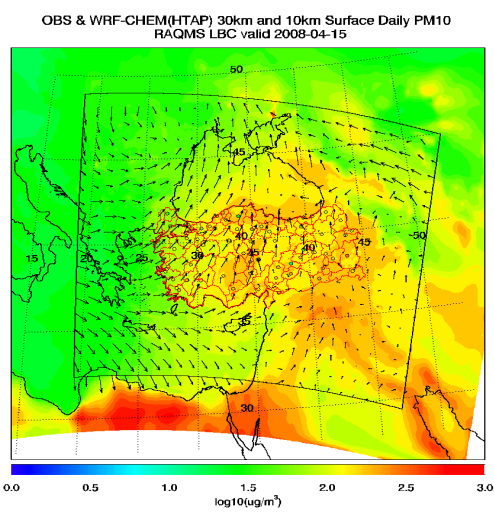
(c)



(d)



(e)



(f)

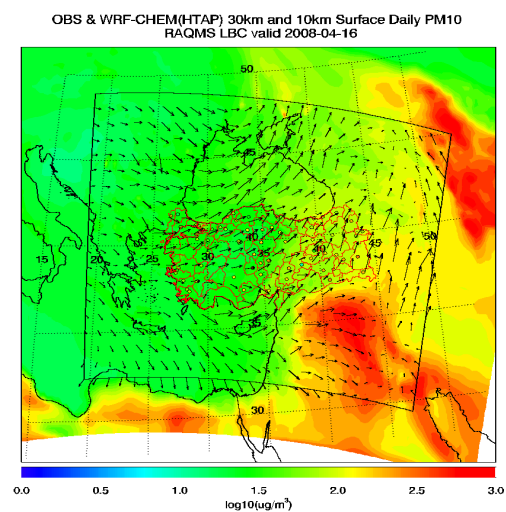
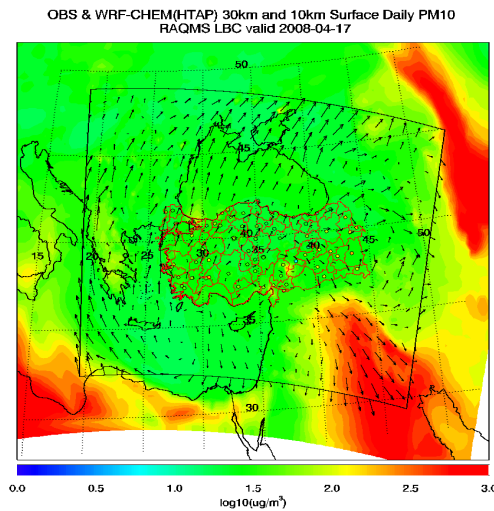


**Figure 3.5 :** WRF-Chem HTAP daily output for outer and nested domain with ground observations (colored circles) for April 11-18, 2008 (a-h, respectively) episode. Surface wind vectors are shown in black arrows.

(g)



(h)

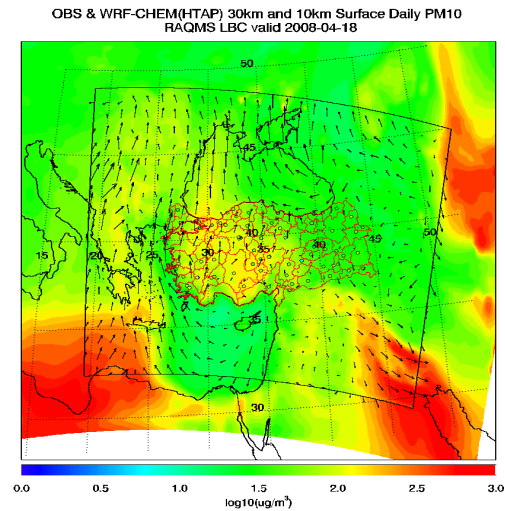


**Figure 3.5 (continued)** : WRF-Chem HTAP daily output for outer and nested domain with ground observations (colored circles) for April 11-18, 2008 (a-h, respectively) episode. Surface wind vectors are shown in black arrows.

For the first few days (between the dates of April 11-14, 2008), dust intrusions affect the western part of Turkey as well as southern Italy and southeastern Balkans (Figure 3.5a-d). For the rest of the episode, after April 15, 2008, the Saharan dust cloud covers Turkey, moving towards eastern part of Turkey by the end of the episode.

Clean air is transported from the northwest into the region towards the end of the episode (starting on April 16, 2008) showing that the region was influenced by relatively clean continental air (Figure 3.5f-g).

Figure 3.6 shows average lateral boundary conditions for dust during the episode represented above (11-18 April, 2008) for the 10 km-nested run for each boundary of the domain (south, north, west and east) in order to understand the impact of dust that is transported from 30km domain into the nest domain.

Dust is transported into the nested domain from the southwest with average value of  $\sim 300 \mu\text{g}/\text{m}^3$  during this episode (11-18 April, 2008). Over Turkey, average dust concentration is around  $150 \mu\text{g}/\text{m}^3$  for the same episode (11-18 April 2008).

The dust cloud reaches up to 6 km in the southwest part of the domain and is then transported over Turkey which is much better agreement with CALIPSO observations (see Figure 2.7). This also shows that utilizing a higher resolution (30km and 10km) WRF-Chem model performs better than the 2x2 degree global RAQMS analysis (see Figure 2.8).

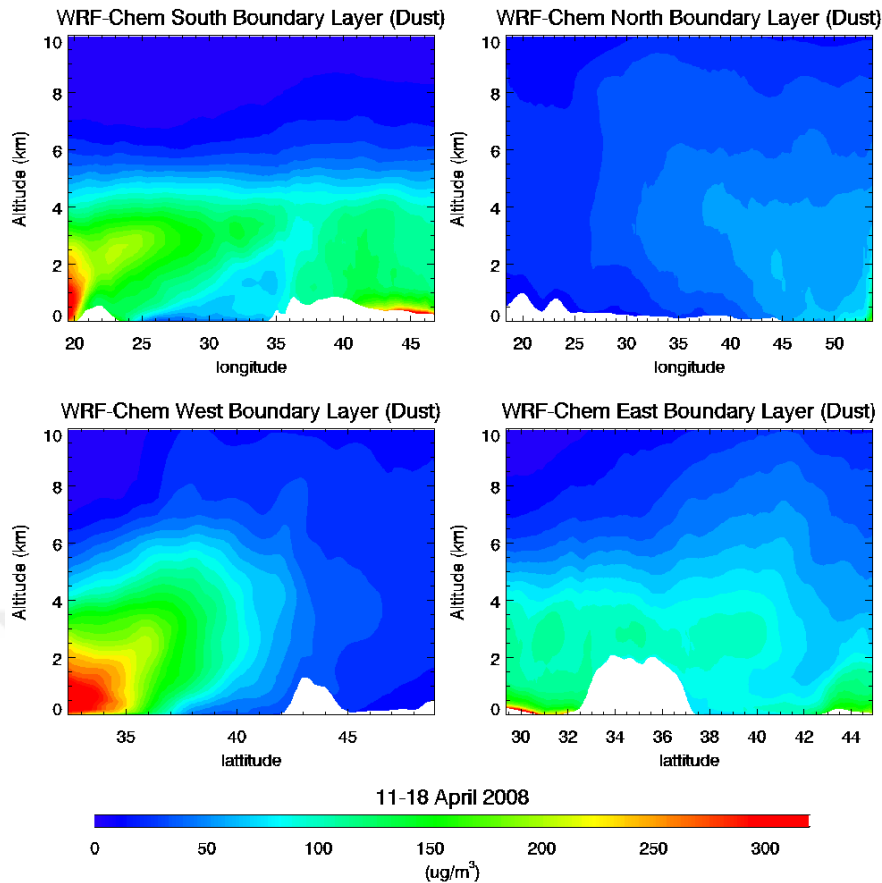


**Figure 3.6 :** Lateral boundary conditions obtained from RAQMS for south, north, west and east directions for WRF-Chem HTAP 10km nested domain.

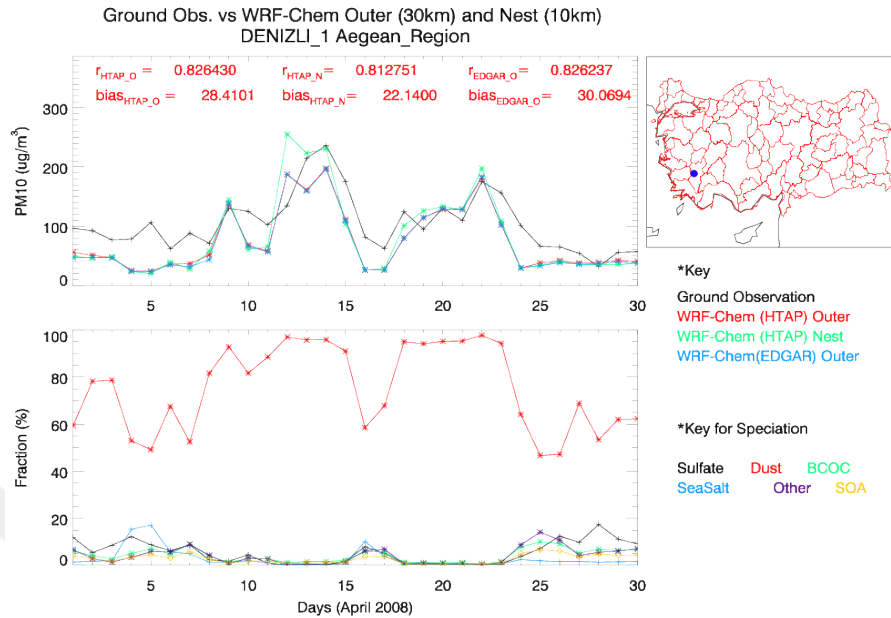
### 3.3 Discussion of the WRF-Chem Experiment

Figures 3.7a and 3.7b show two different stations located in the western part of Turkey. Station Denizli is located in the southwestern part of Turkey at  $37.77^\circ\text{N}$ ,  $29.04^\circ\text{E}$  and was chosen due to having high daily mean  $\text{PM}_{10}$  concentrations ( $236 \mu\text{g}/\text{m}^3$ ) on the high dust event day (April 14, 2008). Station Kocaeli Dilovasi, which is located in the northwestern part of the country ( $40.77^\circ\text{N}$ ,  $29.52^\circ\text{E}$ ) (Figure 3.7b), was chosen due to its location within one of the most industry-based and polluted zones of Turkey with a share of industry in Gross National Product of 73% (Hamzaoglu et al, 2011). Dilovasi, serves 45 different sectors including metal, chemistry and energy for 185 companies in total, and with its bowl shaped topography, tends to trap local emissions, leading to poor air quality in the region (Demiray et al, 2012). The upper panels of Figure 3.7a and b show the time series of ground observations (black), WRF-Chem HTAP outer domain with 30 km horizontal resolution (red), WRF-Chem HTAP nested domain with 10 km horizontal resolution (green), and WRF-Chem EDGAR outer domain with 30 km horizontal resolution (blue). The lower panels Figure 3.7a and b show aerosol



speciation for the WRF-Chem HTAP nested (10km) domain only for two different ground observation stations.

(a)



(b)



**Figure 3.7 :** Time series for ground observations, WRF-Chem HTAP outer (30km) (red) and nested (10km) (green) domains, and WRF-Chem EDGAR outer domain (30km) (blue) (upper panel); and AOD speciation for the WRF-Chem HTAP nested (10km) domain only (lower panel) for two different ground observation stations ((a) Denizli and (b) Kocaeli sites). Locations of both stations are shown on the map with a blue circle. HTAP\_O refers to WRF-Chem HTAP outer domain, HTAP\_N refers to WRF-Chem HTAP nested domain, and EDGAR\_O refers to WRF-Chem EDGAR outer domain in the upper panel. Key for speciation is given for the lower panel with each color representing different species.

For Denizli station, WRF-Chem HTAP and EDGAR outer domains have slightly higher correlation (both around 0.826) than WRF-Chem HTAP nested domain (0.812). WRF-Chem HTAP outer domain has slightly lower bias ( $28.4 \mu\text{g}/\text{m}^3$ ) compared to the WRF-Chem EDGAR outer domain ( $30.06 \mu\text{g}/\text{m}^3$ ) leading to a slightly better prediction of  $\text{PM}_{10}$ . Time series of ground observations and the model runs for Denizli station (Figure 3.6a, upper panel) show the similar patterns except for WRF-Chem HTAP nested domain. WRF-Chem HTAP nested domain has the lowest bias among all the runs with a value of  $22.1 \mu\text{g}/\text{m}^3$ , leading to an overestimation of surface  $\text{PM}_{10}$  values compared to the outer domains. The dominant aerosol type is found to be dust for this station as can be seen from the bottom panel of Figure 3.7a which shows the aerosol speciation for WRF-Chem HTAP nested domain (10km) only. When Saharan dust is transported over Turkey, it dominates the region for both EDGAR and HTAP runs. The Kocaeli station (Figure 3.7b), on the other hand, is located at one of the most polluted zones of Turkey and using two different emission inventories with different resolutions show a significant difference in terms of daily mean values of surface  $\text{PM}_{10}$  concentration and aerosol speciation.

Although the correlation between ground observations and WRF-Chem HTAP outer and nested domains are lower (0.59 and 0.48, respectively) than the WRF-Chem EDGAR outer domain (0.66), HTAP outer and nested domains ( $-11.12 \mu\text{g}/\text{m}^3$  and  $-13.06 \mu\text{g}/\text{m}^3$ , respectively) reduce the bias by  $50 \mu\text{g}/\text{m}^3$  comparing to the WRF-Chem EDGAR outer domain ( $42.02 \mu\text{g}/\text{m}^3$ ). Underestimation of WRF-Chem EDGAR outer domain can be seen in Figure 3.7b upper panel where WRF-Chem HTAP outer and nested domains show a better agreement of predicting surface  $\text{PM}_{10}$  concentrations.

For both of the stations, during the high dust event on April 14 when the maximum  $\text{PM}_{10}$  concentration was observed throughout Turkey, dust is found to be the dominant aerosol species, while during the low dust event days such as April 16 and April 17 the dominant aerosol is found to be a combination of sea salt, sulfate and other primary aerosol for Kocaeli station (Figure 3.7b, lower panel).

At each site, for WRF-Chem EDGAR run when the model predicts low values the model results tend to be lower than ground observations. These underestimates are most likely due to underestimates of local anthropogenic emissions. This points to issues with using the relatively coarse resolution anthropogenic emissions to represent local emissions within the domain. At Denizli station where anthropogenic emissions

are lower than the dust emissions, all models result show similar patterns to each other, on the other hand, at Kocaeli station, where the anthropogenic effect is more dominant; WRF-Chem HTAP results show better prediction and speciation of PM<sub>10</sub> concentration. The higher resolution emission inventory HTAP improves the overall predictions compared to EDGAR results, and among two HTAP runs (30km and 10km) when the dust fraction is less than 50%, WRF-Chem HTAP 30km domain better predicts the local emissions better than HTAP 10km domain.

Emission inventories are the basic input and also a major source of error to atmospheric chemical transport model results. Those errors may be due to the inherent uncertainty and the selection of representative emission factors for a given area (Markakis et al, 2012). In their study, Russel and Denise (2000) discussed the strengths and weaknesses of air quality models. They tried to address the level of uncertainty in air quality model predictions resulting from using different emission inventories but the same meteorology. They stated the major uncertainties are due to the model input that was being processed rather than the model itself. They indicated that the emission inventories were mainly based on a local source and then allocated over the domain causing sub-grid-scale fluctuations, which means emission inventories were not accurately resolved at the same scale as the model. In their study, Im et al. (2014), simulated major gaseous and particulate pollutant levels over Europe in 2008 and compared the results with surface observations from the EMEP stations. It is shown that the lack of representation of both anthropogenic and natural emissions in northern and southern Europe result in significant differences for those regions in the model performance. In another study that was done for Europe, the differences between ground observations and results of the CALIOPE air quality modelling system with a 12 km horizontal resolution were attributed to uncertainties in the chemical speciation of primary pollutants in the emission inventory (Basart et al, 2012). The parameters that affect the accuracy of emissions in Turkey are listed by Markakis et al. (2012) who point to the lack of emission factors mainly for the local emissions and the lack of temporal profiles.



## 4. WRF-CHEM MODIS ASSIMILATION EXPERIMENT

In this chapter, WRF-Chem model with aerosol data assimilation (DA) is utilized with the same model configuration of the previous WRF-Chem study (Chaper 3). The NOAA Gridpoint Statistical Interpolation (GSI) data analysis system is used to assimilate Moderate Resolution Imaging Spectoradiometer (MODIS (collection 6)) Terra aerosol optical depth (AOD) retrievals over the region for April 2008 in order to see the consistency of aerosol DA within this multi-nested modeling framework. Real-time Air Quality Modeling System (RAQMS)  $2^{\circ} \times 2^{\circ}$  global analyses are used to provide the LBC for two 30km runs with and without GSI aerosol DA (Hereafter 30km\_Assim or 30km\_Control). The 30km\_Assim run was then used to provide LBC for two higher resolution (10km horizontal resolution) nested runs to further improve the representation of complex topography and explore the effects of model resolution on aerosol DA. 10km runs are utilized with and without DA (Hereafter 10km\_Assim and 10km\_NoAssim, respectively). This is the first WRF-Chem MODIS DA study investigating natural dust influences on air quality in Anatolian peninsula.

### 4.1 Data Description

#### 4.1.1 Data assimilation GSI/3D-VAR and calculating background error covariances

GSI is unified 3D variational (3DVAR) data assimilation (DA) tool for both global and regional applications that is used at the National Centers for Environmental Prediction (NCEP) (Kleist et al, 2009). 3DVAR system calculates the best fit analysis based on irregularly spaced point observations and a gridded background field which can be taken from a short-term model forecast (Schwartz et al, 2012). Therefore, the main task of 3DVAR technique is the minimization of the cost function (J), which measures the distance between observations and background (model first guess), given by equation (4.1)

$$J(x) = (x - x_b)^T \mathbf{B}^{-1} (x - x_b) + (y - H(x))^T \mathbf{R}^{-1} (y - H(x)) \quad (4.1)$$

In equation 4.1,  $x$  is the analysis vector,  $x_b$  is the forecast or background vector,  $y$  is an observation vector,  $B$  and  $R$  are the background and observation error covariance matrices,  $H$  is an observation operator which converts model variables to observation space. The background error covariance matrix  $B$  is a product of error variances and spatial correlation matrices. The observation covariance matrix  $R$  combines measurement and representativeness errors (Purser et al., 2003; Schwartz et al., 2012; Pagowski et al., 2014). A model may predict all the prognostic variables, but it only updates the analysis variables during DA (Schwartz et al., 2012). In our case, the updated analysis variables are 3D mass mixing ratios of the 14 GOCART aerosol module variables that is implemented within WRF-Chem at each grid point.

The Community Radiative Transfer Model (CRTM) (Han et al., 2006) is used to convert the aerosol mass mixing ratios to AOD (the  $H$  operator in Eq. 4.1) and currently only supports GOCART aerosol species, consequently satellite AOD can only be assimilated with the GOCART model background within GSI (Pagowski et al. 2014). Observation operator,  $H$ , also transforms predicted values to observations by interpolating model grid points to observations points (Schwartz et al., 2012).

The Community Radiative Transfer Model (CRTM), developed at the Joint Center for Satellite Data Assimilation, is primarily used to compute satellite radiance assimilation radiances from microwave and infrared sensors for operational weather forecasting at NOAA. It is extended to calculate MODIS AOD as input by using only aerosol profiles and this recent developed CRTM-AOD module is integrated with the GSI system. CRTM includes GOCART aerosol species profiles which consist of effective radii, refractive indices and standard deviations of each aerosol. The size distribution of aerosols within each bin size is accepted as logarithmic, the particles are assumed to be spherical and externally mixed (Liu et al., 2011; Pagowski et al., 2014).

Considering all those assumptions, Mie scattering code (van de Hulst, 1957) is applied to calculate the mass extinction coefficient for each aerosol type at a particular wavelength for each of the 14 aerosols species at all atmospheric layers in order to calculate column total AOD (Liu et al., 2011; Schwartz et al., 2011; Pagowski et al., 2014).

It is necessary to calculate background error covariance (BEC) statistics for each aerosol variable in order to apply 3DVAR algorithm. We use the same implementation of AOD DA with Liu et al. (2011) for the calculation of BEC statistics. We constrain

the 3-D mass concentration of 14 aerosol species including sulfate, hydrophobic and hydrophilic black carbon (BC1 and BC2, respectively), hydrophobic and hydrophilic organic carbon (OC1 and OC2, respectively), five dust bins ( $D_1$  : 0.2–2.0  $\mu\text{m}$ ;  $D_2$  : 2.0–3.6  $\mu\text{m}$ ;  $D_3$  : 3.6–6.0  $\mu\text{m}$ ;  $D_4$  : 6.0–12.0  $\mu\text{m}$ ; and  $D_5$  : 12.0–20.0  $\mu\text{m}$ ), and four sea salt bins ( $SS_1$  : 0.2–1.0  $\mu\text{m}$ ;  $SS_2$  : 1.0–3.0  $\mu\text{m}$ ,  $SS_3$ : 3.0–10.0  $\mu\text{m}$ ; and  $SS_4$ : 10.0–20.0  $\mu\text{m}$ ) (Pagowski et al., 2014). BEC for each species is calculated using National Meteorological Center (NMC) method (Parrish and Derber, 1992). Differences of 24 and 12 h 00:00 UTC WRF/Chem forecasts of the aerosol species during the month of April, 2008 are used to compute the aerosol BECs for both the 30km and 10km nests. 30km meteorological fields are initialized and LBC are obtained from 6 hourly NOAA NCEP GFS (Global Forecast System) analyses. 30km aerosol LBC are obtained from 6 hourly RAQMS 2x2 degree global analyses. Two nested domain (10km) experiments were designed to evaluate the impact of AOD DA on predicted  $\text{PM}_{10}$  concentrations over Turkey by using the same LBC obtained from 30km domain. Both 10km experiments used the same physical and chemistry options, but one experiment did not employ DA (10km\_NoAssim) and the other employed 3DVAR DA (10km\_Assim) that updated the 14 aerosol profiles of GOCART aerosol module.

#### **4.1.2 MODIS aerosol optical depth (AOD) retrieval product**

The MODIS is a twin sensor aboard NASA's Terra and Aqua satellites with the ability to characterize the spatial and temporal characteristics of the global aerosol optical depth fields. MODIS provides radiance measurements in 36 channels at three spatial resolutions: 250 m (2 channels), 500 m (5 channels), and 1 km (29 channels) from 0.41 to 15  $\mu\text{m}$  (410–1500 nm) (Remer et al., 2005). The MODIS aerosol algorithm consists of two different algorithms. Dark target algorithm derives aerosols over land and ocean (from both Aqua and Terra), which is what we used in our DA experiment, (Remer et al., 2005) while the deep blue algorithm derives aerosols over bright land surfaces (only available from Aqua) (Hsu et al., 2004; Sayer et al., 2013; Pagowski et al., 2014). MODIS retrieved aerosol characteristic was provided at seven wavelengths: 470, 550, 660, 870, 1240, 1630, and 2130 nm (Liu et al., 2011).

In our implementation, assimilated observations include the most recent release (collection 06) (Levy et al., 2013) of level 2 total AOD aerosol optical depth retrievals at 550 nm from MODIS on the Terra satellite. MODIS data come in HDF format at 5 min segments of the satellite's orbit. Each pixel corresponds to 10 km  $\times$  10 km

horizontal resolution at the surface. Since GSI requires observations in BUFR (Binary Universal Form for the Representation of meteorological data, Dragosavac, 2007) format, software is used to convert from HDF to BUFR for the GSI (Pagowski et al., 2014).

One of the major uncertainties in the MODIS AOD retrieval is cloud contamination. The main cloud contamination is unresolved residual cirrus clouds that can lead high biases in the retrieved AOD (Kaufman et al, 2005). To minimize cloud artifacts, we use a cloud fraction threshold of 30%. Pixels having cloud cover more than 30% are eliminated.

#### 4.2 Results of the WRF-Chem MODIS Assimilation Experiments

Figure 4.1 shows the time series comparisons for daily  $PM_{10}$  concentration of WRF-Chem 30km\_Assim (MODIS) with RAQMS-LBC and WRF-Chem 30km\_Control (HTAP) with RAQMS-LBC runs (Kabatas et al, 2016) to ground observations. WRF-Chem 30km assimilation run tends to increase the high values of  $PM_{10}$  concentration during the high dust event (11-15 April 2008) compared to WRF-Chem 30km Control run. For the rest of the episode, 30km\_Assim run shows slightly lower values than the 30km Control run. Both 30km runs lower the low values the observed  $PM_{10}$  concentration, while they overestimate the high observed  $PM_{10}$  values.

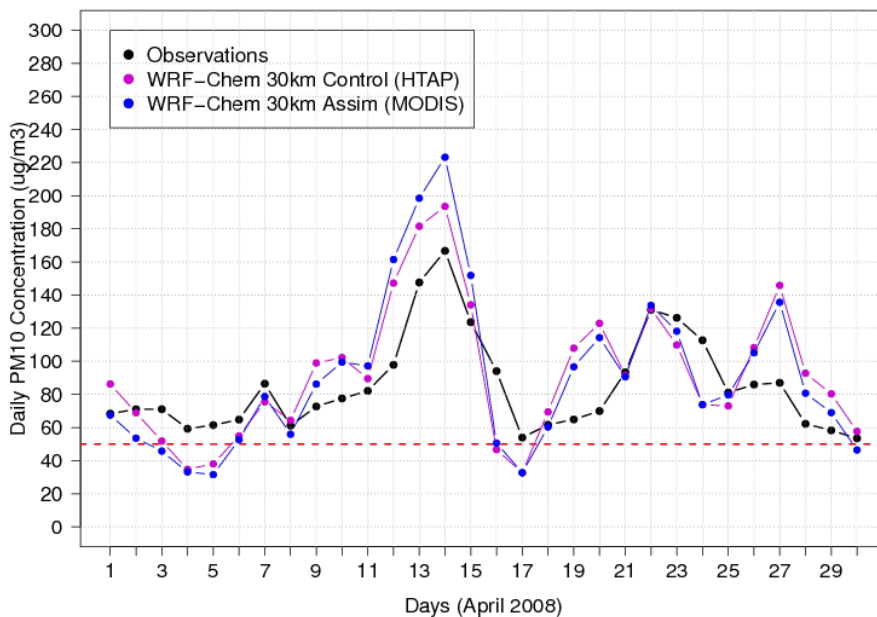


**Figure 4.1 :** Time series comparisons for daily  $PM_{10}$  concentration of WRF-Chem 30km\_Assim and WRF-Chem 30km\_Control runs (Kabatas et al, 2016) to ground observations.



Overall, two runs are consistent to each other as they capture same the pattern with the ground observations (Boxplot analysis of the ground observations can be seen from the figures 2.1 and 2.2).

WRF-Chem 30km\_Assim, WRF-Chem 10km\_NoAssim and 10km\_Assim box plot results are presented in Figures 4.2a, b and c, respectively. Lower and upper hinges of the boxplot represent 10<sup>th</sup> and 90<sup>th</sup> percentile of the data. Red dashed lines indicate the threshold of European Commission daily PM<sub>10</sub> standard (50 µg/m<sup>3</sup>). Red dots show the mean values and the horizontal line shows the median of the data. Figure 4.2d shows comparison of daily PM<sub>10</sub> concentration of ground observations, WRF-Chem 30km\_Assim, WRF-Chem 10km\_NoAssim and 10km\_Assim.

It can be seen that the both 10km and 30km model analysis captures the overall temporal evolution very well as it is consistent with the daily mean observations (Figure 2.2). However, among the two 10km nest experiments, the one that did not employ DA have slightly higher values than the one employed DA on the high dust event days. On April 14, when the high dust event occurred, all WRF-Chem runs tend to overestimate the values while they underestimate low PM<sub>10</sub> events on April 17 as well as the first few days of beginning of April 2008.

(a)

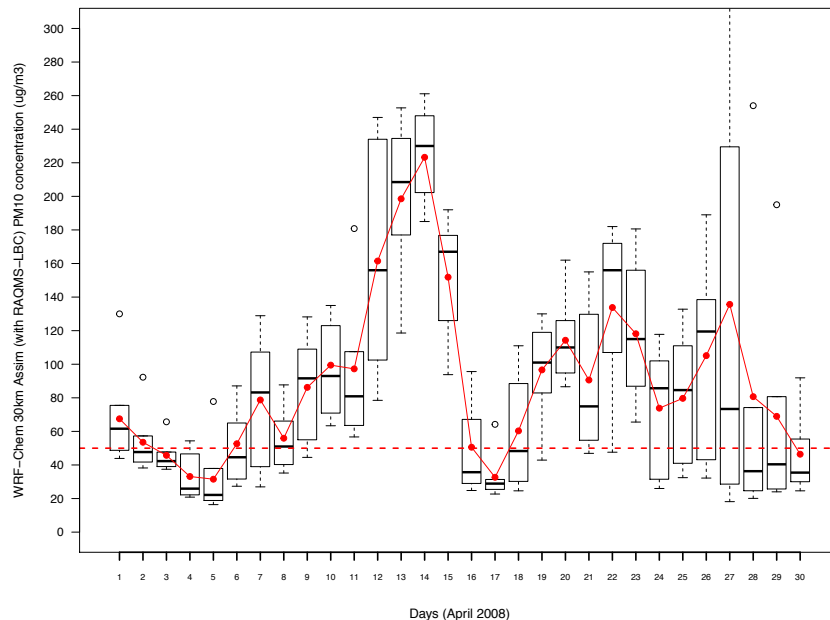
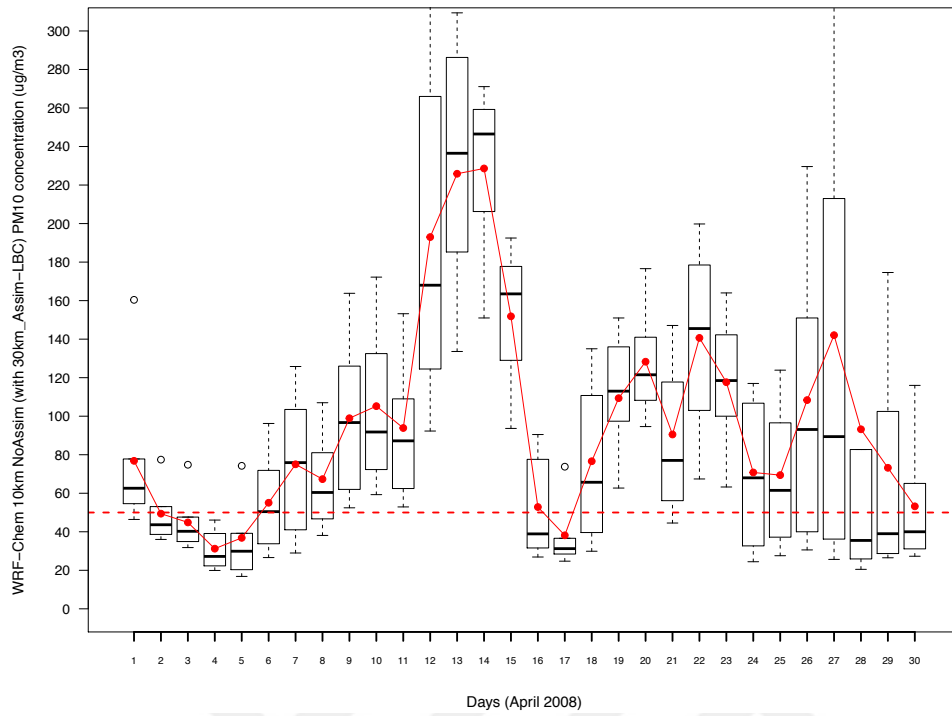


**Figure 4.2 :** WRF-Chem 30km\_Assim with RAQMS LBC (a), WRF-Chem 10km\_NoAssim with 30km\_Assim LBC (b), WRF-Chem 10km\_Assim with 30km\_Assim LBC (c) and time series comparisons for daily PM<sub>10</sub> concentration of three WRF-Chem runs and ground observations (d). Red dashed lines indicate the threshold of European Commission daily PM<sub>10</sub> standard (50 µg/m<sup>3</sup>).

(b)



(c)

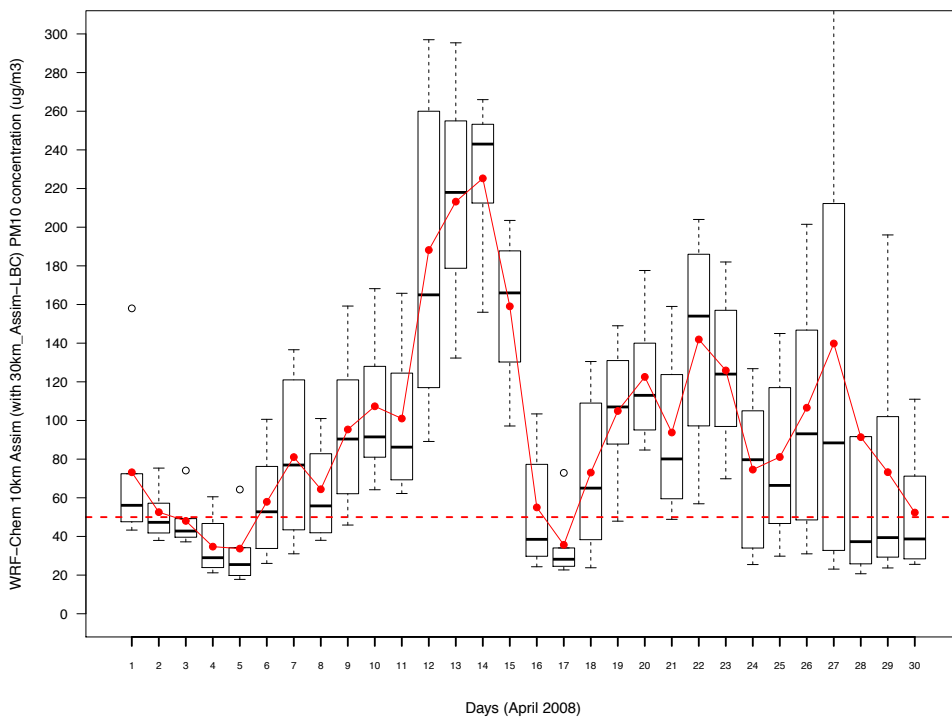


**Figure 4.2 (continued)** : WRF-Chem 30km\_Assim with RAQMS LBC (a), WRF-Chem 10km\_NoAssim with 30km\_Assim LBC (b), WRF-Chem 10km\_Assim with 30km\_Assim LBC (c) and time series comparisons for daily PM<sub>10</sub> concentration of three WRF-Chem runs and ground observations (d). Red dashed lines indicate the threshold of European Commission daily PM<sub>10</sub> standard ( $50 \mu\text{g}/\text{m}^3$ ).

(d)

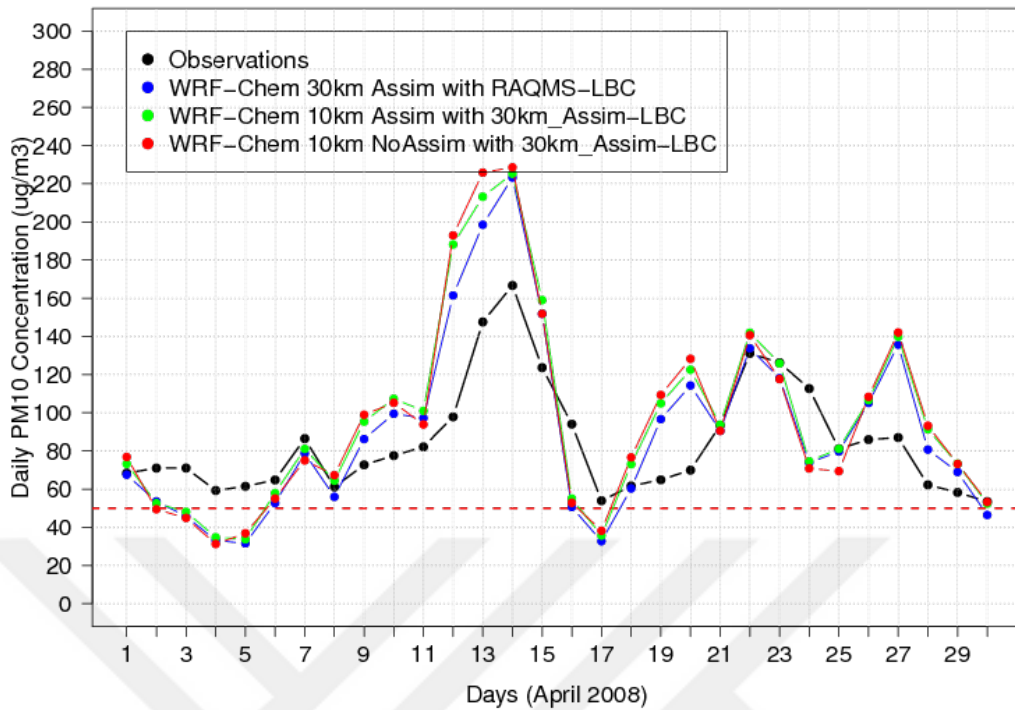


**Figure 4.2 (continued)** : WRF-Chem 30km\_Assim with RAQMS LBC (a), WRF Chem 10km\_NoAssim with 30km\_Assim LBC (b), WRF-Chem 10km\_Assim with 30km\_Assim LBC (c) and time series comparisons for daily PM<sub>10</sub> concentration of three WRF-Chem runs and ground observations (d). Red dashed lines indicate the threshold of European Commission daily PM<sub>10</sub> standard (50  $\mu\text{g}/\text{m}^3$ ).

Although all mean values obtained from ground observations show higher values than European Commission daily PM<sub>10</sub> standard (50  $\mu\text{g}/\text{m}^3$ ), model analyses during the episode is lower than this standard. When we compare average model outputs with the observation means, we find that both 10km (10km\_NoAssim and 10km\_Assim) analyses show higher level of variability in the PM<sub>10</sub> values compared to 30km\_Assim run. Among the 10km runs though, 10km\_NoAssim run show higher level of variability than the 10km\_Assim run. So, assimilation lowers the variability especially for the days on April 12<sup>th</sup>, 13<sup>th</sup>, 14<sup>th</sup> around the time when high dust event occurred.

Figures 4.3a, b and c show scatterplot comparisons of individual daily ground observations to the 30km\_Assim with RAQMS LBC, the WRF-Chem 10km\_Assim with 30km\_Assim LBC, and the WRF-Chem 10km\_NoAssim with 30km\_Assim LBC runs, respectively. All runs overestimate the ground observations with observations minus model biases of -5  $\mu\text{g}/\text{m}^3$ , -10  $\mu\text{g}/\text{m}^3$ , and -11  $\mu\text{g}/\text{m}^3$  for 30km\_Assim, 10km\_NoAssim and 10km\_Assim runs, respectively. The number of data points falling within the maximum density bin is higher in 10km\_NoAssim, yet the correlation of

10km\_NoAssim run to ground observations is slightly lower (0.504) than 30km\_Assim and 10km\_Assim runs (0.523 and 0.527, respectively).

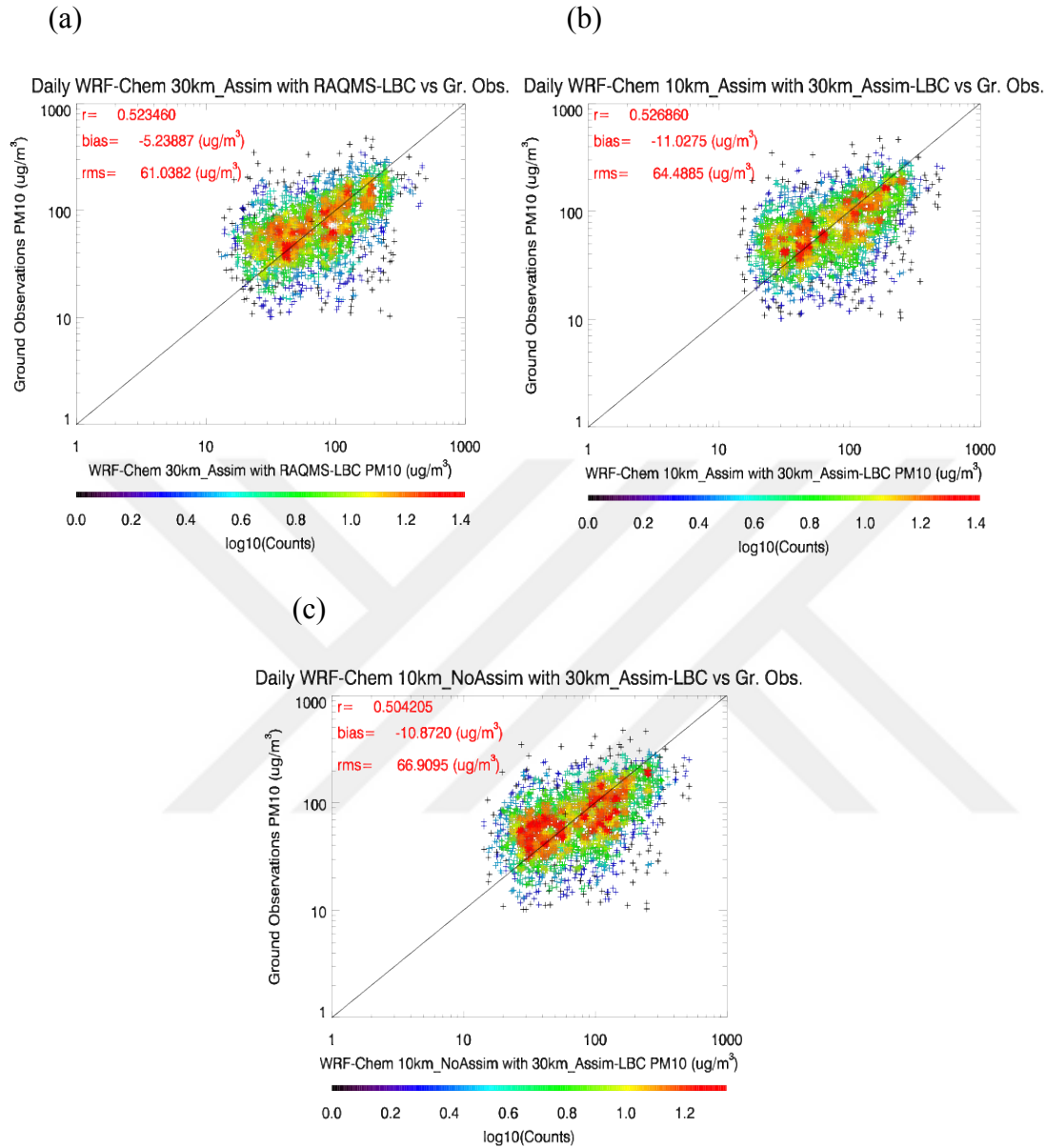


**Figure 4.3:** Scatter plots for WRF-Chem 30KM\_Assim with RAQMS-LBC (a), for WRF-Chem 10km\_Assim with 30km\_Assim-LBC (b), and WRF-Chem 10km\_Assim with 30km\_NoAssim-LBC (c) runs, respectively.

Although the correlation between 30km\_Assim and 10km\_Assim runs to ground observations are almost the same, 10km\_Assim lowers the bias by slightly overestimating the frequency of relatively high observed  $\text{PM}_{10}$  values (This can be seen from Figure 4.2d as well). Root mean squared (RMS) error of 30km\_Assim is smaller than 10km\_Assim and 10km\_NoAssim runs ( $61.04 \mu\text{g/m}^3$ ,  $64.49 \mu\text{g/m}^3$ ,  $66.91 \mu\text{g/m}^3$ , respectively) indicating a better agreement with observations compared to the higher resolution nested runs.

### 4.3 Discussion of the WRF-Chem Assimilation Experiments

Daily comparison of surface PM<sub>10</sub> measurements to model outputs shows that higher resolution domains (10km\_Assim and 10km\_NoAssim) overestimate daily surface mean PM<sub>10</sub> values more than lower resolution domain (30km\_Assim) for the high dust event days. Figure 4.4 shows the time series of the impact of aerosol DA expressed at PM<sub>10</sub> differences averaged over the surface sites for 30km runs (30km\_Assim minus 30km\_Control) (black line) and 10km runs (10km\_Assim minus 10km\_NoAssim) (red line).

Differences between the two 10km runs are generally smaller than the two 30km runs, particularly around the high dust event days (14 April  $\pm$ 2 days). For example, on April 1, where the difference between assimilation and control runs for both 30km and 10km are both negative, the difference between two 10km runs (10km\_Assim and 10km\_NoAssim) is  $\sim$ -5  $\mu\text{g}/\text{m}^3$ , where the difference between two 30km runs (30k\_Assim and 30km\_Control) is  $\sim$ -20  $\mu\text{g}/\text{m}^3$ . On April 13, where the 30km and 10km differences are the opposite sign, the difference between two 10km runs is  $\sim$ -13  $\mu\text{g}/\text{m}^3$ , which is the highest difference between the two 10km runs. For the same day, the difference between the two 30km runs is  $\sim$ 18  $\mu\text{g}/\text{m}^3$ .

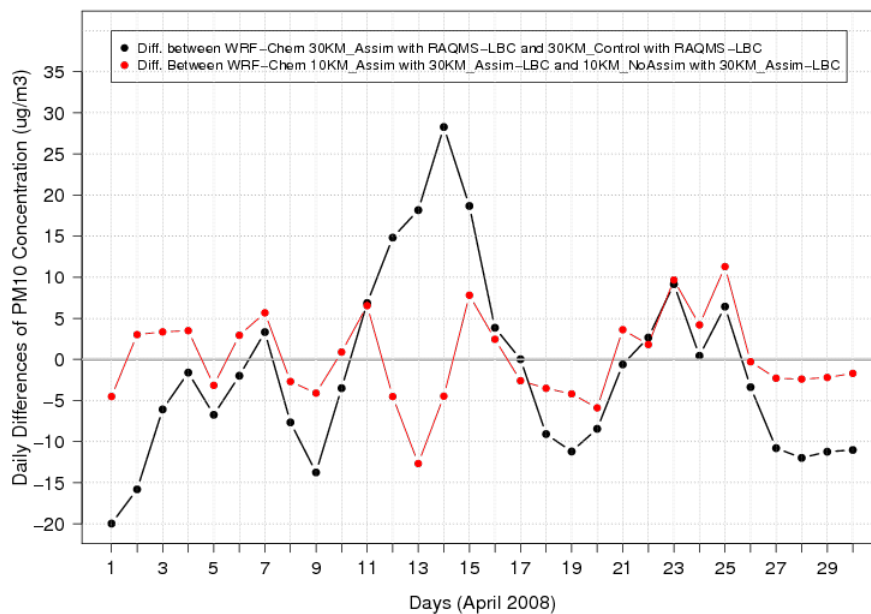


**Figure 4.4 :** Timeseries of PM<sub>10</sub> differences averaged over the sites for 30km runs (30km\_Assim and 30km\_Control) and 10km runs (10km\_Assim and 10km\_NoAssim).

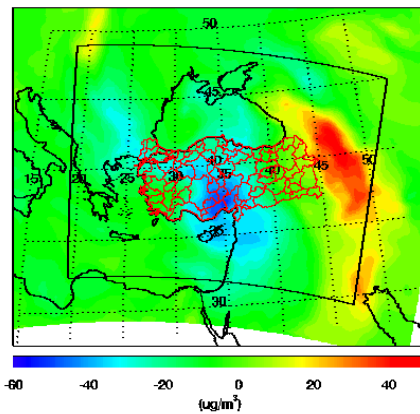
In their study, Tang et al. (2007) stated that LBC is a major contributor to uncertainty in the regional air quality models. In mesoscale atmospheric models, such as WRF-

Chem, global models are being used to obtain the LBC in order to import the influence of external forcings. Although the use of global model LBCs can improve regional air quality predictions, due to the uncertainties in the global models, differences in model formations (i.e. chemical mechanisms) and the horizontal resolution changes between the global and the regional models, additional uncertainties are introduced. The RAQMS model that we used to obtain LBC for 30km WRF-Chem domain uses the same chemical mechanism as the WRF-Chem run utilized in this study, yet coarse resolution of RAQMS might add uncertainties within the 30km resolution regional model. In order to explore differences in aerosol AOD assimilation between the high resolution domain (10km) and the 30km runs, we have interpolated 30km\_Assim run to the 10km grid (hereafter 30km\_Assim) and calculated the differences between 30km\_Assim and 10km\_NoAssim run to further investigate the consistency of the aerosol assimilation at different resolution domains.

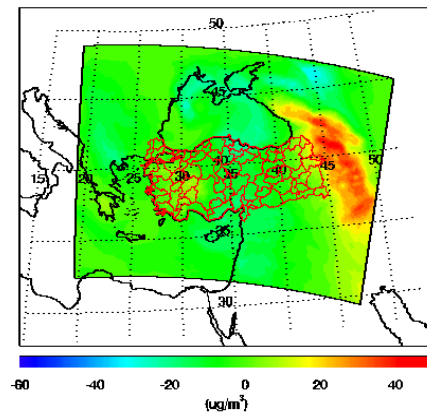
Figure 4.5 upper left panel shows the daily surface PM<sub>10</sub> differences of the two 30km runs (30km\_Assim and 30km\_Control), upper right panel shows the differences between the two 10km runs (10km\_Assim and 10km\_NoAssim) and the difference between 30km\_Assim interpolated to the 10km grid and 10km\_NoAssim is shown in the lower left panel for April 1, 2008. Differences between 30km\_Assim and 30km\_Control run are  $\sim -50 \mu\text{g}/\text{m}^3$  over the central and the northwestern part of Anatolia on April 1, 2008, which indicates that AOD assimilation has lowered surface PM<sub>10</sub> compared to the 30km\_Control run (As also can be seen from Figure 4.1).

In the eastern part of the domain, the difference increases up to  $\sim 50 \mu\text{g}/\text{m}^3$  indicating that AOD assimilation has increased surface PM<sub>10</sub> compared to the 30km\_Control run. Over the central Anatolia, 10km runs show smaller differences (between  $-10$  to  $+10 \mu\text{g}/\text{m}^3$ ) than found in the 30km experiments (This can be seen from Figure 4.4 as well). For the eastern part of the domain, the difference between 10km runs shows the same pattern as in 30km differences with higher values in the 10km assimilation run. The difference between 30km\_Assim and 10km\_NoAssim in the central part of Turkey is  $\sim -20 \mu\text{g}/\text{m}^3$  which results from the 30km\_Assim having lower predictions than 10km\_NoAssim, while it is  $\sim 30 \mu\text{g}/\text{m}^3$  in the eastern of the Anatolia, indicating 30km\_Assim has higher predictions than the 10km\_NoAssim run. The difference between 10km\_NoAssim and 30km\_Assim is larger than the difference between two 10km runs, which are almost the same over the Central Anatolia.

WRF-Chem 30KM\_Assim with RAQMS-LBC and 30KM\_Control with RAQMS-LBC Differences of Surface Daily PM10 2008-04-01



WRF-Chem 10KM\_Assim with 30KM\_Assim-LBC and 10KM\_NoAssim with 30KM\_Assim-LBC Differences of Surface Daily PM10 2008-04-01



WRF-Chem 30KM\_Assim Interp. over 10KM Grid and 10KM\_NoAssim with 30KM\_Assim-LBC Differences of Daily Surface PM10 2008-04-01

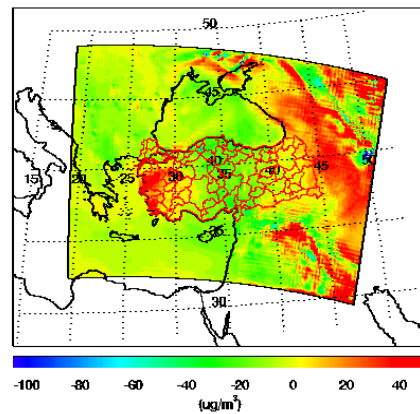
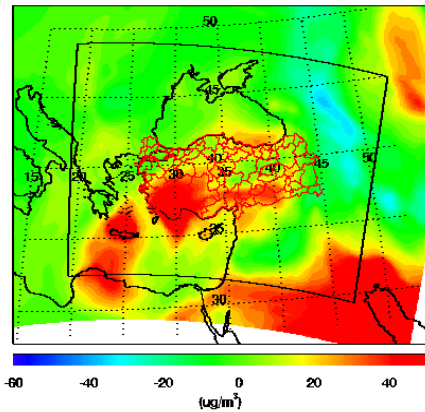


**Figure 4.5:** Difference of surface daily PM<sub>10</sub> concentration between 30km\_Assim with RAQMS-LBC and 30km\_Control with RAQMS-LBC (upper left panel), 10km\_Assim with 30km\_Assim-LBC and 10km\_NoAssim with 30km\_Assim-LBC (upper right panel), 30km\_Assim interpolation over 10 km grid and 10km\_NoAssim with 30km\_Assim-LBC (lower left panel) for April 1, 2008.

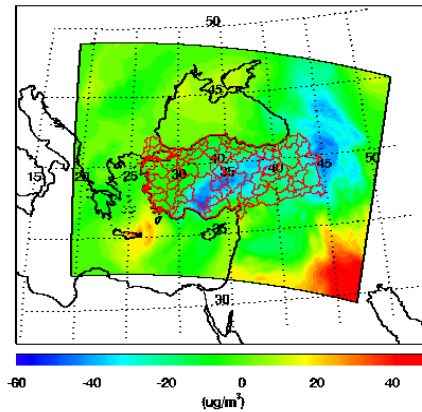
Due to higher resolution emissions introduced as the horizontal resolution increases, both 10km runs tend to predict higher values than the coarse resolution domain. However, among the 10km runs, the one that does not employ DA tends to increase it more whereas the run that employs DA tends to move the predictions back towards the surface PM<sub>10</sub> observations. In the eastern part, however, this influence is negligible since assimilation already predicts high values in 30km domain and again since 10km\_Assim corrects the 10km\_NoAssim predictions, the impacts of assimilation in the 30km domain and 10km domain tend to be similar.

Figure 4.6 shows the same difference maps for April 13, 2008 which is a high dust event day. In this case, the 30km run differences and 10km run differences averaged at the surface observation sites have the opposite signs ( $18 \mu\text{g}/\text{m}^3$  and  $-13 \mu\text{g}/\text{m}^3$ , respectively, see Figure 4.4).

WRF-Chem 30KM Assim with RAQMS-LBC and 30KM Control with RAQMS-LBC Differences of Surface Daily PM10 2008-04-13



WRF-Chem 10KM Assim with 30KM Assim-LBC and 10KM NoAssim with 30KM Assim-LBC Differences of Surface Daily PM10 2008-04-13



WRF-Chem 30KM Assim Interp. over 10KM Grid and 10KM NoAssim with 30KM Assim-LBC Differences of Daily Surface PM10 2008-04-13

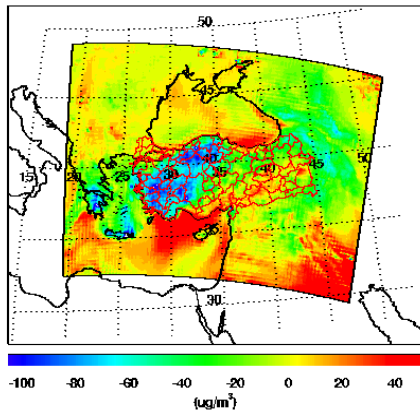


**Figure 4.6:** Difference of surface daily PM<sub>10</sub> concentration between 30km\_Assim with RAQMS-LBC and 30km\_Control with RAQMS-LBC (upper left panel), 10km\_Assim with 30km\_Assim-LBC and 10km\_NoAssim with 30km\_Assim-LBC (upper right panel), 30km\_Assim interpolation over 10 km grid and 10km\_NoAssim with 30km\_Assim-LBC (lower left panel) for April 13, 2008.

Differences between two 30km runs is  $\sim 40 \mu\text{g}/\text{m}^3$  indicating that AOD assimilation has increased surface PM<sub>10</sub> compared to the 30km\_Control run (Also see Figure 4.1). Differences between the two 10km runs tend to be negative meaning that AOD assimilation has decreased surface PM<sub>10</sub> compared to the 10km\_NoAssim run (See Figure 4.2d). The large negative differences between the 30km\_Assim run and 10km\_NoAssim shows that the 10km\_NoAssim run is much higher than the 30km\_Assim run over central Turkey on April 13. This is mainly because the assimilation enhances the dust transport affecting 30km domain on April 13, resulting in overestimation compared to surface observations. 30km domain then influences 10km domain by carrying this enhancement in through LBC and causing additional PM<sub>10</sub> over prediction in 10km domain. Since the difference between the two 10km runs is smaller than 30km\_Assim and 10km\_NoAssim, it can be said assimilation within



the 10km domain again tends to move the  $PM_{10}$  prediction closer to the observations within the 10km domain on high dust event day (See Figure 4.2d).

Schaap et al (2015) indicated the importance of grid resolution especially for the urban signal. Downscaling from a coarser domain to a finer one adds a lot of detail, and this causes an increase in high emission areas as the grid size decreases. In our experiment, the finer domain predicted higher values than the coarse one, and among the 10km runs, the one does not apply DA tends to have higher predicted values than the one that employed DA. Considering both 10km runs (10km\_Assim and 10km\_NoAssim) have the same LBC obtained from 30km\_Assim run, it can be stated that within the 10km domains, assimilation forces the predictions towards the surface observations on high dust event day with larger signal than the one on low dust event day due to effect of the local emitted components of surface  $PM_{10}$  (Figure 4.4).



## 5. CONCLUSIONS

In this study, we have utilized the atmospheric models to explain the possible effect of Saharan dust on high levels of  $PM_{10}$  measured in Turkey. First of all, we analyzed Real-Time Air Quality Modeling System (RAQMS) results, which is a unified, online global aerosol and chemistry assimilation and forecasting system that was run at  $2 \times 2$  degrees in order to quantify the impact of Saharan dust transport over Anatolian Peninsula in April 2008 (Kabatás et al, 2014). Observations show that  $PM_{10}$  levels change according to the time of the year. During the cold season, high  $PM_{10}$  levels are usually related to low boundary layer height and local pollution. In warm seasons, however,  $PM_{10}$  concentrations are reasonably lower than the cold season. Since Saharan dust outbreaks occur in the transition seasons, high levels of measured  $PM_{10}$  in April 2008 is thought to be related to Saharan dust outbreak. Satellite data is used for validation and Terra MODIS and Aqua MODIS agreed on high AOD values starting from the desert area moving over the Mediterranean Sea, and finally to Turkey.

Dust is found to be the major component of the overall  $PM_{10}$  concentration calculated from RAQMS output (96.6% of total  $PM_{10}$  concentration simulated via RAQMS is due to dust load). Daily averages of surface level  $PM_{10}$  concentrations at the Turkey ground sites are obtained from RAQMS to compare with in situ observations. The results suggest a significant contribution of Sahara dust to high levels of  $PM_{10}$  in Turkey with RAQMS and in situ time series showing similar patterns. The two data sets are found to be in agreement with a correlation coefficient of 0.87, although RAQMS over predicts the surface  $PM_{10}$  up to a factor of 5. Comparisons between CALIPSO, RAQMS and WRF along the CALIPSO track suggest that RAQMS underestimates aerosol lofting over Turkey due to a shallow surface inversion within the RAQMS model that is likely not present in the real atmosphere, as confirmed by a higher resolution WRF simulation. This underestimate in aerosol lofting leads to over estimates in surface  $PM_{10}$  concentrations.

In order to overcome the deficiencies caused by the coarse resolution analysis, we utilized a higher resolution, online-coupled WRF-Chem system to investigate spatial

and temporal distribution of Saharan mineral dust transport over Eastern Mediterranean. The results are found to be significantly improved compared to the RAQMS study.

WRF-Chem version 3.5.1 was employed using the simple GOCART aerosol option and was configured to cover Eastern Mediterranean with 30 km horizontal resolution. RAQMS lateral boundary conditions were used for 30km run. The 30km run was then used to provide lateral boundary conditions for a second higher resolution (10km horizontal resolution) nested run to minimize the errors in representing complex topography.

For anthropogenic emission two different emission inventories used. EDGAR is used for 30 km (WRF-Chem EDGAR outer) horizontal resolution run only, in order to have a base line to see the difference between the two emission inventories, and HTAP emission inventory is used for both 30km (WRF-Chem HTAP outer) and 10 km (WRF-Chem HTAP nest) horizontal resolution domains. The correlations between ground observations to the WRF-Chem HTAP outer and nested domain runs are found to be 0.471 and 0.478, respectively, while the correlation between ground observations to the WRF-Chem EDGAR outer domain is found to be 0.494. Root mean square (RMS) errors are calculated as  $\sim 61 \mu\text{g}/\text{m}^3$  for WRF-Chem HTAP outer domain and  $\sim 64 \mu\text{g}/\text{m}^3$  for WRF-Chem HTAP nested domain. For WRF-Chem EDGAR outer domain, RMS is calculated to be  $\sim 59 \mu\text{g}/\text{m}^3$ . Although EDGAR run has lower RMS indicating to a better fit comparing to HTAP runs, it underestimates the ground observations. Introducing higher emission inventory within the model results in WRF-Chem HTAP outer and nested domains to have lower bias ( $-6.7 \mu\text{g}/\text{m}^3$  and  $-11.1 \mu\text{g}/\text{m}^3$ , respectively) than WRF-Chem EDGAR outer domain ( $2.1 \mu\text{g}/\text{m}^3$ ).

When dust is the dominant aerosol (dust fraction is more than 50%), the correlations between ground observations from all 118-ground stations and the WRF-Chem HTAP 30km, 10km and WRF-Chem EDGAR 30km runs are found to be 0.45, 0.48 and 0.49, respectively. When dust fraction is less than 50% correlations between the ground observations to the two HTAP 30km and 10km runs are found to be 0.31 and 0.25, while, the correlation between the observations to WRF-Chem EDGAR run is found to be 0.07. This shows that WRF-Chem HTAP runs can adequately capture local emissions that influence the ground observations better than WRF-Chem EDGAR run during periods of lower dust aerosol loading. Among two HTAP runs (30km and

10km), the WRF-Chem 30km HTAP run can better predict the PM<sub>10</sub> that is associated with the local emissions especially when dust is not the dominated aerosol than WRF-Chem HTAP 10KM run, which also explains the high RMSE results for 10km HTAP run.

A high dust event during April 11-18, 2008 was identified from ground observations and was investigated. The most dominant aerosol type for the episode is found to be dust, with other aerosols and sulfate as the second and third dominant aerosol types during periods with low surface aerosol concentrations, suggesting the transported dust cloud over Turkey dominates the whole region. According to the ground observations, the highest daily PM<sub>10</sub> concentration was observed on April 14, which can also be seen from both the 30 km and 10 km WRF-Chem forecasts. April 17 is the day when minimum mean daily PM<sub>10</sub> concentrations were observed and all model runs agree with this as well. All outer and nested model runs tend to increase the PM<sub>10</sub> concentration relative to observations during high events by 30 µg/m<sup>3</sup> and decrease the PM<sub>10</sub> concentration during periods of low PM<sub>10</sub> by 30 µg/m<sup>3</sup>.

Daily comparison of the both WRF-Chem EDGAR and HTAP 30km run and WRF-Chem HTAP 10km run to ground observations shows that the nested domain has an overall larger low bias than outer domains do, although the correlations between the runs and the ground observations are almost the same. In order to understand the differences between model and ground observations, two ground stations are chosen from the western part of Turkey to avoid eastern part's complex topography. Station Denizli is located at 37.77 °N, 29.04 °E, and is chosen due to having a high daily concentration of PM<sub>10</sub> (236 µg/m<sup>3</sup>) measured on the day when daily maximum PM<sub>10</sub> concentration was observed throughout Turkey.

The second station, Kocaeli Dilovası, is located at 40.77 °N, 29.52 °E and is chosen due to its being located within the most polluted zone of Turkey. At Denizli station, all model runs agreed with each other since dust is the dominant aerosol species. At Kocaeli station, however, other aerosols and sulfate aerosol were found to contribute to high levels of PM<sub>10</sub> concentration since this station is located within one of the most industry-based regions of Turkey. This contribution can be seen from the model forecast that utilized the higher resolution HTAP emission inventory. Among WRF-Chem HTAP runs, however, outer domain better represents the local emissions when dust is not a dominant aerosol than HTAP 10km domain. WRF-Chem EDGAR outer

domain cannot adequately capture local emissions that influence the ground observations which results in larger differences between model prediction and ground observations during periods of lower aerosol loading. The representativeness of the positioning of 118 ground-based air quality monitoring sites distributed in 81 cities of Turkey arises as well as the temporal and spatial resolution of the model emission inventories, which are not adequate to represent the local emissions. It showed that this deficiency can be improved by using a higher resolution emission inventories.

After identifying the effect of different emission inventories on quantification of PM<sub>10</sub> concentrations, satellite data assimilation is considered as a next step the consistency of the multi-scale modeling system. By using the same configuration that was used before for WRF-Chem experiment, we utilized NOAA Gridpoint Statistical Interpolation (GSI) data analysis system that is used to assimilate MODIS (collection 6) AOD retrievals over the region for April 2008. 30km and 10km runs are conducted with and without DA (30km\_Assim, 30km\_Control and 10km\_Assim, 10km\_NoAssim, respectively).

DA experiments showed that all WRF-Chem runs tend to overestimate the high PM<sub>10</sub> events (i.e. around April 14, 2008) while they underestimate the low PM<sub>10</sub> events and among all models, higher resolution 10km domains yield higher predicted surface PM<sub>10</sub> concentration than coarse 30km domain for high dust event days. Both 10km simulations show higher level of variability in the surface PM<sub>10</sub> values compared to 30km\_Assim run. Among the 10km runs, 10km\_NoAssim run shows higher level of variability than the 10km\_Assim run, which indicates that assimilation lowers the variability especially for the days when high dust event occurred.

All runs overestimate the ground observations with biases of  $-5 \mu\text{g}/\text{m}^3$ ,  $-10 \mu\text{g}/\text{m}^3$ , and  $-11 \mu\text{g}/\text{m}^3$  for 30km\_Assim, 10km\_NoAssim and 10km\_Assim runs, respectively. Correlations between the 10km\_NoAssim run to ground observations is found to be slightly lower (0.504) than 30km\_Assim and 10km\_Assim runs (0.523 and 0.527, respectively).

In order to understand the differences between the PM<sub>10</sub> forecast and assess the consistency between the 30km and 10km assimilation runs, we compared the impacts of assimilation in the 30km and 10km experiments at the surface observation sites. Based on the PM<sub>10</sub> differences averaged over the surface sites for 30km runs and 10km runs, April 1 and April 13, 2008 are chosen in order to further explore the consistency

of the aerosol assimilation at 30 and 10km resolution, and we compare the 30km\_Assim (interpolated to the 10km grid) to the 10km\_NoAssim experiment.

On April 1, over the central Anatolia, within the higher resolution domain, the predictions tend to increase due to the 30km\_Assim domain influence through the LBC. This increase in higher resolution domain is corrected by employing assimilation by moving the predictions towards the observations. For the eastern part of the domain on April 1, the impacts of assimilation are similar for the 30 and 10km experiments indicating LBC impact is small.

On April 13, when dust is the dominant aerosol, 30km\_Assim run shows higher PM<sub>10</sub> concentrations than the 30km\_Control run. The local emissions, as well as LBC from the 30km domain, add additional enhancements to 10km domain resulting large negative differences between 30km\_Assim and 10km\_NoAssim domains. Relatively small differences between the two 10km domains again shows that assimilation tends to move the 10km predictions closer to the surface observations during this high dust event.

This demonstrates that, in our study, although the nested domains tend to over predict the PM<sub>10</sub> concentrations comparing to the 30km domain, assimilation of satellite AOD retrievals moves the model forecasts towards the surface observations within the 10km resolution domains especially on high dust event days.

These results represented here are the first WRF-Chem/WRF-Chem DA study investigating natural dust influences (dust and anthropogenic impact together) on air quality in the Eastern Mediterranean, especially in Anatolian Peninsula. We tried to address the uncertainties in the atmospheric models caused by dust, and approaches presented here are useful tools in order to investigate dust impact on air quality, but many more challenges remain and need to be addressed in the follow-up studies. We hope this study will enlighten the future researches and help us to fully understand the characteristics of aerosols and their impact on air quality.





## REFERENCES

- Anderson, J. O., Thundiyil, J. G., and Stolbach, A.** (2012). Clearing the Air: A Review of the Effects of Particulate Matter Air Pollution on Human Health. *J. Med. Toxicol.*, 8, 166–175.
- Atkinson, R. W., Anderson, H. R., Sunyer, J., Ayres, J., Baxxini, M., Vonk, J.M., ...Katsouyanni, K.** (2001). Acute Effects of Particulate Air Pollution on Respiratory Admissions. *Am J Respir Crit Care Med*; 164, 1860–1866.
- Ayberk, H., Kucukosmanoglu, A., and Cebeci, H.** (2010). The structure and importance of fire suppressing organizations in Turkey. *Scientific Research and Essays*, 5 (5), 456-460.
- Baklanov, A., Schlünzen, K., Suppan, P., Baldasano, J., Brunner, D., Aksoyoglu, S., ...Zhang, Y.** (2014). Online coupled regional meteorology chemistry models in Europe: current status and prospects. *Atmos. Chem. Phys.*, 14, 317–398, doi:10.5194/acp-14-317-2014.
- Banks, J. R., Brindley, H. E., Flamant, C., Garay, M. J., Hsu, N. C., Kalashnikov, O. V., ...Sayer, A. M.** (2013). Intercomparison of satellite dust retrieval products over the west African Sahara during the Fennec campaign in June 2011. *Remote Sens. Environ.*, 136, 99–116.
- Basart, S., Pay, M.T., Jorba, O., Perez, C., Jimenez-Guerrero, P., Schulz, M., and Baldasano, J.M.** (2012). Aerosols in the CALIOPE air quality modelling system: evaluation and analysis of PM levels, optical depths and chemical composition over Europe. *Atmospheric Chemistry and Physics*, 12 (7), 3363–3392.
- Bellouin, N., and Haywood, J.** (2015). AEROSOLS, Climatology of Tropospheric Aerosols, *Encyclopedia of Atmospheric Sciences (Second edition)*, 40-47.
- Benedetti, A., Morcrette, J.J., Boucher, O., Dethof, A., Engelen, R.J., Fisher, M., ...Suttie, M.** (2009). Aerosol analysis and forecast in the ECMWF integrated forecast system: 2. Data assimilation. *J. Geophys. Res.*, 114, D13205.
- Bocquet, M., Elbern, H., Eskes, H., Hirtl, M., Žabkar, R., Carmichael, G. R., ...Seigneur, C.** (2015). Data assimilation in atmospheric chemistry models: current status and future prospects for coupled chemistry meteorology models. *Atmos. Chem. Phys.*, 15, 5325–5358.
- Bouchlaghem, K., Nsom, B., Latrache N., and Kacem, H. H.** (2009). Impact of Saharan dust on PM10 concentration in the Mediterranean Tunisian coasts. *Atmos. Res.*, 92, 531–539.
- Chen, D., Li, Q., Stutz, J., Mao, Y., Zhang, L., Pikelnaya, O., and Tsai, J.** (2013).

WRF-Chem simulation of NO<sub>x</sub> and O<sub>3</sub> in the LA Basin during CalNex 2010, *Atmos. Environ.*, 81, 421–432.

- Chen, S., Zhao, C., Qian, Y., Leung, L. R., Huang, J., Huang, Z., ...Li, J.** (2014). Regional modeling of dust mass balance and radiative forcing over East Asia using WRF-Chem, *Aeolian Research*, 15, 15-30.
- Chin, M., Rood, R. B., Lin, S. J., Müller, J. F., and Thompson, A. M.** (2000). Atmospheric sulfur cycle simulated in the global model GOCART: Model description and global properties, *J. Geophys. Res.*, 105, 24671–24687.
- Chin, M., Ginoux, P., Kinne, S., Torres, O., Holben, B. N., Duncan, B. N., ...Nakajima, T.** (2002). Tropospheric aerosol optical thickness from the GOCART model and comparisons with satellite and Sun photometer measurements, *J. Atmos. Sci.*, 59, 461–483.
- Chin, M., Ginoux, P., Lucchesi, R., Huebert, B., Weber, R., Anderson, T., ...Thornton, D.** (2003). A global aerosol model forecast for the ACE-Asia field experiment. *J. Geophys. Res.*, 108(D23), 8654, doi:10.1029/2003JD003642.
- Collins, W. D., Rasch, P. J., Eaton, B. E., Khattatov, B. V., Lamarque, J., and Zender, C. S.** (2001). Simulating aerosols using a chemical transport model with assimilation of satellite aerosol retrievals: Methodology for INDOEX, *J. Geophys. Res.*, 106 (D7), 7313– 7336.
- Communication From the Commission to the Council and the European Parliament.** (2006) Establishing an Environment Strategy for the Mediterranean.
- Cziczo, D. J., Froyd, K.D., Hoose, C., Jensen, E. J., Diao, M., Zondlo, M. A., ...Murphy, D. M.** (2013). Clarifying the Dominant Sources and Mechanisms of Cirrus Cloud Formation. *Science*, 340, 6138, 1320-1324.
- Daly, A and Zannetti, P.** (2007). Air Pollution Modeling-An Overview. Chapter 2 of “Ambient Air Pollution” ASST and The EnviroComp Institute.
- Demiray, A.D., Yolcubal, I., Akyol, N.H., and Cobanoglu, G.** (2012). Biomonitoring of airborne metals using the Lichen *Xanthoria parietina* in Kocaeli Province. *Turkey Ecol. Indic.*, 18, 632–643.
- Dragosavac, M.** (2007). BUFR User’s Guide, ECMWF Technical note.
- Engelstaedter, S., and Tegen, I.** (2006). Washington, R. North African dust emissions and transport. *Earth-Science Reviews*, 79, 73–100.
- Fast, J. D., Gustafson Jr., W. I., Easter, R. C., Zaveri, R. A., Bernard, J. C., Chapman, E. G., ...Peckham, S. E.** (2006). Evolution of ozone, particulates, and aerosol direct radiative forcing in the vicinity of Houston using a fully coupled meteorology-chemistry-aerosol model. *J. Geophys. Res.*, 111, D21305.
- Follette Cook, M. B., Pickering, K. E., Crawford J. H., Duncan, B. N., Loughner, C. P., Diskin, G. S., ...Weinheimer, A. J.** (2015). Spatial and temporal variability of trace gas columns derived from WRF/Chem regional model output: Planning for geostationary observations of atmospheric

- composition. *Atmospheric Environment*, 118, 28-44.
- Foltz, G. R., and McPhaden, M. J.** (2008). Trends in Saharan dust and tropical Atlantic climate during 1980 – 2006. *Geophys. Res. Lett.*, 35, L20706.
- Freitas, S. R., Longo, K.M., Alonso, M.F., Pirre, M., Marecal, V., Grell, G., ...Gacita, M.S.** (2011). PREP-CHEM-SRC 1.0: a preprocessor of trace gas and aerosol emission fields for regional and global atmospheric chemistry models, *Geoscientific Model Development*, 4, 419-433.
- Fuzzi, S., Baltensperger, U., Carslaw, K., Decesari, S., Denier van der Gon, H., Facchini, M. C., ...Gilardoni, S.** (2015). Particulate matter, air quality and climate: lessons learned and future needs. *Atmos. Chem. Phys.*, 15, 8217-8299.
- Gerasopoulos, E., Kouvarakis, G., Babasakalis, P., Vrekoussis, M., Putaud, J.P., and Mihalopoulos, N.** (2006). Origin and variability of particulate matter (PM<sub>10</sub>) mass concentrations over the Eastern Mediterranean. *Atmos. Environ.*, 40, 4679–4690.
- Ginoux, P., Chin, M., Tegen, I., Prospero, J., Holben, B., Dubovik, O., and Lin, S. J.** (2001). Sources and distributions of dust aerosols simulated with the GOCART model. *J. Geophys. Res.*, 106, 20225–20273.
- Gkikas, A., Houssos, E. E., Hatzianastassiou, N., Papadimas, C. D., and Bartzokas, A.** (2012). Synoptic conditions favouring the occurrence of aerosol episodes over the broader Mediterranean Basin. *J. Meteorol. Soc.*, 138, 932–949. DOI:10.1002/qj.978.
- Goudie, A.S and Middleton, N. J.** (2001). Saharan dust storms: nature and consequences. *Earth-Science Reviews*, 56,1-4, 179-204.
- Grantz, D. A., Garner, J. H. B., and Johnson, D. W.** (2003). Ecological effects of particulate matter. *Environ. Int.*, 29, 213–239.
- Grell, G. A., Peckham, S. E., Schmitz, R., McKeen, S. A., Frost, G., Skamarock, W. C., and Eder, B.** (2005). Fully coupled “online” chemistry within the WRF model. *Atmospheric Environment*, 39, 6957–6975.
- Griffin, D. W., Garrison, V. H., Herman, J. R., and Shinn, E. A.** (2001). African desert dust in the Caribbean atmosphere: Microbiology and public health. *Aerobiologia*, 17, 203–213.
- Griffin, D. W.** (2007). Atmospheric movement of microorganisms in clouds of desert dust and implications for human health. *Clin. Microbiol. Rev.*, 20, 459–477.
- Grishkan, I., Schlesinger, P., and Mamane, Y.** (2012). Influence of dust storms on concentration and content of fungi in the atmosphere of Haifa, Israel, *Aerobiologia*, 28, 557–564.
- Guerzoni, S., Molinarolo, E., and Chester, R.** (1997). Saharan dust inputs to the western Mediterranean Sea: depositional patterns, geochemistry and sedimentological implications. *Deep Sea Research Part II: Tropical Studies in Oceanography*, 44, 631-654.
- Hamzaoglu O., Etiler N., Yavuz C.I., and Cağlayan C.** (2011). The causes of deaths in an industry-dense area: example of Dilovası (Kocaeli). *Turk J Med*

*Sci.*, 41, 369–375.

- Han, Y., van Delst, P., Liu, Q., Weng, F., Yan, B., Treadon, R., and Derber, J.** (2006). JCSDA Community Radiative Transfer Model (CRTM)—Version 1. *NOAA Tech. Rep. NESDIS*, 122, 33.
- Han, Z., Li, J., Xia, X., and Zhang, R.** (2012). Investigation of direct radiative effects of aerosols in dust storm season over East Asia with an online coupled regional climate-chemistry-aerosol model. *Atmospheric Environment*, 54, 688-699.
- Han, Z., Li, J., Guo, W., Xiong, Z., and Zhang, W.** (2013). A study of dust radiative feedback on dust cycle and meteorology over East Asia by a coupled regional climate-chemistry-aerosol model. *Atmospheric Environment*, 68, 54-63.
- Hatzianastassiou, N., Gkikas, A., Mihalopoulos, N., Torres, O., and Katsoulis, B. D.** (2009). Natural versus anthropogenic aerosols in the eastern Mediterranean basin derived from multiyear TOMS and MODIS satellite data, *J. Geophys. Res.*, 114, D24202.
- Hinds, William C.** (1999). *Aerosol Technology* (2nd ed.). Wiley – Interscience.
- Hsu, N. C., Tsay, S. C., King, M. D., and Herman, J. R.** (2004). Aerosol properties over bright-reflecting source regions. *IEEE Trans. Geosci. Remote*, 42, 557–569.
- Hsu, A., Emerson, J., Levy, M., Sherbinin, A., Johnson, L., Malik, O., ...Jaiteh, M.** (2014). The 2014 Environmental Performance Index. *New Haven, CT, Yale Center for Environmental Law & Policy*.
- Huang, J., Wang, T., Wang, W., Li, Z., and Yan, H.** (2014). Climate effects of dust aerosols over East Asian arid and semiarid regions. *J. Geophys. Res. Atmos.*, 119, doi:10.1002/2014JD021796.
- Im, U., Daskalakis, N., Markakis, K., Vrekoussis, M., Hjorth, J., Myriokefalitakis, S., ...Kanakidou, M.** (2014). Simulated air quality and pollutant budgets over Europe in 2008, *Sci Total Environ.*, 470–471, 270–28.
- Israelevich, P., Ganor, E., Alpert, P., Kishcha, P., and Stupp, A.** (2012). Predominant transport paths of Saharan dust over the Mediterranean Sea to Europe. *J. Geophys. Res.*, 117, D02205, doi:10.1029/2011JD016482, 17842-17847.
- Janjić, Z. I.** 1994: The Step-Mountain Eta Coordinate Model: Further Developments of the Convection, Viscous Sublayer, and Turbulence Closure Schemes. *Mon. Wea. Rev.*, 122: 927–945.
- Janssens-Maenhout, G., Dentener, F., van Aardenne, J., Monni S., Pagliari, V., Orlandini, L., ...Keating, T.** (2012). EDGAR-HTAP: a harmonized gridded air pollution emission dataset based on national inventories.
- Jimenez-Guerrero, P., Perez, C., Jobra, O., and Baldasano, J.** (2008). Contribution of Saharan dust in an ingrated air quality system and its on-line assessment, *Geophys. Res. Lett.*, 35, L03814.
- Kabatas, B., Unal, A., Pierce, R.B., Kindap, T., and Pozzoli, L.** (2014). The contribution of Saharan dust in PM<sub>10</sub> concentration levels in Anatolian

Peninsula of Turkey, *Sci. Total Environ.*, 488–489, 413–421.

- Kallos, G., Papadopoulos, A., Katsafados, P., and Nickovic, S.** (2006). Transatlantic Saharan dust transport: Model simulation and results. *J. Geophys. Res.*, 111, D09204.
- Kallos, G., Astitha, M., Katsafados, P., and Spyrou, C.** (2007). Long-range transport of anthropogenically and naturally produced particulate matter in the Mediterranean and North Atlantic: current state of knowledge. *J. Appl. Meteorol. Clim.*, 46, 1230–1251.
- Kanakidou, M., Mihalopoulos, N., Kindap, T., Im, U., Vrekoussis, M., Gerasopoulos, E., ...Moubasher, H.** (2011). Megacities as hot spots of air pollution in the East Mediterranean, *Atmos. Environ.*, 45, 1223–1235.
- Karanasiou, A., Moreno, N., Moreno, T., Viana, M., de Leeuw, F., and Querol, X.** (2012). Health effects from Sahara dust episodes in Europe: Literature review and research gaps, *Environ. Int.*, 47, 107–114.
- Karydis, V. A., Kumar, P., Barahona, D., Sokolik, I. N., and Nenes, A.** (2011). On the effect of dust particles on global cloud condensation nuclei and cloud droplet number. *J. Geophys. Res.*, 116, D23204, doi:10.1029/2011JD016283.
- Kaufman, Y. J., Koren, I., Remer, L.A., Tanre, D., Ginoux, P., and Fan, S.** (2005a). Dust transport and deposition observed from the Terra MODIS spacecraft over the Atlantic Ocean, *J. Geophys. Res.*, 110, D10S12, doi:10.1029/2003JD004436.
- Kaufman, Y. J., Remer, L., Tanre, D., Li, R., Kleidman, R., Mattoo, S., ...Koren, I.** (2005b). A critical examination of the residual cloud contamination and diurnal sampling effects on MODIS estimates of aerosol over ocean. *IEEE T. Geosci. Remote*, 43 (12), 2886–2897.
- Kavgacı, A., Carni, A., Basaran, S., Basaran, M. A., Košir, P., Marinšek, A., and Šilc, U.** (2010). Long-term post-fire succession of *Pinus brutia* forest in the east Mediterranean. *Int. J. Wildland Fire*, 19, 599–605.
- Khan, B., Stenchikov, G., Weinzierl, B., Kalenderski, S., and Osipov, S.** (2015). Quantifying dust plume formation and aerosol size distribution during the Saharan Mineral Dust Experiment in North Africa. *Tellus B*.
- Kleist, D. T., Parrish, D. F., Derber, J. C., Treadon, R., Wu, W.S., and Lord, S.** (2009). Introduction of the GSI into the NCEP global data assimilation system. *Weather Forecast.*, 24, 1691–1705.
- Kocak, M., Mihalopoulos, N., and Kubilay, N.** (2007). Contributions of natural sources to high PM10 and PM2.5 events in the eastern Mediterranean. *Atmos. Environ.*, 41 (18), 3806–3818.
- Kubilay, N., Nickovic, S., Moulin, C., and Dulac, F.** (2000). An illustration of the transport and deposition of mineral dust onto the eastern Mediterranean, *Atmos. Environ.*, 34, 1293–1303.
- Kumar, R., Naja, M., Pfister, G. G., Barth, M. C., Wiedinmyer, C., and Brasseur, G. P.** (2012). Simulations over South Asia using the Weather Research and Forecasting model with Chemistry (WRFChem): chemistry

evaluation and initial results. *Geosci. Model Dev.*, 5, 619–648, doi:10.5194/gmd-5-619-2012.

- Kumar, R., Barth, M. C., Pfister, G. G., Naja, M., and Brasseur, G. P.** (2014). WRF-Chem simulations of a typical pre-monsoon dust storm in northern India: influences on aerosol optical properties and radiation budget. *Atmos. Chem. Phys.*, 14, 2431-2446, doi:10.5194/acp-14-2431-2014.
- Lelieveld J., Berresheim, H., Borrmann, S., Crutzen, P. J., Dentener, F. J., Fischer, H., ...Ziereis, H.** (2002). Global air pollution crossroads over the Mediterranean. *Science*, 298, 794–799.
- Levin, Z., Teller, A., Ganor, E., and Yin, Y.** (2005). On the interactions of mineral dust, sea-salt particles, and clouds: A measurement and modeling study from the Mediterranean Israeli Dust Experiment campaign. *J. Geophys. Res.*, 110 (D20), D20202, doi:10.1029/2005JD005810.
- Levy, R. C., Mattoo, S., Munchak, L. A., Remer, L. A., Sayer, A. M., Patadia, F., ...Hsu, N. C.** (2013). The Collection 6 MODIS aerosol products over land and ocean. *Atmos. Meas. Tech.*, 6, 2989-3034, doi:10.5194/amt-6-2989-2013.
- Liu, Z., Liu, Q., Lin, H. C., Schwartz, C. S., Lee, Y. H. and Wang, T.** (2011). Three-dimensional variational assimilation of MODIS aerosol optical depth: Implementation and application to a dust storm over East Asia, *J. Geophys. Res.*, 116, D23206.
- Mallone, S., Stafoggia, M., Faustini, A., Gobbi, J. P., Marconi, A., and Forastiere, F.** (2011). Saharan dust and associations between particulate matter and daily mortality in Rome, Italy. *Environ. Health Perspect.*, 119, 1409 – 1414.
- Martin, R. V.** (2008). Satellite remote sensing of surface air quality. *Atmospheric Environment*, 42, 7823–7843.
- Markakis, K., Im, U., Unal, A., Melas, D., Yenigun, O., and Incecik, S.** (2012). Compilation of a GIS based high spatially and temporally resolved emission inventory for the greater Istanbul area. *Atmos. Pollut. Res.*, 3, 112–125.
- Michalakes, J., Chen, S., Dudhia, J., Hart, L., Klemp, J., Middlecoff, J., ...Skamarock, W.** (2001): Development of a Next Generation Regional Weather Research and Forecast Model. Developments in Teracomputing: Proceedings of the Ninth ECMWF Workshop on the Use of High Performance Computing in Meteorology. Eds. *Walter Zwiefelhofer and Norbert Kreitz. World Scientific*, 269-276.
- Mitsakou, C., Kallos, G., Papantoniou, N., Spyrou, C., Solomos, S., Astitha, M., ...Housiadas, C.** (2008). Saharan dust levels in Greece and received inhalation doses. *Atmos. Chem. Phys.*, 8, 7181– 7192.
- Mustafic H., Jabre, P., Caussin, C., Murad, M. H., Escolano, S., Tafflet, M., Perier, M.C., ...Joven, X.** (2012). Main Air Pollutants and Myocardial Infarction A Systematic Review and Meta-analysis. *American Medical Association*, 307, 713-721.

- Nel, A.** (2005). Air pollution-related illness: effects of particles. *Science*, 308, 804–806.
- Natarajan, M., Pierce, R. B., Schaack, T. K., Lenzen, A. J., Al Saadi, J. A., Soja, A. J., ... Worden, J. R.** (2012). Radiative forcing due to enhancements in tropospheric ozone and carbonaceous aerosols caused by Asian fires during spring 2008. *J. Geophys. Res.*, 117, D06307, doi:10.1029/2011JD016584.
- Nawrot, T. S., Perez, L., Künzli, N., Munters, E., and Nemery, B.** (2011). Public health importance of triggers of myocardial infarction: a comparative risk assessment. *Lancet*, 377, 732–740.
- Niu, T., Gong, S. L., Zhu, G. F., Liu, H. L., Hu, X. Q., Zhou, C. H., ... Wang, Y. Q.** (2008). Data assimilation of dust aerosol observations for the CUACE/dust forecasting system. *Atmos. Chem. Phys.*, 8, 3473–3482, doi:10.5194/acp-8-3473-2008.
- Olivier, J., Bouwman, A., van der Maas, C., Berdowski, J., Veldt, C., Bloos, J., ... Haverlag, J.** (1996). Description of EDGAR Version 2.0: A Set of Global Emission Inventories of Greenhouse Gases and Ozone-Depleting Substances for All Anthropogenic and Most Natural Sources on a per Country Basis and on a  $1 \times 1$  Degree Grid, *RIVM Report 771060 002/TNO-MEP Report R96/119*, National Institute of Public Health and the Environment, Bilthoven, the Netherlands.
- Pagowski, M., Liu, Z., Grell, G. A., Hu, M., Lin, H.C., and Schwartz, C. S.** (2014). Implementation of aerosol assimilation in GSI and WRF-Chem. *Geosci. Model Dev.*, 7, 1621–1627.
- Papayannis, A., Balis, D., Amiridis, V., Chourdakis, G., Tsaknakis G., Zeferos, C., ... Grabowski, J.** (2005). Measurements of Saharan dust aerosols over the eastern Mediterranean using elastic backscatter-Raman lidar, spectrophotometric and satellite observations in the frame of the EARLINET project. *Atmos. Chem. Phys.*, 5, 2065–2079.
- Parrish, D. F., and J. C. Derber.** (1992). The National Meteorological Center's spectral statistical interpolation analysis system. *Mon. Wea. Rev.*, 120, 1747–1763.
- Perlwitz, J., and R. L. Miller** (2010). Cloud cover increase with increasing aerosol absorptivity- A counterexample to the conventional semi-direct aerosol effect. *J. Geophys. Res.*, 115, D08203.
- Peters, A., Skorkovsky J., Kotesovec F., Brynda J., Spix C., Wichmann H.E., ... Heinrich J.** (2000). Associations between Mortality and Air Pollution in Central Europe Environ. *Health Perspect.*, 108, 283–287.
- Pey, J., Querol, X., Alastuey, A., Forastiere, F., and Stafoggia, M.** (2013). African dust outbreaks over the Mediterranean Basin during 2001–2011: PM<sub>10</sub> concentrations, phenomenology and trends, and its relation with synoptic and mesoscale meteorology. *Atmos. Chem. Phys.*, 13, 1395–1410, doi:10.5194/acp-13-1395.
- Pierce, R. B., Al-Saadi, J. A., Schaack, T., Lenzen, A., Zapotocny, T., Johnson, D., ... Sandholm, S. T.** (2003). Regional Air Quality Modeling System (RAQMS) predictions of the tropospheric ozone budget over East Asia.

*J. Geophys. Res.*, 108 (D21), 8825–8835, doi:10.1029/2002JD003176, 2003.

- Pierce, R. B., Schaack, T. K., Al-Saadi, J., Fairlie, T. D., Kittaka, C., Lingenfelter, ...Fishman, J.** (2007). Chemical data assimilation estimates of continental US ozone and nitrogen budgets during INTEX-A, *J. Geophys. Res.*, 112, D12S21.
- Prins, E. M., and Menzel, W. P.** (1994). Trends in South American biomass burning detected with the GOES VAS from 1983 to 1991. *J. Geophys. Res.*, 99, 16, 719-16,735.
- Prospero, J.M., Charlson, R. J., Mohnen, V., Jaenicke, R., Delany, A. C., Meyers, J., ...Rahn, K.** (1983). The atmospheric aerosol system: An overview. *Reviews of Geophysics and Space Physics*, 21, 1607-1629.
- Pope III, C. A., Burnett, R. T., Thurston, G. D., Thun, M. J., Calle, E. E., Krewski, D., ...Godleski, J. J.** (2004). Cardiovascular Mortality and Long-Term Exposure to Particulate Air Pollution: Epidemiological Evidence of General Pathophysiological Pathways of Disease. *Circulation*, 109, 71-77.
- Purser, R., Wu, W., Parrish, D., and Roberts, N.** (2003). Numerical aspects of the application of recursive filters to variational statistical analysis. Part I: Spatially homogeneous and isotropic gaussian covariances, *Mon. Weather Rev.*, 131, 1524–1535.
- Querol, X., Alastuey, A., Ruiz, C. R., Artinano, B., Hansson, H. C., Harrison, R. M., ...Schneider, J.** (2004). Speciation and origin of PM<sub>10</sub> and PM<sub>2.5</sub> in selected European cities. *Atmos. Environ.*, 38, 6547–6555.
- Querol, X., Pey, J., Pandolfi, M., Alastuey, A., Cusack, M., Pérez, N., ...Kleanthous, S.** (2009). African dust contributions to mean ambient PM<sub>10</sub> mass-levels across the Mediterranean Basin. *Atmospheric Environment*, 43, 4266–4277.
- Remer, L. A., Kaufman, Y. J., Tanre, D., Mattoo, S., Chu, D. A., Martins, J. V., ...Holben, B. N.** (2005). The MODIS aerosol algorithm, products and validation. *J. Atmos. Sci.*, 62 (4), 947–973.
- Rodríguez, S., Querol, X., Alastuey, A., Kallos, G., and Kakaliagou, O.** (2001). Saharan dust contributions to PM<sub>10</sub> and TSP levels in Southern and Eastern Spain. *Atmos. Environ.*, 35, 2433–2447.
- Rodríguez, S., Alastuey, A., Alonso-Perez, S., Querol, X., Cuevas, E., Abreu-Afonso, J., ...dela Rosa, J.** (2011). Transport of desert dust mixed with North African industrial pollutants in the subtropical Saharan Air Layer. *Atmos. Chem. Phys.*, 11, 6663-6685.
- Russell, A. and Dennis, R.** (2000). NARSTO critical review of photochemical models and modeling. *Atmos. Environ.*, 34, 2283–2324.
- Saide, P. E., Carmichael, G. R., Liu, Z., Schwartz, C. S., Lin, H. C., da Silva, A. M., ...Hyer, E.** (2013). Aerosol optical depth assimilation for a size-resolved sectional model: impacts of observationally constrained, multi-wavelength and fine mode retrievals on regional scale analyses and forecasts. *Atmos. Chem. Phys.*, 13, 10425–10444.



- Sajani S. Z., Miglio R., Bonasoni, P., Cristofanelli, P., Marinoni, A., Sartini, C., ...Lauriola, P.** (2011). Saharan dust and daily mortality in Emilia-Romagna (Italy). *Occup Environ Med*., 68, 446–51.
- Sayer, A. M., Hsu, N. C., Bettenhausen, C., and Jeong, M. J.** (2013). Validation and uncertainty estimates for MODIS Collection 6 “Deep Blue” aerosol data. *J. Geophysical Research*, 118, 7864-7872.
- Schaack, T. K., Zapotocny, T. H., Lenzen, A. J., and Johnson, D. R.** (2004). Global Climate Simulation with the University of Wisconsin Global Hybrid Isentropic Coordinate Model., *J. Climate*, 17, 2998–2016.
- Schaap, M., Cuvelier, C., Hendriks, C., Bessagnet, B., Baldasano, J. M., Colette, A., ...Wind, P.** (2015). Performance of European chemistry transport models as function of horizontal resolution. *Atmos. Environment*, 112, 90–105.
- Schultz, M. and Rast, S.** (2007). Emission datasets and methodologies for estimating emissions, available at: <http://retro.enes.org>, RETRO Report D1-6.
- Schwartz, C. S., Liu, Z., Lin, H.C., and McKeen, S. A.** (2012). Simultaneous three-dimensional variational assimilation of surface fine particulate matter and MODIS aerosol optical depth. *J. Geophys. Res.*, 117, D13202, doi:10.1029/2011JD017383.
- Sekiyama, T. T., Tanaka, T. Y., Shimizu, A., and Miyoshi, T.** (2010). Data assimilation of CALIPSO aerosol observations. *Atmos. Chem. Phys.*, 10, 39–49.
- Sessions, W. R., Fuelberg, H. E., Kahn, R. A., and Winker, D. M.** (2011). An investigation of methods for injecting emissions from boreal wildfires using WRF-Chem during ARCTAS. *Atmos. Chem. Phys.*, 11, 5719-5744, doi:10.5194/acp-11-5719-2011.
- Shi, Y., Zhang, J., Reid, J. S., Holben, B. N., Hyer, E. J., and Curtis, C.** (2011). An analysis of the collection 5 MODIS over-ocean aerosol optical depth product for its implication in aerosol assimilation. *Atmos. Chem. Phys.*, 11, 557-565.
- Shinn, E. A., Smith, G. W., Prospero, J. M., Betzer, P., Hayes, M. L., Garrison, V., ...Barber, R. T.** (2000). African dust and the demise of Caribbean Coral Reefs. *Geophys. Res. Lett.*, 27, 3029–3032.
- Skamarock, W. C., Klemp, J. B., and Dudhia, J.** (2001). Prototypes for the WRF (Weather Research and Forecasting) model. Preprints, Ninth Conf. on Mesoscale Processes, Fort Lauderdale. FL. *Amer. Meteor. Soc.*, J11–J15.
- Skamarock, W. C. and Klemp, J. B.** (2005). A time-split non-hydrostatic atmospheric model. *J. Comput. Phys.*, 227, 3465–3485.
- Smoydzin, L., Teller, A., Tost, H., Fnais, M., and Lelieveld, J.** (2012). Impact of mineral dust on cloud formation in a Saharan outflow region. *Atmos. Chem. Phys.*, 12, 11383–11393.
- Streets, D. G., Canty, T., Carmichael, G. R., de Foy, B., Dickerson, R. R., Duncan, B. N., ...Wecht, K. J.** (2013). Emissions estimation from satellite retrievals: A review of current capability. *Atmos. Envir.*, 77, 1011-1042.

- Swap, R., Garstang, M., Greco, S., Talbot, R., and Kallberg, P.** (1992). Saharan dust in the Amazon basin. *Tellus B*, 44 (2) 133–149.
- Talagrand, O.** (1997). Assimilation of Observations, an Introduction. *J. Meteorological Society of Japan*, 75, 191-209.
- Tanaka, T. Y., and Chiba M.** (2006). A numerical study of the contribution of dust source regions to the global dust budget. *Glob. Planet Change*, 52, 88-104.
- Tang, Y., Carmichael, G. R., Thongboonchoo, N., Chai, T., Horowitz, L. W., Pierce, R. B., ...Brune, W. H.** (2007). The influence of lateral and top boundary conditions on regional air quality prediction: a multi-scale study coupling regional and global chemical transport models. *J. Geophys. Res.*, 112, D10S18.
- Tie, X., Madronich, S., Li, G. H., Ying, Z. M., Zhang, R., Garcia, A., ...Liu, Y.** (2007). Characterizations of chemical oxidants in Mexico City: a regional chemical/dynamical model (WRF-Chem) study. *Atmos. Environ.*, 41, 1989–2008.
- Tie, X., Geng, F., Guenther, A., Cao, J., Greenberg, J., Zhang, R., ...Cai, C.** (2013). Megacity impacts on regional ozone formation: observations and WRFChem modeling for the MIRAGE-Shanghai field campaign. *Atmos. Chem. Phys.*, 13, 5655–5669.
- Tobias, A., Perez, L., Diaz, J., Linares, C., Pey, J., Alastuey, A., ...Querol, X.** (2011). Short-term effects of particulate matter on daily mortality during Saharan dust outbreaks: A case-crossover analysis in Madrid (Spain). *Sci. Total Environ.*, 412–413, 386–389.
- Twohy, C. H., Kreidenweis, S. M., Eidhammer, T., Browell, E. V., Heymsfield, A. J., Bansemer, A. R., ...Van den Heever, S. C.** (2009). Saharan dust particles nucleate droplets in eastern Atlantic clouds. *Geophys. Res. Lett.*, 36, L01807.
- van de Hulst, H. C.** (1957), *Light Scattering by Small Particles*, 470, John Wiley, New York.
- Verma, S., Worden, J., Pierce, B., Jones, D. B. A., Al-Saadi, J., Boersma, F., ...Worden, H.** (2009). Ozone production in boreal fire smoke plumes using observations from Tropospheric Emissions Spectrometer and the Ozone Monitoring Instrument. *J. Geophys. Res.*, 114, D02303.
- Vodonos, A., Friger, M., Katra, I., Avnon, L., Krasnov, H., Koutrakis, P., ...Novack, V.** (2014). The impact of desert dust exposure on hospitalization due to the exacerbation of chronic obstructive pulmonary disease. *Air Qual. Atmos. Health*, 7, 433-439.
- Wang, Y., Sartelet, K. N., Bocquet, M., Chazette, P., Sicard, M., D'Amico, G., ...Dulac, F.** (2014). Assimilation of lidar signals: application to aerosol forecasting in the western Mediterranean basin. *Atmos. Chem. Phys.*, 14, 12031–12053.
- Winker, D. M., Hunt, W. H., and McGill, M. J.** (2007). Initial performance assessment of CALIOP. *Geophys. Res. Lett.*, 34, L19803.

- World Health Organization.** (2006). Air quality guidelines. Global update 2005. Particulate Matter, Ozone, Nitrogen Dioxide and Sulfur Dioxide. *World Health Organization*.
- Wu, W.S., Purser, R. J., and Parrish, D. F.** (2002). Three-dimensional variational analysis with spatially inhomogeneous covariances. *Mon. Wea. Rev.*, 130, 2905–2916.
- Zhang, J., Reid, J. S., Westphal, D. L., Baker, N. L., and Hyer, E. J.** (2008). A system for operational aerosol optical depth data assimilation over global oceans, *J. Geophys. Res.*, 113, D10208.
- Zhao, C., Liu, X., Ruby Leung, L., and Hagos, S.** (2011). Radiative impact of mineral dust on monsoon precipitation variability over West Africa. *Atmos. Chem. Phys.*, 11, 1879–1893.
- Zhao, X.** (2012). Asian Dust Detection from the Satellite Observations of Moderate Resolution Imaging Spectroradiometer (MODIS). *Aerosol and Air Quality Research*, 12, 1073–1080.



## CURRICULUM VITAE

**Name Surname** : Burcu Kabataş  
**Place and Date of Birth** : Istanbul 03.04.1984  
**E-Mail** : kabatasb@gmail.com

### EDUCATION

- **B.Sc.** : 2008, ITU, Faculty of Aeronautics and Astronautics, Meteorological Engineering Department.
- **M.Sc.** : 2011, ITU, Faculty of Maritime, Department of Maritime Transportation and Management Engineering.

### PROFESSIONAL EXPERIENCE AND REWARDS:

- 2009-2010, Research Scholar, University of Wisconsin-Madison, Space Science and Engineering Center.
- 2011-2013, Research Assistant, TUBITAK (Scientific and Technological Research Council of Turkey) Contract 110Y078: Quantification of the effect of Sahara Dust on Air Pollution in Turkey, Istanbul, Turkey.
- 2014-2016, Research Scholar, University of Wisconsin-Madison, Space Science and Engineering Center.
- Best Scientific Poster, 1<sup>st</sup> Place, at NOAA/NESDIS Cooperative Research Program (CoRP) 11<sup>th</sup> Annual Student Science Symposium, 2015, Maryland, USA.

### PUBLICATIONS, PRESENTATIONS AND PATENTS ON THE THESIS:

- **Kabatas, B.**, Unal, A., Pierce, R.B., Kindap, T., and Pozzoli, L., 2014: Quantification of Saharan dust on Anatolian Peninsula via RAQMS Modeling, Special Session of the Air Quality Management at Urban, Regional and Global Scales, 4th International Symposium and IUAPPA Regional Conference (AQM2012), September 10-13, 2012 Istanbul Turkey.

- **Kabatas, B.**, Unal, A., Pierce, R.B., Rogal, M., Schaack, T. Lenzen, A., 2015: Nested RAQMS/WRF-CHEM/GSI aerosol data assimilation experiments during the April 2008 Saharan Dust Event, September 16-17, 2015 University of Maryland, Collage Park, MD, USA.
- **Kabatas, B.**, Unal, A., Pierce, R.B., Rogal, M., Schaack, T. Lenzen, A., accepted on October 4, 2016: Dust influences in the Eastern Mediterranean: Multi-scale assimilation of MODIS AOD, AGU Fall Meeting, San Francisco, CA, USA.
- **Kabatas, B.**, Unal, A., Pierce, R.B., Kindap, T., and Pozzoli, L. 2014. The contribution of Saharan dust in PM<sub>10</sub> concentration levels in Anatolian Peninsula of Turkey, *Sci. Total Environ.*, 488–489, 413–421.

#### **OTHER PUBLICATIONS, PRESENTATIONS AND PATENTS:**

**Kabatas, B.**, Menzel, W.P., Bilgili, A., Gumley, L. E., 2012: Comparing Ship Track Droplet Sizes Inferred from Terra and Aqua MODIS Data, Geophysical Research Abstracts Vol. 14, EGU2012-12064-1.

**Kabatas, B.**, Menzel, P., Bilgili, A., Gumley, L. E., 2013. Comparing Ship-Track Droplet Sizes Inferred from Terra and Aqua MODIS Data, *J. Appl. Meteor. Climat.*, 52, 230-241, doi:10.1175/JAMC-D-11-0232.1.